Forschungszentrum Karlsruhe
Technik und Umwelt

Wissenschaftliche Berichte
FZKA 6507

Neutron Physics Calculations for ADS Targets

I. Broeders, C. H. M. Broeders

Institut für Kern- und Energietechnik
Programm Nukleare Sicherheitsforschung

Oktober 2000

Forschungszentrum Karlsruhe

Technik und Umwelt

Wissenschaftliche Berichte

FZKA 6507

Neutron Physics Calculations for ADS Targets

I. Broeders, C. H. M. Broeders

Institut für Kern- und Energietechnik
Programm Nukleare Sicherheitsforschung

Forschungszentrum Karlsruhe GmbH, Karlsruhe
2000

Als Manuskript gedruckt

Forschungszentrum Karlsruhe GmbH
Postfach 3640, 76021 Karlsruhe

Mitglied der Hermann von Helmholtz-Gemeinschaft
Deutscher Forschungszentren (HGF)

ISSN 0947-8620

Neutron Physics Calculations for ADS Targets

Abstract

The LAHET Code System (LCS) is used to investigate the neutron physics of a liquid lead target hit by a high energy proton beam. The main goals of the performed analysis are the calculation of the spatial dependence of the energy deposition in the beam window and in the liqiud lead target and the calculation of the neutron flux density spectra in the beam window and in different zones of the target. Moreover, the reaction products (nucleons, mesons, deuterons, tritons, ^{3}He, α-particles and residual nuclei) which result from the spallation process in a lead-bismuth target are investigated.

Some of the calculations mentioned above have also been carried out with the beta test version of the MCNPX code, provided by LANL/USA, that was established by merging of LAHET and MCNP.

In the Appendix, calculations for neutron flux density spectra up to 1GeV in different regions (target, inner and outer core region, radial blanket) of an accelerator-driven system (ADS) are presented.

The results described in this report were used for the thermohydraulic layout of the window- and target-cooling and contributed to benchmark intercomparisons.

Neutronenphysikalische Rechnungen für Targets beschleunigergetriebener Systeme

Zusammenfassung

Mit Hilfe des LAHET Code Systems (LCS) wird das neutronenphysikalische Verhalten eines Flüssigblei-Targets bei Auftreffen eines hochenergetischen Protonenstrahls untersucht. Die Hauptziele der neutronenphysikalischen Analyse sind die Untersuchung der Ortsabhängigkeit der Energiefreisetzung im Strahlfenster und im Flüssigblei-Target und die Berechnung der Neutronenflussdichte-Spektren im Fenster und in verschiedenen Zonen des Targets. Außerdem werden die Reaktionsprodukte (Nukleonen, Mesonen, Deuteronen, Tritonen, ^{3}He, α-Teilchen und Restkerne) untersucht, die beim Spallationsprozess in einem Blei-Wismut-Target gebildet werden.

Zum Vergleich von Ergebnissen ist für einige der Untersuchungen auch die Beta Test Version des MCNPX Codes eingesetzt worden, die von LANL/USA verfügbar gemacht wurde und eine Vereinigung der Programme LAHET und MCNP darstellt.

Im Anhang werden Rechnungen für Neutronenflussdichte-Spektren bis 1GeV in verschiedenen Bereichen (Target, innere und äussere Corezone, radiales Blanket) eines beschleunigergetriebenen Systems (ADS) diskutiert.
Die in diesem Bericht beschriebenen Ergebnisse wurden für die thermohydraulische Auslegung der Fenster- und Target-Kühlung benutzt und trugen zu Vergleichen im Rahmen eines Benchmarks bei.

Contents

List of Figures

List of Tables

Chapter 1

Introduction

The spallation target and the beam window are very important components of an accelerator-driven system (ADS). In a previous report, calculations for the energy deposition in the target and in the beam window of a liquid lead target have been presented [1]. The model for the target had been derived from the layout of the IAEA-ADS neutronic benchmark reactor [2, 3], shown in Fig. A.1; (a hemispherical beam window was added to the inner lead region with the center of the hemisphere on the reactor axis 35cm above the reactor midplane). Meanwhile similar investigations have been carried out for a more detailed target design based on [4, 5], and shown in Fig. 2.1.

Our main goal is the determination of the spatial distribution of the energy deposition in the target. We also investigate neutron flux density spectra, reaction rates and the reaction products (particles and residual nuclei) of the spallation process.

Most of the calculations have been carried out with the LAHET Code System (LCS) [6] which mainly consists of LAHET (Los Alamos version of the High Energy Transport Code HETC) [7], [8] and of MCNP (Monte Carlo N-Particle transport code) [9]. For the nuclear model parameters that have to be chosen by the input of LAHET [7] we used the default values, with the only exception that we specified a preequilibrium phase following the intranuclear cascade.

For our calculations with LAHET we used the following models and methods:
(in parentheses the corresponding LCS input variables)

- The Bertini model [10] is used for the simulation of the intranuclear cascade (IEXISA=0)
- A preequilibrium model [11, 12] is applied following the intranuclear cascade (IPREQ=1)
- The RAL (Rutherford and Appleton Laboratories) evaporation-fission model is used [13] (IEVAP=0). For light nuclei the evaporation model is replaced by the Fermi breakup model (IFBRK=1) (see [7] and references given there)

- The Gilbert-Cameron-Cook-Ignatyuk [14] level density model is used (ILVDEN=0)
- The neutron elastic scattering data file /LCS/ELSTIN which is part of the LCS system is used (NOELAS=23)
- The nucleon-pion transport option is applied (NBERTP=1)

Chapter 2

Energy Deposition in Different Zones of a Liquid Lead Target Hit by a 600MeV Proton Beam

Here we present neutron physics investigations for a liquid lead target. The model of the target used in the calculations is based on [4] and shown in Figure 2.1. The different zones taken into account in the calculation are marked in the figure and explained below. Our main goal is the determination of the spatial distribution of the energy deposion in the target. As a first orientation we calculate the average energy deposition in the different zones (zones 1 to 17)

The **proton beam** enters the target from above. In the LCS input the position of the proton source is at r=0cm, z=212cm. The energy of the protons is 600MeV, the cross section of the proton beam is a circle of radius 7.5 cm. The intensity distribution of the protons is parabolic over the beam radius (corresponding ISOPT=1 in the source specification of LAHET [6]).

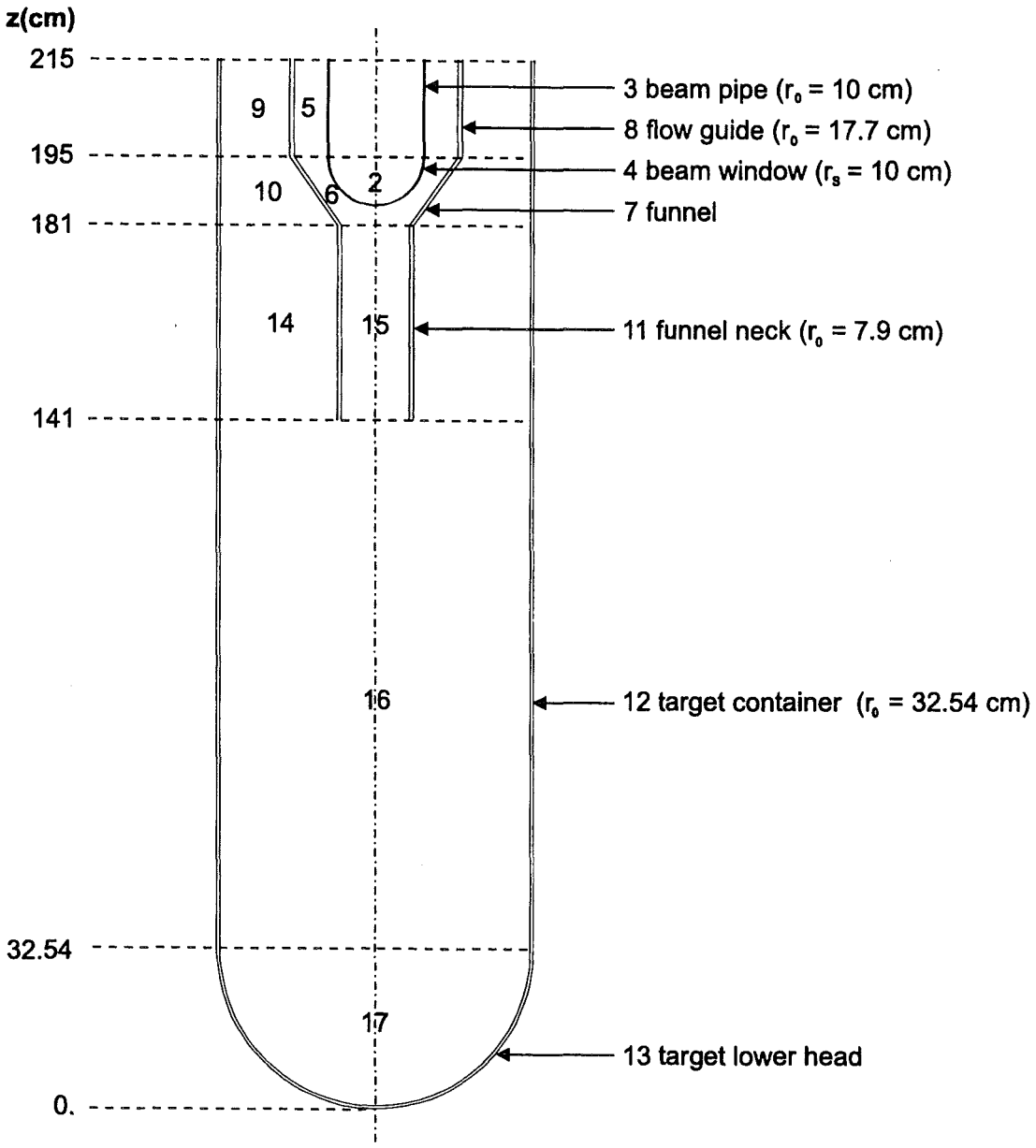

Figure 2.1: Geometry model of the target used for the calculations with the LCS codes

zones 1,2: highly diluted helium in beam pipe

zone 3: beam pipe steel HT9 ($r_i = 9.7cm, r_o = 10.0cm$)

zone 4: beam window, steel HT9

outer surface: radius of the hemisphere: ($r_s = 10cm$)

inner surface: ellipsoid ($r_a = 9.7cm, r_b = 9.85cm$)

r_a semiaxis perpendicular to target axis,

r_b semiaxis parallel to target axis

zones 5, 6, 9, 10,

14, 15, 16, 17: liquid lead zones

zone 5 : lead around vacuum tube

zone 6 : lead between window and funnel

zone 7 : funnel (steel HT9)

zone 8 : flow guide: steel HT9 ($r_i = 16.8cm$, $r_o = 17.7cm$)

zone 9 : lead outside flow guide

zone 10: lead outside funnel

zone 11: funnel neck: steel HT9 ($r_i = 7.0cm, r_o = 7.9cm$)

zone 12: target container: (HT9) ($r_i = 31.94cm, r_o = 32.54cm$)

zone 13: target lower head: (HT9) hemispherical shell

radius of the inner sphere: $r_{si} = 31.94cm$

radius of the outer sphere: $r_{so} = 32.54cm$

zone 14: lead outside funnel neck

zone 15: lead inside funnel neck

zone 16: lead below funnel neck

zone 17: lead inside target lower head

r_i and r_o are inner and outer radii of cylinders with the same axis as the target.

2.1 Calculation of the energy deposition in different zones of the target

As a first step we calculated the energy deposition in zones 1 - 17 of the target shown in Figure 2.1.
The calculations have been carried out for 100.000 protons.
The results are given in Tables 2.1 and 2.2.
For zones 1 - 17 the results for the energy deposition obtained from the LAHET calculation, and from the MCNP calculation and the corresponding statistical (relative) errors [9] are given. The total energy deposition is the sum from the LAHET- and the MCNP-results. The statistical error of the total energy deposition , $err_{(total)}$, has been calculated from: $err_{total} =$
$(err_{(LAHET)} \cdot value_{(LAHET)} + err_{(MCNP)} \cdot value_{(MCNP)})/(value_{(LAHET)} + value_{(MCNP)})$,
where $err_{(LAHET)}$ and $err_{(MCNP)}$ are the statistical errors resulting from the LAHET calculation and from the MCNP calculation, respectively, $value_{(LAHET)}$ and $value_{(MCNP)}$ are the mean values of the energy deposition calculated from LAHET or MCNP respectively, (see additional columns in Tables 2.1, 2.2).
The result in Table 2.1 is for the target shown in Fig. 2.1 with HT9 steel [15] in zones 3, 4, 7, 8, 11, 12 and 13 (reference case, case A). In Table 2.2 results are shown for the case that the steel HT9 in regions 3 (beam pipe), 4 (window), 7 (funnel guide), 8 (flow guide), 11 (funnel neck), 12 (target container), and 13 (target lower head) has been replaced by liquid lead (case B).
As is seen from Tables 2.1 and 2.2 there is only a small difference in the total energy deposition in the *window* (zone 4): in the window of HT9 steel the total energy deposition is $2.80273 \cdot 10^{-2}$[MeV/(proton$\cdot cm^3$)] in the liquid lead window the energy deposition is $2.74485 \cdot 10^{-2}$[MeV/(proton$\cdot cm^3$)].
The comparison for all zones (1 - 17) is given in Table 2.3:
Differences of more than 10% are found in regions 1 and 2 (diluted ^4He in the beam pipe and in the window). Moreover, differences of more than 10% are found in the zones that are made of steel in the reference target, namely in region 8 (flow guide above the window), region 12 (target container), region 13 (target lower head) and region 17 (lead within target lower head). In region 11 (funnel neck) the difference between the calculation with liquid lead in all regions and the calculation for the original target (case A) is about 11%, only slightly more than 10 %: deviations that are clearly higher than 10 % are found in regions where the average energy deposition is low: $6.7 \cdot 10^{-5}$MeV/(proton$\cdot cm^3$) and less.

This is to be compared to the maximum average energy deposition in region 15 (funnel neck) which is about $4.8 \cdot 10^{-2}$MeV/(proton$\cdot cm^3$).
The comparison for all zones shows that for a first guess it might be allowed - in order to simplify the input of the geometry - to replace the material in the steel regions by lead. This simplification is mainly of interest for investigations of the spatial dependence of the energy deposition, where subzones have to be specified (see section 1.5)
This replacement simplifies the geometry input for LAHET and for MCNP: The whole target may be subdivided into partial volumes of the same shape, cylinders and annular rings of the same inner and outer radii and of the same height without taking care of the individual shape of regions of different material composition, e.g. HT9 steel in regions 3, 4, 7, 8, 11, 12 and 13 of the target shown in Fig. 2.1

Table 2.1: Liquid lead target with HT9 (case A, reference case)
densities of energy deposition calculated from LAHET and from MCNP
$[MeV/(proton \cdot cm^3)]$ corresponding to $[kW/(mA \cdot cm^3)]$

zone	LAHET		MCNP		total	
1	2.26765E-07	.3170	0.00000E+00	.0000	2.26765E-07	.3170
2	2.74776E-06	.1870	0.00000E+00	.0000	2.74776E-06	.1870
3	3.01070E-04	.1180	2.05365E-04	.0283	5.06435E-04	.0816
4	2.70443E-02	.0110	9.82994E-04	.0345	2.80273E-02	.0118
5	2.28468E-05	.0560	8.67446E-05	.0132	1.09591E-04	.0221
6	2.22428E-02	.0020	1.62902E-03	.0150	2.38719E-02	.0029
7	7.29003E-04	.0470	3.58707E-04	.0086	1.08771E-03	.0343
8	1.40059E-05	.0880	5.26072E-05	.0102	6.66131E-05	.0266
9	3.71127E-06	.0450	1.86721E-05	.0089	2.23833E-05	.0149
10	3.08242E-05	.0220	8.74282E-05	.0057	1.18252E-04	.0099
11	1.02362E-02	.0100	7.41159E-04	.0064	1.09774E-02	.0098
12	1.39230E-05	.0760	8.48354E-06	.0066	2.24065E-05	.0497
13	5.12753E-08	1.0000	1.40756E-08	.3512	6.53509E-08	.8603
14	1.89794E-04	.0080	1.21872E-04	.0037	3.11666E-04	.0063
15	4.62740E-02	.0020	1.83078E-03	.0085	4.81048E-02	.0022
16	7.47776E-06	.0210	5.98504E-06	.0107	1.34628E-05	.0164
17	3.10217E-08	.3910	4.23286E-08	.2171	7.33503E-08	.2906
all zones	6.39509E-04	.0010	6.26334E-05	.0043	7.02143E-04	.0013

Table 2.2: Liquid lead target (case B)

densities of energy deposition calculated from LAHET and from MCNP $[MeV/(proton \cdot cm^3)]$ corresponding to $[kW/(mA \cdot cm^3)]$

zone	LAHET		MCNP		total	
1	4.28355E-07	.2510	0.00000E+00	.0000	4.28355E-07	.2510
2	3.44025E-06	.1720	0.00000E+00	.0000	3.44025E-06	.1720
3	2.71738E-04	.0780	2.65857E-04	.0512	5.37595E-04	.0647
4	2.59779E-02	.0090	1.47058E-03	.0476	2.74485E-02	.0111
5	2.46007E-05	.0550	7.85219E-05	.0140	1.03123E-04	.0238
6	2.21497E-02	.0020	1.52944E-03	.0145	2.36792E-02	.0028
7	4.98676E-04	.0280	3.48242E-04	.0110	8.46918E-04	.0210
8	7.42292E-06	.1300	4.29283E-05	.0135	5.03512E-05	.0307
9	3.84388E-06	.0440	1.91388E-05	.0087	2.29827E-05	.0146
10	3.08628E-05	.0210	8.68996E-05	.0057	1.17762E-04	.0097
11	8.98418E-03	.0100	7.61319E-04	.0087	9.74550E-03	.0099
12	6.78885E-06	.0520	6.43859E-06	.0107	1.32274E-05	.0319
13	0.00000E+00	.0000	2.15244E-08	.4194	2.15244E-08	.4194
14	1.90099E-04	.0080	1.21257E-04	.0035	3.11357E-04	.0062
15	4.63086E-02	.0020	1.75381E-03	.0083	4.80624E-02	.0022
16	7.40935E-06	.0210	6.12733E-06	.0106	1.35367E-05	.0163
17	5.86727E-08	.4300	4.45851E-08	.2325	1.03258E-07	.3447
all zones	6.35326E-04	.0010	6.11879E-05	.0041	6.96514E-04	.0013

The total energy loss in the target is:
case A: (HT9 in regions 3, 4, 7,8, 11, 12, 13)
total energy loss: 476.83MeV/proton
from LAHET calculation: 434.30 (.001)
from MCNP calculation: 42.54 (.0043)
case B: (liquid lead in all regions)
total energy loss: 474.01MeV/proton
from LAHET: 431.46 (.001)
from MCNP: 41.55 (.0041)

Table 2.3 comparison of energy deposition $[MeV/(proton \cdot cm^3]$ **for case A and case B** (mean values and statistical errors)

zone	HT9 in zones 3, 4, 7, 8, 11, 12, 13 (case A)		all zones liquid lead (case B)		(B - A)/A [%]
1	2.26765E-07	.3170	4.28355E-07	.2510	88.9
2	2.74776E-06	.1870	3.44025E-06	.1720	25.2
3	5.06435E-04	.1213	5.37595E-04	.0933	6.2
4	2.80273E-02	.0362	2.74485E-02	.0484	-2.1
5	1.09591E-04	.0575	1.03123E-04	.0568	-5.9
6	2.38719E-02	.0151	2.36792E-02	.0146	-0.8
7	1.08771E-03	.0478	8.46918E-04	.0301	-2.2
8	6.66131E-05	.0886	5.03512E-05	.1307	-24.4
9	2.23833E-05	.0459	2.29827E-05	.0449	2.7
10	1.18252E-04	.0227	1.17762E-04	.0218	-0.4
11	1.09774E-02	.0119	9.74550E-03	.0133	-11.2
12	2.24065E-05	.0763	1.32274E-05	.0531	-41.0
13	6.53509E-08	1.0599	2.15244E-08	.4194	-67.1
14	3.11666E-04	.0088	3.11357E-04	.0087	-0.1
15	4.81048E-02	.0087	4.80624E-02	.0085	-0.09
16	1.34628E-05	.0236	1.35367E-05	.0235	0.6
17	7.33503E-08	.4472	1.03258E-07	.4888	40.8
all zones	7.02143E-04	.0044	6.96514E-04	.0042	-0.80

2.2 Proton range in different materials as a function of proton energy

The energy deposition in the beam window and in the target is mainly due to the energy loss of protons and other charged particles. The charged particles lose their energy mainly by ionization of the atoms of the beam window and of the target.
Table 2.4 shows the contributions of different physical processes to the energy deposition in the beam window (cell4), the lead region between window and funnel (cell6), the lead region within the funnel neck (cell15) and for the entire target.

Table 2.4: LAHET/HTAPE results for the energy deposition ([MeV/proton]) in zone 4, zone 6, zone 15 and for the whole target shown in Fig. 2.1 contribution of different reaction types

lahet/htape - calculation of energy deposition
600MeV circular beam r=7.5cm parabolic profile
100.000 proton histories

energy deposition in cell 4

beam window (steel HT9)

	time total	
coulomb loss h-1	3.61629D+00	.008
coulomb loss pi+-	4.51458D-02	.069
coulomb loss mu+-	0.00000D+00	.000
coulomb loss K+-	0.00000D+00	.000
coulomb loss pbar	0.00000D+00	.000
coulomb loss h-2	2.90638D-02	.094
coulomb loss h-3	4.87618D-03	.153
coulomb loss he-3	7.19117D-03	.270
coulomb loss he-4	3.41505D-02	.072
nuclear recoil	4.09966D-02	.044
excitation	7.39249D-02	.031
pi0 decay gammas	2.37031D-01	.100
kin. eng. of e+,e-	0.00000D+00	.000
positron mass	0.00000D+00	.000
kin. eng. of muons	2.37170D-03	.134
mu+ mass	5.56709D-02	.137
mu- mass	2.11320D-04	.707
total deposition	4.14692D+00	.011

energy deposition in cell 6

(lead between window and funnel)

	time total	
coulomb loss h-1	8.82273D+01	.002
coulomb loss pi+-	1.09416D+00	.023
coulomb loss mu+-	0.00000D+00	.000
coulomb loss K+-	0.00000D+00	.000
coulomb loss pbar	0.00000D+00	.000
coulomb loss h-2	4.65401D-01	.022
coulomb loss h-3	2.77010D-01	.023
coulomb loss he-3	1.44864D-02	.125
coulomb loss he-4	1.74478D+00	.014
nuclear recoil	1.64860D+00	.025
excitation	1.43041D+00	.007
pi0 decay gammas	3.46441D+00	.025
kin. eng. of e+,e-	0.00000D+00	.000
positron mass	0.00000D+00	.000
kin. eng. of muons	5.65718D-02	.028
mu+ mass	1.35446D+00	.028
mu- mass	2.43018D-03	.217
total deposition	9.97800D+01	.002

energy deposition in cell 15

lead inside funnel neck

	time total	
coulomb loss h-1	2.70289D+02	.002
coulomb loss pi+-	1.02677D+00	.026
coulomb loss mu+-	0.00000D+00	.000
coulomb loss K+-	0.00000D+00	.000
coulomb loss pbar	0.00000D+00	.000
coulomb loss h-2	5.50339D-01	.021
coulomb loss h-3	2.76318D-01	.022
coulomb loss he-3	1.33487D-02	.141

coulomb loss he-4	2.09337D+00	.012
nuclear recoil	3.09433D+00	.018
excitation	3.63640D+00	.004
pi0 decay gammas	2.72244D+00	.026
kin. eng. of e+,e-	0.00000D+00	.000
positron mass	0.00000D+00	.000
kin. eng. of muons	4.95375D-02	.030
mu+ mass	1.17800D+00	.030
mu- mass	2.95848D-03	.196
total deposition	2.84933D+02	.002

total energy deposition

	time total	
coulomb loss h-1	4.01686D+02	.001
coulomb loss pi+-	2.42908D+00	.018
coulomb loss mu+-	0.00000D+00	.000
coulomb loss K+-	0.00000D+00	.000
coulomb loss pbar	0.00000D+00	.000
coulomb loss h-2	1.18733D+00	.014
coulomb loss h-3	5.86309D-01	.015
coulomb loss he-3	5.36455D-02	.084
coulomb loss he-4	4.10920D+00	.008
nuclear recoil	5.38150D+00	.013
excitation	9.21901D+00	.003
pi0 decay gammas	6.63310D+00	.017
kin. eng. of e+,e-	0.00000D+00	.000
positron mass	0.00000D+00	.000
kin. eng. of muons	1.22221D-01	.019
mu+ mass	2.88391D+00	.019
mu- mass	8.03078D-03	.125
total deposition	4.34299D+02	.001

We have used the option of the LAHET code to calculate the proton ranges in different materials as a function of the proton energy. The results are shown in Figure 2.2 for

proton energies up to 1GeV and in Figure 2.3 for proton energies up to 9GeV.
It is seen from Figure 2.2 that for proton energies between 0.33MeV and 1GeV the proton range is nearly equal in liquid lead and in steel HT9. In rhenium and tungsten the proton range is much smaller. The solid line in Figure 2.2 shows the range of α-particles in steel HT9.
At higher energies the proton range in liquid lead becomes slightly smaller than the one for steel HT9 as is shown in Figure 2.3
A proton of given energy deposits less of its energy in a thin layer of material with **large** proton range than it deposits in a thin layer of material with **small** proton range. That means that less energy will be deposited in a beam window of steel than in a tungsten window.

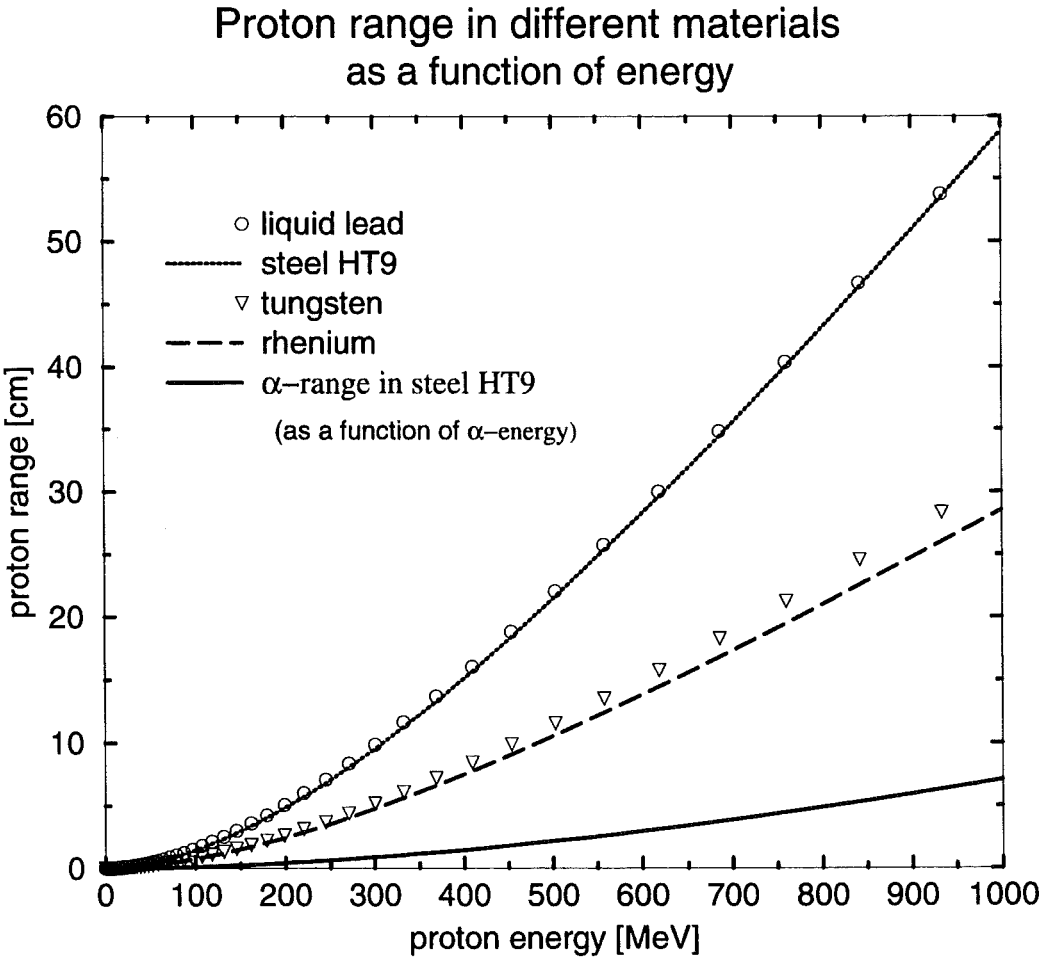

Figure 2.2: Proton range in different materials for proton energies up to 1GeV

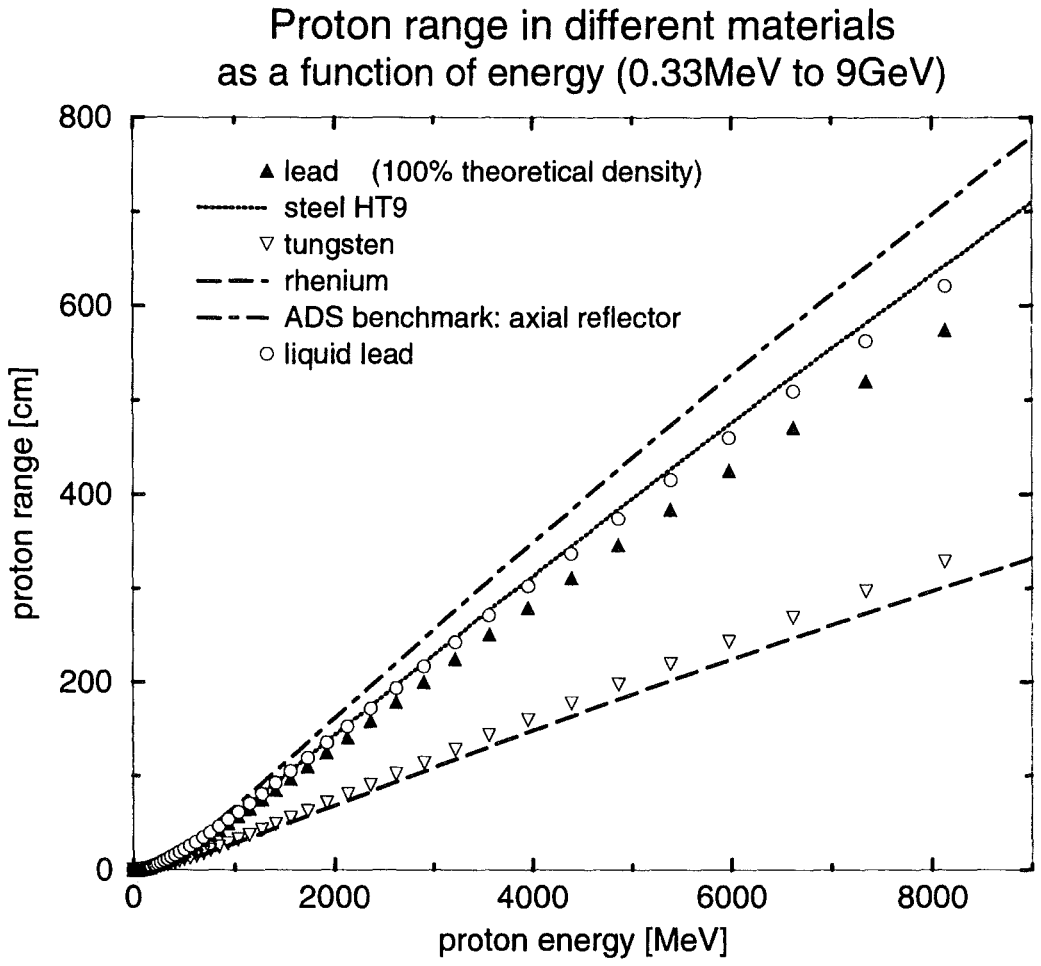

Figure 2.3: Proton range in different materials for proton energies up to 9GeV

2.3 Particle production in the target by spallation processes

The modules LAHET and HTAPE of the LCS system [6] allow the calculation of the energy distributions of the produced particles in the different geometric zones defined in the input. Here we calculate only the *total* number (integral over energy) of different particles (neutrons, protons, neutral and charged π-mesons , deuterons, tritons, ^3He, and α-particles) in the target (sum over zones 1 - 17) and in the target window (zone 4 in Fig. 2.1). 14.87 neutrons/proton (n/p) are produced in the reference target, (case A), 12.86 of them with energy $E_n \leq$ 20MeV. The number of neutrons that are produced in the intranuclear cascade (inc) is 4.333 (n/p) in case A and 4.412 (n/p) in case B (in case B all materials in the target are liquid lead, except in regions 1 and 2 which are filled with diluted ^4He).

The number of neutrons emitted in the evaporation process is 10.42 for the target with HT9 parts (case A) and 10.74 for the target with liquid lead only (case B). The number of protons emitted per incident proton is about 2.121 in case A and 1.956 in case B (see Tables 2.6 and 2.7).

The π-mesons are produced in the intranuclear cascade (inc). The kinetic energy necessary for π-meson production is the sum of the rest energy of the pion (about 140MeV) plus the recoil energy of the struck particle. The energy necessary for the production of a π-meson in the reaction $p + p \rightarrow p + p + \pi$ is 290MeV [16]. muons arise from the decay of pions, which have very short halflives. The properties of π-mesons and muons are given in Table 2.5 taken from [8]. (As is well known, the halflife, T, is correlated to the mean lifetime, given in Table 2.5, τ, by $T = \tau \cdot ln2$. Deuterons, tritons, ^3He-nuclei and α-particles are emitted in evaporation processes. Neutrons and protons are emitted in both, intranuclear cascade (inc) and evaporation (neutrons also in high energy fission).

Neutrons that are produced by reactions with incident neutrons of primary energy $\leq$20MeV, e.g. in (n,2n)-, (n,3n)-, ... reactions are not included in the following tables. Tables 2.6 and 2.7 only give the results of LAHET/HTAPE, not those of MCNP.

Table 2.5: Decay Properties of pions and muons

particle	mean lifetime τ_0 [sec]	$c \cdot \tau_0$ [m]	decay model
π^+	$2.6 \cdot 10^{-8}$	7.8	$\pi^+ \rightarrow \mu^+ \quad \nu_\mu$
π^-	$2.6 \cdot 10^{-8}$	7.8	$\pi^- \rightarrow \mu^- \quad \nu_\mu$
μ^+	$2.2 \cdot 10^{-6}$	~ 660.0	$\mu^+ \rightarrow e^+ \quad \nu_e \quad \nu_\mu$
			$\mu^- \rightarrow e^- \quad \nu_\mu \quad \nu_e$
π^0	$0.87 \cdot 10^{-16}$	$\sim 10^{-8}$	$\pi^0 \rightarrow \gamma\gamma \quad (98.799\ \%)$
			$\pi^0 \rightarrow \gamma e^+ e^- \quad (1.198\ \%)$
			(additional decay modes of π^0 are:
			$\pi^0 \rightarrow \gamma\gamma\gamma$ and $\pi^0 \rightarrow e^+e^-e^+e^-$ [17])

Table 2.6: Particles produced per proton in the target / in the target window
Case A: (target with HT9 steel in regions 3, 4, 7, 8, 11, 12, 13, see Fig. 2.1). Calculations have been carried out for a 600MeV proton beam with radius 7.5cm and parabolic profile

	TARGET (zones 1 - 17 in Fig. 2.1)		WINDOW (zone 4)	
particle	mean value	statistical error	mean value	statistical error
neutron	14.87	(.003)	5.901e-2	(.031)
inc	4.333	(.003)	2.576e-2	(.034)
evaporation	10.42	(.003)	3.277e-2	(.034)
el. scatter	0.1104	(.011)	4.900e-4	(.143)
proton	2.121	(.003)	5.229e-2	(.039)
inc	1.694	(.003)	2.707e-2	(.033)
evaporation	0.4268	(.011)	2.522e-2	(.056)
el. scatter	0.0		0.0	
pi+	3.021e-2	(.018)	1.310e-3	(.087)
pi0	3.452e-2	(.017)	1.100e-3	(.095)
pi-	1.927e-2	(.023)	5.180e-4	(.139)
deuteron	1.002e-1	(.012)	2.528e-3	(.077)
triton	5.827e-2	(.014)	5.100e-4	(.148)
he-3	2.910e-3	(.077)	3.600e-4	(.200)
alpha	2.154e-1	(.008)	3.160e-3	(.068)

Table 2.7: Particles produced per proton in the target / target window
Case B: liquid lead in all regions (except regions 1 and 2). Calculations have been carried out for a 600MeV proton beam with radius 7.5cm and parabolic profile

	TARGET (zones 1 - 17 in Fig. 2.1)		WINDOW (zone 4)	
particle	mean value	statistical error	mean value	statistical error
neutron	15.26	(.003)	1.418e-1	(.033)
inc	4.412	(.003)	4.050e-2	(.035)
evaporation	10.74	(.003)	1.011e-1	(.034)
el. scatter	0.1060	(.001)	2.500e-4	(.200)
proton	1.956	(.003)	2.611e-2	(.035)
inc	1.650	(.003)	2.000e-2	(.036)
evaporation	0.3058	(.007)	6.110e-3	(060)
el. scatter	0.0		0.0	
pi+	2.965e-2	(.019)	8.600e-4	(.109)
pi0	3.143e-2	(.017)	9.200e-4	(.105)
pi-	1.933e-2	(.023)	5.180e-4	(.139)
deuteron	9.625e-2	(.012)	2.030e-3	(.086)
triton	5.944e-2	(.014)	1.490e-3	(.096)
he-3	1.400e-3	(.085)	4.000e-5	(.500)
alpha	2.108e-1	(.008)	4.599e-3	(.065)

The values for the neutron production given in Tables 2.6 and 2.7 before are the results of LAHET/HTAPE. That means that neutron production by nuclear reactions with neutrons of primary energy $E_n \leq 20$MeV e.g. (n,2n), (n,3n) is not taken into account. The neutrons produced in these reactions are calculated by MCNP. The following results are taken from the table named 'neutron weight balance due to physical events' of the MCNP output.

Table 2.8: Neutron production per primary proton in the target / target window due to reactions with neutrons with $E_n \leq 20\text{MeV}$ (specification of the proton beam like in Tables 2.6 and 2.7)

case A

neutron gain per proton	total	(n,xn)	capture
target	$6.0694 \cdot 10^{-1}$	$8.4376 \cdot 10^{-1}$	$-2.3683 \cdot 10^{-1}$
window	$-1.0755 \cdot 10^{-3}$	$8.6239 \cdot 10^{-4}$	$-1.9379 \cdot 10^{-3}$

case B

neutron gain per proton	total	(n,xn)	capture
target	$7.1641 \cdot 10^{-1}$	$9.0996 \cdot 10^{-1}$	$-1.9353 \cdot 10^{-1}$
window	$2.3684 \cdot 10^{-3}$	$2.6084 \cdot 10^{-3}$	$-2.3999 \cdot 10^{-4}$

Taken together from Tables 2.6, 2.7 and 2.8, the total number of neutrons produced per proton is:

total number of neutrons produced per primary proton

case A	target:	15.48	window:	$5.793 \cdot 10^{-2}$
case B	target:	15.98	window:	$1.442 \cdot 10^{-1}$

The particle numbers given in Tables 2.6, 2.7, and 2.8 are the particles produced per beam proton. A proton current of 1mA corresponds to $6.242 \cdot 10^{15}$ protons/sec. That means that for a 6mA proton current the particle numbers given in Tables 2.6, 2.7 and 2.8 have to be multiplied by $3.745 \cdot 10^{16}$

According to our calculations a proton current of 6mA produces in total:

in the HT9 window:	$1.96 \cdot 10^{15}$ protons/sec	$2.17 \cdot 10^{15}$ neutrons/sec
in the lead window:	$9.78 \cdot 10^{14}$ protons/sec	$5.40 \cdot 10^{15}$ neutrons/sec

2.4 Spatial distribution of the energy deposition in the target window

In the previous section the energy deposition has been calculated for zones. The average total energy density deposited in the HT9 window (zone 4) was found to be $2.80273 \cdot 10^{-2}$MeV/(proton$\cdot cm^3$). (see Table 2.1)
In this section we study the energy deposition in different parts of the window. These results are an important item for the thermodynamical behavior and the thermohydraulics concerned with cooling of the window and a suitable target design.
In the geometry shown in Fig. 2.1 we introduce additional concentric cylinders with radii 0.5cm, 1.0cm, 1.5cm, ... 10.0cm.
Now we subdivide the window in such a way that we treat in the Monte Carlo calculations (with LCS) subzones (cells) of the window that are inside cylinder 1 ($r_{cyl} = 0.5cm$), inside cylinder 2 ($r_{cyl} = 1.0cm$) and outside cylinder 1, inside cylinder 3 ($r_{cyl} = 1.5cm$) and outside cylinder 2, ... inside cylinder 20 ($r_{cyl} = 10cm$) and outside cylinder 19 ($r_{cyl} = 9.5cm$).
The calculations with LAHET and MCNP have been carried out for 200.000 proton histories. The results for the energy deposition [MeV/(proton $\cdot cm^3$)] (corresponding to $[kW/(mA \cdot cm^3)]$) in different parts of the window are given in Table 2.9 for the HT9 window (case A) and in Table 2.10 for the "pseudo" liquid lead window (case B).

In Tables 2.9 and 2.10 the energy density deposited in the window is shown for different regions of the radius of the cylindrical target. The highest energy density in the window is found in the vicinity of the cylinder axis ($r_{cyl} \leq 0.5cm$). In the next two regions of the window ($0.5cm \leq r_{cyl} \leq 1.0cm$) and ($1.0cm \leq r_{cyl} \leq 1.5cm$) the energy density is decreasing as expected. However the energy density is increasing again for ($1.5cm \leq r_{cyl} \leq 2.0cm$). For $r_{cyl} \geq 2.0cm$ the energy density in the window is decreasing monotonically. This behaviour of the dependence of the energy density as a function of the target radius (more precisely: of the distance from the target axis) is found for the window of steel HT9 (caseA) as well as for the liquid lead window (case B).
From this non-monotonic behaviour we conjecture that the subzones (cells) defined are too small to give reliable results in Monte Carlo calculations with the given number of histories.

Table 2.9: Average energy deposition in subzones of the HT9 window

$[MeV/(proton \cdot cm^3)] = [kW/(mA \cdot cm^3)]$

the subzones are identified by coaxial cylindrical shells within the target

r_{cyl} in column 1 gives the range of the ring of each cylindrical shell

radius [cm]	LAHET	MCNP	total
$r_{cyl} \leq 0.5$	2.44210E-01 (.0860)	2.58530E-03 (.2943)	2.46795E-01 (.0882)
$0.5 \leq r_{cyl} \leq 1.0$	2.23726E-01 (.0460)	1.38774E-03 (.1454)	2.25113E-01 (.0466)
$1.0 \leq r_{cyl} \leq 1.5$	2.06859E-01 (.0440)	1.23794E-03 (.0900)	2.08097E-01 (.0443)
$1.5 \leq r_{cyl} \leq 2.0$	2.11174E-01 (.0290)	1.42219E-03 (.1142)	2.12596E-01 (.0296)
$2.0 \leq r_{cyl} \leq 2.5$	2.00669E-01 (.0310)	1.62806E-03 (.0989)	2.02297E-01 (.0315)
$2.5 \leq r_{cyl} \leq 3.0$	1.94751E-01 (.0260)	1.69880E-03 (.0906)	1.96450E-01 (.0266)
$3.0 \leq r_{cyl} \leq 3.5$	1.72236E-01 (.0210)	1.54388E-03 (.0978)	1.73780E-01 (.0217)
$3.5 \leq r_{cyl} \leq 4.0$	1.63633E-01 (.0260)	1.42908E-03 (.0847)	1.65062E-01 (.0265)
$4.0 \leq r_{cyl} \leq 4.5$	1.47196E-01 (.0210)	1.22419E-03 (.0799)	1.48421E-01 (.0215)
$4.5 \leq r_{cyl} \leq 5.0$	1.38929E-01 (.0250)	1.28762E-03 (.0869)	1.40217E-01 (.0256)
$5.0 \leq r_{cyl} \leq 5.5$	1.14000E-01 (.0200)	1.10407E-03 (.0866)	1.15104E-01 (.0206)
$5.5 \leq r_{cyl} \leq 6.0$	9.21453E-02 (.0210)	9.88956E-04 (.0953)	9.31342E-02 (.0218)
$6.0 \leq r_{cyl} \leq 6.5$	6.69870E-02 (.0230)	6.82434E-04 (.0748)	6.76695E-02 (.0235)
$6.5 \leq r_{cyl} \leq 7.0$	4.23229E-02 (.0280)	5.30689E-04 (.0731)	4.28536E-02 (.0286)
$7.0 \leq r_{cyl} \leq 7.5$	1.50255E-02 (.0420)	3.49009E-04 (.0760)	1.53745E-02 (.0428)
$7.5 \leq r_{cyl} \leq 8.0$	1.42313E-03 (.1210)	2.37680E-04 (.0641)	1.66081E-03 (.1129)
$8.0 \leq r_{cyl} \leq 8.5$	1.28653E-03 (.1310)	1.97906E-04 (.0546)	1.48443E-03 (.1208)
$8.5 \leq r_{cyl} \leq 9.0$	9.82457E-04 (.1200)	1.87294E-04 (.0522)	1.16975E-03 (.1091)
$9.0 \leq r_{cyl} \leq 9.5$	9.56553E-04 (.2240)	1.71229E-04 (.0469)	1.12778E-03 (.1971)
$9.5 \leq r_{cyl} \leq 10.0$	6.75831E-04 (.0890)	1.29703E-04 (.0313)	8.05534E-04 (.0797)

Table 2.10: Average energy deposition in subzones of the liquid lead window

$[MeV/(proton \cdot cm^3)] = [kW/(mA \cdot cm^3)]$

the subzones are identified by coaxial cylindrical shells within the target

r_{cyl} in column 1 gives the range of the annulus of each cylindrical shell

radius [cm]	LAHET	MCNP	total
$r_{cyl} \leq 0.5$	2.54027E-01 (.0990)	1.39277E-02 (.3740)	2.67954E-01 (.1133)
$0.5 \leq r_{cyl} \leq 1.0$	2.14798E-01 (.0490)	9.07545E-03 (.2173)	2.23873E-01 (.0558)
$1.0 \leq r_{cyl} \leq 1.5$	1.95379E-01 (.0280)	7.18815E-03 (.1726)	2.02567E-01 (.0331)
$1.5 \leq r_{cyl} \leq 2.0$	2.09375E-01 (.0290)	9.01696E-03 (.1619)	2.18392E-01 (.0345)
$2.0 \leq r_{cyl} \leq 2.5$	2.01803E-01 (.0300)	9.50325E-03 (.1453)	2.11306E-01 (.0352)
$2.5 \leq r_{cyl} \leq 3.0$	1.84293E-01 (.0220)	7.26661E-03 (.1289)	1.91559E-01 (.0261)
$3.0 \leq r_{cyl} \leq 3.5$	1.70360E-01 (.0220)	6.79474E-03 (.1025)	1.77154E-01 (.0251)
$3.5 \leq r_{cyl} \leq 4.0$	1.56718E-01 (.0200)	6.50520E-03 (.0973)	1.63223E-01 (.0231)
$4.0 \leq r_{cyl} \leq 4.5$	1.46113E-01 (.0220)	6.55657E-03 (.0889)	1.52669E-01 (.0249)
$4.5 \leq r_{cyl} \leq 5.0$	1.29000E-01 (.0200)	4.72618E-03 (.1126)	1.33726E-01 (.0233)
$5.0 \leq r_{cyl} \leq 5.5$	1.09771E-01 (.0190)	3.89516E-03 (.0914)	1.13667E-01 (.0215)
$5.5 \leq r_{cyl} \leq 6.0$	8.76503E-02 (.0210)	3.24031E-03 (.0967)	9.08906E-02 (.0237)
$6.0 \leq r_{cyl} \leq 6.5$	6.64428E-02 (.0240)	3.31590E-03 (.1049)	6.97587E-02 (.0278)
$6.5 \leq r_{cyl} \leq 7.0$	4.08518E-02 (.0260)	2.15699E-03 (.1008)	4.30088E-02 (.0298)
$7.0 \leq r_{cyl} \leq 7.5$	1.45809E-02 (.0410)	1.38323E-03 (.0966)	1.59641E-02 (.0458)
$7.5 \leq r_{cyl} \leq 8.0$	1.33508E-03 (.1380)	9.02772E-04 (.0878)	2.23785E-03 (.1177)
$8.0 \leq r_{cyl} \leq 8.5$	1.01196E-03 (.1420)	7.62594E-04 (.0931)	1.77455E-03 (.1210)
$8.5 \leq r_{cyl} \leq 9.0$	9.97268E-04 (.1270)	6.64350E-04 (.0804)	1.66162E-03 (.1084)
$9.0 \leq r_{cyl} \leq 9.5$	5.89843E-04 (.1050)	5.73954E-04 (.0640)	1.16380E-03 (.0848)
$9.5 \leq r_{cyl} \leq 10.0$	5.82184E-04 (.0970)	4.74981E-04 (.0531)	1.05717E-03 (.0773)

In order to obtain a monotonically decreasing energy density as a function of the distance from the cylinder axis we redefine the subregions in the window: instead of ($1.0cm \leq r_{cyl} \leq 1.5cm$) (subregion a) and $1.5cm \leq r_{cyl} \leq 2.0cm$ (subregion b) we define the common region ($1.0cm \leq r_{cyl} \leq 2.0cm$) within the window.
The volume of subregion a is: $6.04159 \cdot 10^{-1} cm^2$
the volume of subregion b is: $8.65273 \cdot 10^{-1} cm^2$.
The average energy density in the combined subregions a and b is: $2.10746 \cdot 10^{-1}$MeV/(proton$\cdot cm^3$).
Accordingly subregions c and d are defined:
subregion c: $2.0cm \leq r_{cyl} \leq 2.5cm$ volume of subregion c: $1.14796cm^3$
subregion d: $2.5cm \leq r_{cyl} \leq 3.0cm$ volume of subregion d: $1.45792cm^3$
the average energy density in the combined subregions c and d is: $1.99026 \cdot 10^{-1}$MeV/(proton$\cdot cm^3$).

For the liquid lead window we obtained:
The average energy density in the combined subregions a and b: ($1.0cm \leq r_{cyl} \leq 2.0cm$) is: $2.11888 \cdot 10^{-1}$MeV/(proton$\cdot cm^3$).
The average energy density in the combined subregions c and d ($2.0cm \leq r_{cyl} \leq 3.0cm$) is: $2.00258 \cdot 10^{-1}$MeV/(proton$\cdot cm^3$).

2.5 Spatial distribution of the energy deposition in the target

The next step of our study was the investigation of the **spatial distribution** of the energy deposition in the *target*. For this purpose we introduced into our basic geometry which is shown in Fig. 2.1 coaxial cylinders with radii $r_{cyl} = 1cm$, $r_{cyl} = 2cm$, ...,$r_{cyl} = 7.9cm$, $r_{cyl} = 9cm$, $r_{cyl} = 10cm$.
The radius of 7.9cm was chosen, because $7.0 \leq r_{cyl} \leq 7.9cm$ covers the radial range of the funnel neck (zone 11 in Fig. 2.1). Moreover we introduced the following additional planes:

z=	194.5	194.0	193.5	193.0	...175.0
z=	173.0	171.0	169.0	167.0	...143.0
z=	136.0	131.0	126.0	121.0	...101.0
z=	91.0	81.0	71.0		...11.0

With these cylinders and planes we defined subzones (coaxial cylindrical rings) for which we calculated the energy depositions.
In the MCNP calculations the number of tallies per calculation is restricted to 100 [9]. The number of subzones (cells) for which we want to calculate the energy deposition is 720: number of radial ranges (=10) multiplied by the number of axial ranges (=72), this exceeds the number of possible tallies in MCNP. Therefore we carried out our LCS calculations (LAHET/MCNP) separately for each radial range, that means together 10 LCS calculations. Examples for these subregions in the geometric models are shown in Fig. 2.5 ($0cm \leq r_{cyl} \leq 1cm$), Fig. 2.6 ($4cm \leq r_{cyl} \leq 5cm$) and Fig. 2.7: ($9cm \leq r_{cyl} \leq 10cm$). Fig. 2.4 shows that part of Fig. 2.1 which is in the vicinity of the beam window. In Fig. 2.4 also the proton beam is indicated. For a circular beam with parabolic profile the probability density along the beam radius is given by [6]:
$p(r) = \frac{2}{\pi \cdot a^2}(1 - \frac{r^2}{a^2})$
the probality density is vanishing for $r > a$.
For a=7.5cm p(r=0)= 0.01132 and p(r=a)=0.
For a total proton current of 6mA this means:
the proton current is $6.791 \cdot 10^{-2}$ mA in the beam center
the proton current is $5.093 \cdot 10^{-2}$ mA at r=a/2=3.75cm
the proton current is $2.971 \cdot 10^{-2}$ mA at r=0.75a=5.625cm
the proton current is $1.290 \cdot 10^{-2}$ mA at r=0.9a=6.75cm
the proton current is $1.351 \cdot 10^{-2}$ mA at r=0.99a=7.425cm
the proton current is equal to zero for $r \geq 7.5cm$
The results for all cells are shown in Table 2.11.
MCNP does not evaluate tallies in an internal vacuum. If those are specified, the job is terminated by an error message. Therefore the vacuum within the beam pipe and within the beam window (zones 1 and 2 in Fig. 2.1) was replaced by ^4He of particle number density $2.67 \cdot 10^{-20}[(10^{24} \cdot cm^{-3})]$ in the calculations with LAHET and MCNP. This corresponds to the particle number density calculated from the density of He which is 0.1785 g/l at $0°C$ and 1atm multiplied by 10^{-15} and may be regarded as diluted He.
From Table 2.11 and Fig. 2.1 it is seen that the energy deposition in the vacuum (diluted He) is very small, in the order of 10^{-22} or $10^{-21} kW/(mA \cdot cm^3)$. Some energy densities within the 'vacuum' zones are much larger. This is mainly due to results of LAHET, since the contribution of MCNP is very small in all zones with diluted He. According to the LAHET/HTAPE output these relatively large values for the energy deposition are due to the kinetic energy of muons and to muon mass (the μ rest energy is 105.659MeV [16]).

However, the statistical error for these results is given to be 100 % after 200.000 proton histories.

In Table 2.11a the energy densities calculated from LAHET and from MCNP and the sum are given for the the cells within the cylindrical shell with $4cm \leq r_{cyl} \leq 5cm$, these cells are shown in Fig. 2.6.

In Table 2.11a the mean values of the energy deposition are given and the statistical errors. The statistical error of the total energy deposition has been calculated in the same way as in Tables 2.1 and 2.2.

Fig. 2.8 shows a graphical representation of the results obtained by the visualization program TECPLOT®.

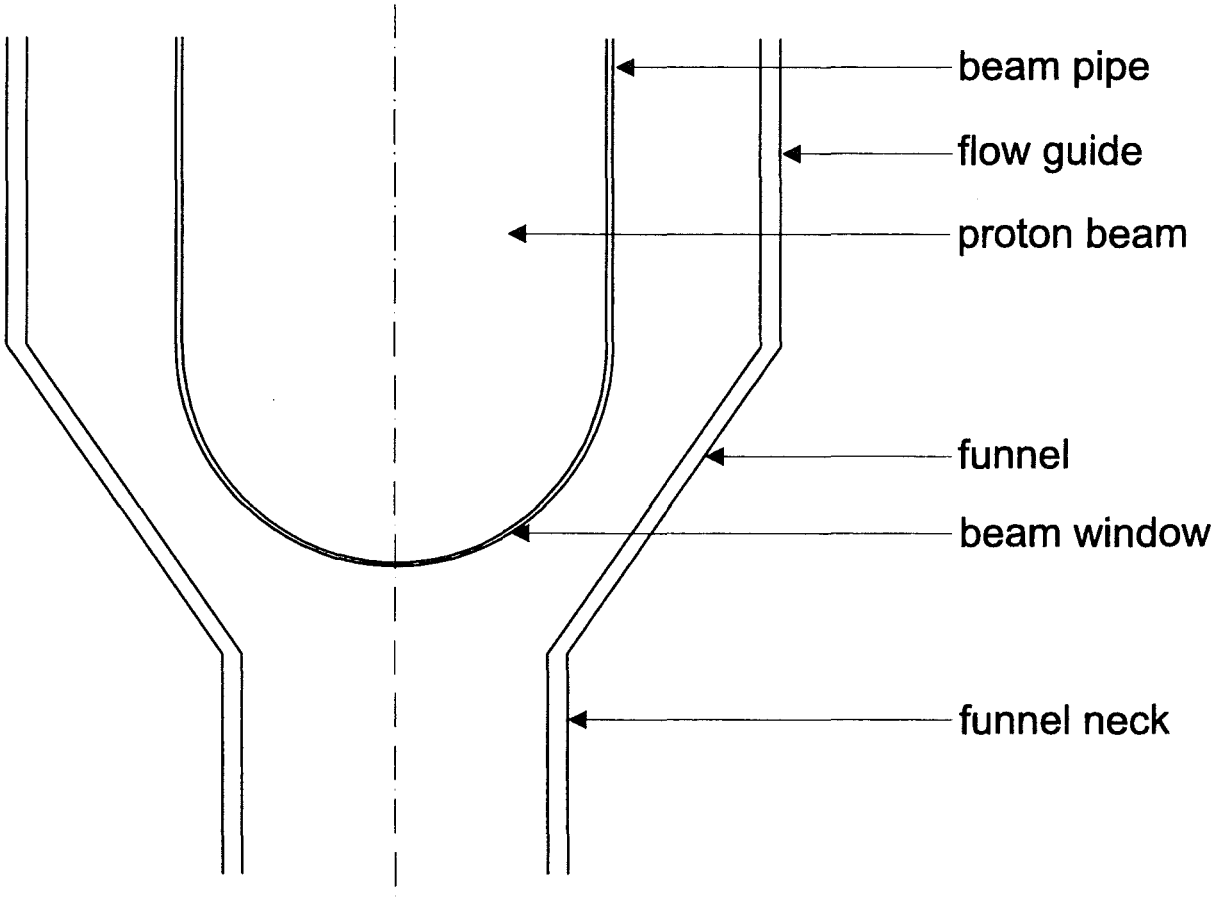

Figure 2.4: Geometric model of the target in the vicinity of the window

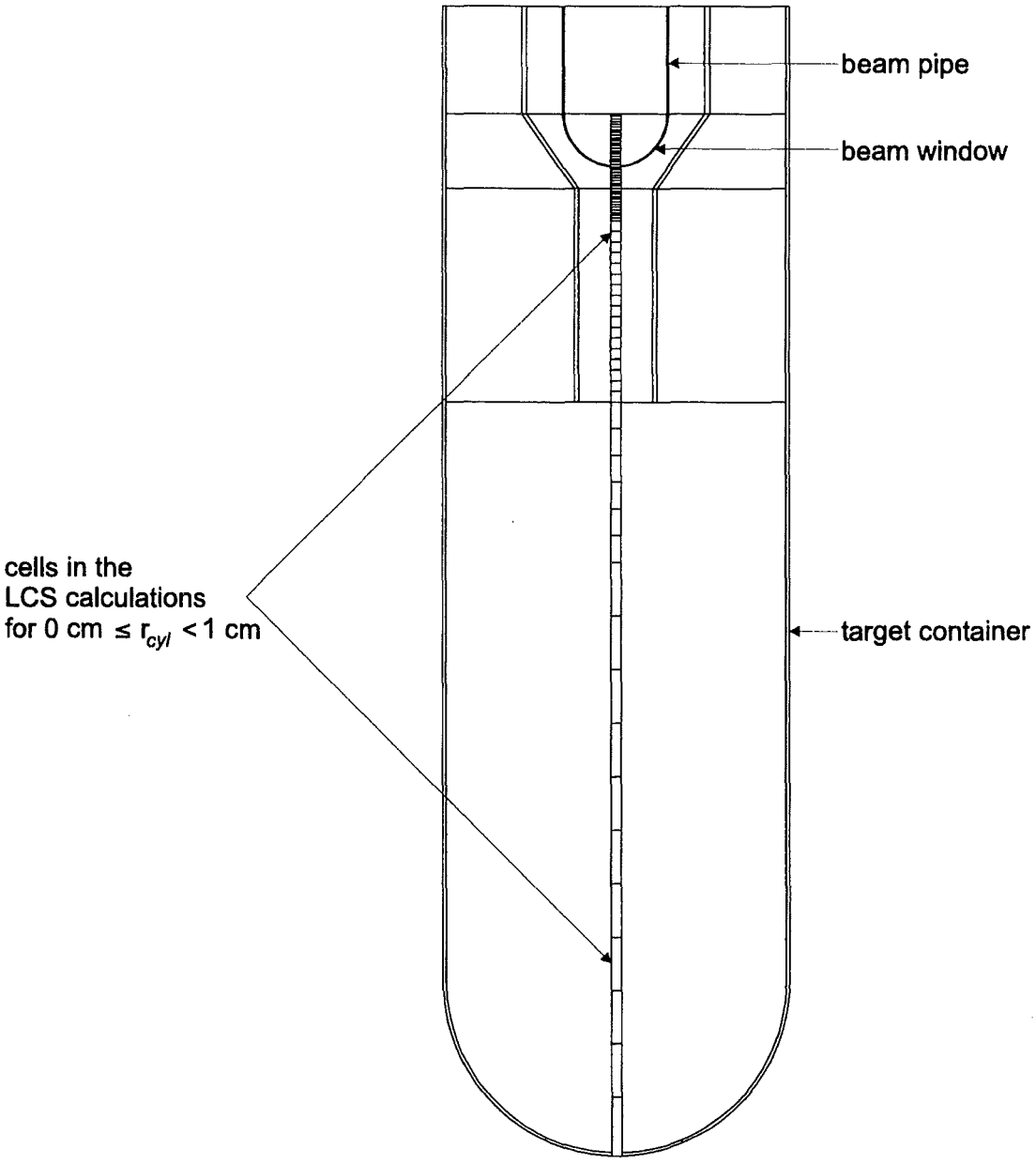

Figure 2.5: Geometric model of the target for the calculation with the LCS program showing subzones for $0cm \leq r_{cyl} < 1cm$

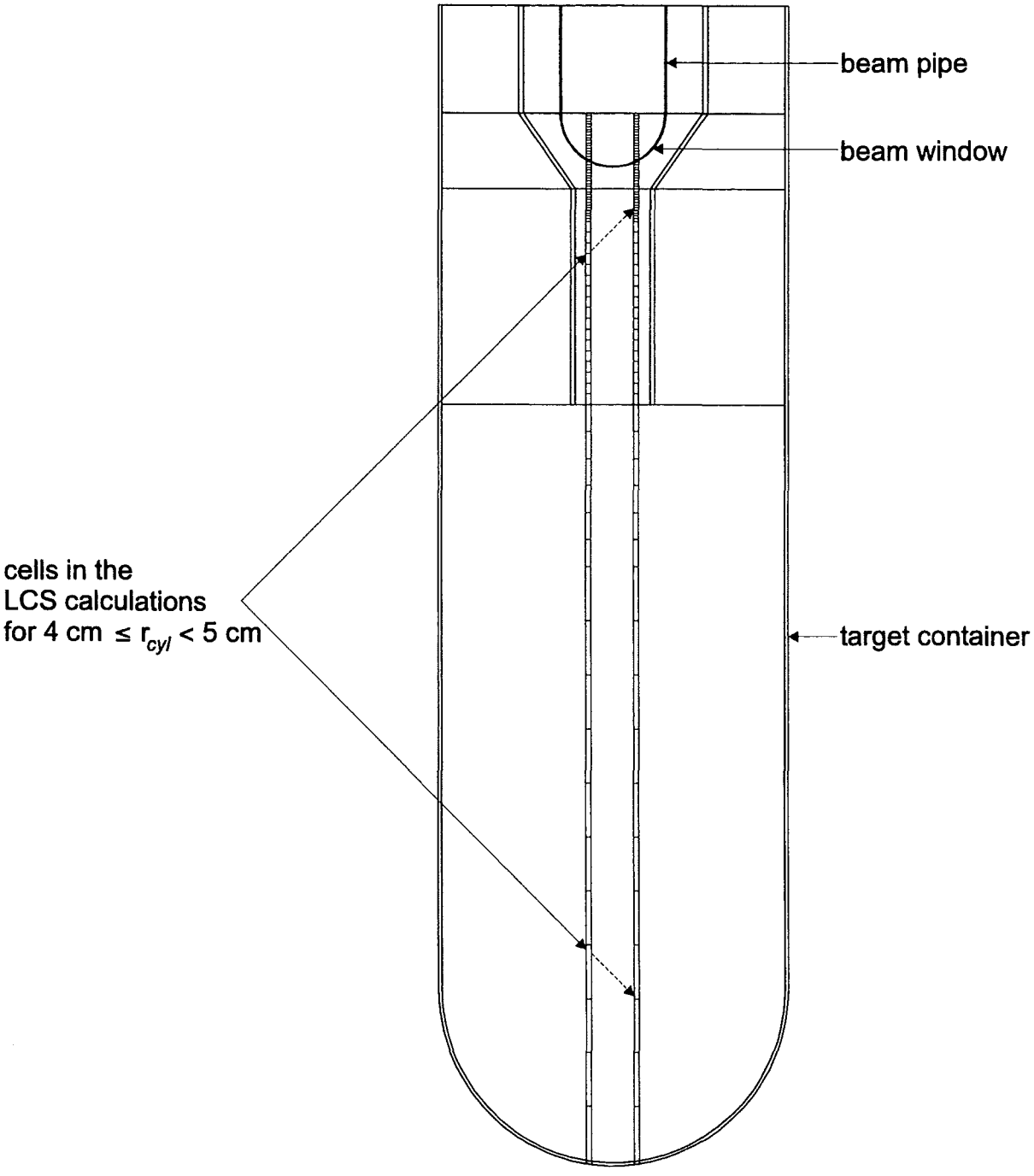

Figure 2.6: Geometric model of the target for the calculation with the LCS program showing subzones for $4cm \leq r_{cyl} < 5cm$

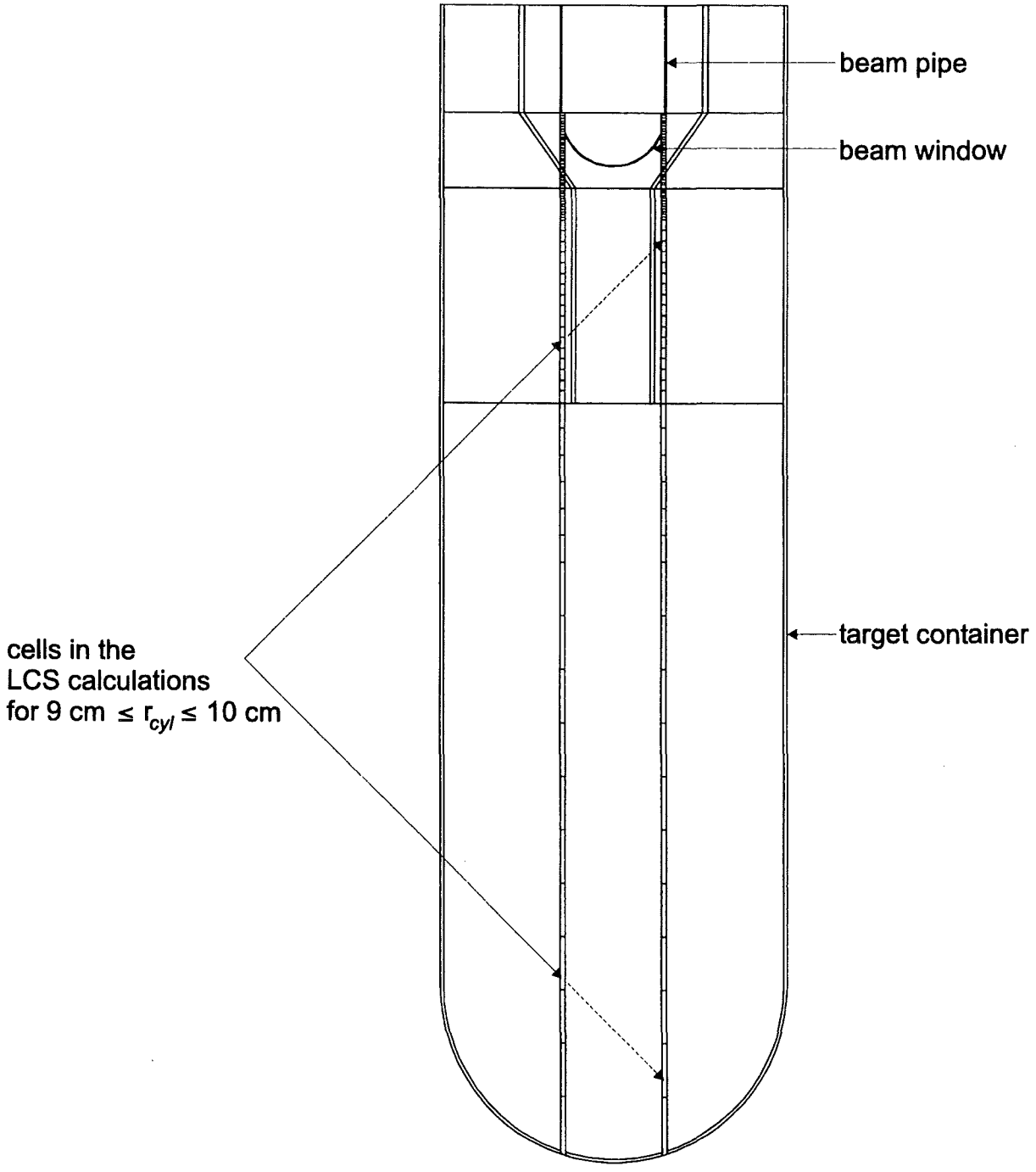

Figure 2.7: Geometric model of the target for the calculation with the LCS program showing subzones for $9cm \leq r_{cyl} \leq 10cm$

Table 2.11: Spatial distribution of energy deposition in the target of an ADS $[MeV/(proton \cdot cm^3)] = [kW/(mA \cdot cm^3)]$

r [cm]:	0 - 1	1 - 2	2 - 3	3 - 4	4 - 5
z [cm]					
195.0 -	3.40615E-22	3.53024E-22	3.43446E-22	3.33098E-22	9.84085E-06
194.5 -	3.55641E-22	3.64988E-22	3.55187E-22	3.45934E-22	3.48052E-22
194.0 -	3.86571E-22	3.65285E-22	3.73377E-22	3.60211E-22	3.64906E-22
193.5 -	4.05785E-22	3.79579E-22	3.90803E-22	3.79304E-22	3.81929E-22
193.0 -	4.25682E-22	3.91803E-22	4.13298E-22	4.00454E-22	4.01574E-22
192.5 -	4.44515E-22	4.09548E-22	4.34084E-22	1.21196E-05	4.21020E-22
192.0 -	4.77617E-22	4.54437E-22	4.53636E-22	4.51924E-22	4.40252E-22
191.5 -	4.93434E-22	2.93675E-05	4.84885E-22	4.70110E-22	1.28595E-05
191.0 -	5.25665E-22	5.13873E-22	5.13746E-22	4.93912E-22	4.90222E-22
190.5 -	5.43949E-22	5.31070E-22	5.51475E-22	5.29160E-22	5.20671E-22
190.0 -	8.24720E-05	5.78578E-22	5.83348E-22	5.63101E-22	5.52498E-22
189.5 -	6.43421E-22	6.18717E-22	6.25689E-22	6.09824E-22	9.09155E-06
189.0 -	6.99427E-22	6.64748E-22	1.62469E-05	1.18672E-05	6.24935E-22
188.5 -	7.18971E-22	3.60011E-05	1.68222E-05	7.06927E-22	6.77498E-22
188.0 -	8.16347E-22	2.74907E-05	7.96844E-22	7.67477E-22	7.42056E-22
187.5 -	8.81810E-22	8.44629E-22	1.66141E-05	8.33086E-22	9.50782E-06
187.0 -	9.77468E-22	3.01208E-05	1.67292E-05	9.24038E-22	8.57999E-06
186.5 -	1.08240E-21	1.07757E-21	1.72155E-05	1.41799E-05	1.44768E-01
186.0 -	1.25683E-21	1.23461E-21	1.22554E-21	1.18325E-21	1.49131E-01
185.5 -	2.37036E-01	2.16631E-01	2.07047E-01	1.84575E-01	1.51177E-01
185.0 -	2.44203E-01	2.30021E-01	2.13053E-01	1.91338E-01	1.51599E-01
184.5 -	2.44081E-01	2.32910E-01	2.17715E-01	1.92469E-01	1.48843E-01
184.0 -	2.38443E-01	2.29648E-01	2.14874E-01	1.96409E-01	1.45178E-01
183.5 -	2.46111E-01	2.30709E-01	2.12522E-01	1.90694E-01	1.43242E-01
183.0 -	2.46482E-01	2.19944E-01	2.12688E-01	1.82730E-01	1.46540E-01
182.5 -	2.34584E-01	2.31628E-01	2.04913E-01	1.82418E-01	1.44107E-01
182.0 -	2.33229E-01	2.21538E-01	1.98971E-01	1.80468E-01	1.39498E-01
181.5 -	2.26283E-01	2.24417E-01	1.99936E-01	1.75614E-01	1.32405E-01
181.0 -	2.20893E-01	2.07521E-01	1.97838E-01	1.72806E-01	1.30192E-01

180.5 -	2.10049E-01	1.98837E-01	1.94929E-01	1.63447E-01	1.27373E-01
180.0 -	2.09111E-01	1.97443E-01	1.90618E-01	1.65458E-01	1.24377E-01
179.5 -	2.00944E-01	1.96473E-01	1.80883E-01	1.59196E-01	1.23476E-01
179.0 -	2.02701E-01	1.87694E-01	1.82233E-01	1.58992E-01	1.20416E-01
178.5 -	1.81886E-01	1.87228E-01	1.73069E-01	1.53560E-01	1.16324E-01
178.0 -	1.92907E-01	1.84553E-01	1.72238E-01	1.49959E-01	1.16227E-01
177.5 -	1.84635E-01	1.75912E-01	1.64059E-01	1.48347E-01	1.12386E-01
177.0 -	2.01264E-01	1.72482E-01	1.63428E-01	1.41176E-01	1.10217E-01
176.5 -	1.91294E-01	1.66731E-01	1.59065E-01	1.36740E-01	1.05315E-01
176.0 -	1.84829E-01	1.64953E-01	1.58015E-01	1.36071E-01	1.03181E-01
175.5 -	1.71841E-01	1.58134E-01	1.52200E-01	1.32649E-01	9.98293E-02
175.0 -	1.66217E-01	1.54945E-01	1.43228E-01	1.25413E-01	9.60621E-02
173.0 -	1.44665E-01	1.39753E-01	1.31155E-01	1.13203E-01	8.83069E-02
171.0 -	1.29568E-01	1.28744E-01	1.18946E-01	1.04463E-01	8.01864E-02
169.0 -	1.25215E-01	1.17976E-01	1.10413E-01	9.51321E-02	7.37384E-02
167.0 -	1.12913E-01	1.08449E-01	1.02805E-01	8.79910E-02	6.81127E-02
165.0 -	1.04370E-01	1.03145E-01	9.60386E-02	8.18876E-02	6.30935E-02
163.0 -	9.66116E-02	9.93401E-02	9.21660E-02	7.80289E-02	6.13556E-02
161.0 -	9.68645E-02	1.01536E-01	9.47379E-02	8.12307E-02	6.65711E-02
159.0 -	1.10585E-01	1.11406E-01	1.01933E-01	8.39355E-02	6.03902E-02
157.0 -	1.58167E-02	1.43479E-02	1.23798E-02	1.03513E-02	3.95285E-03
155.0 -	7.87718E-04	8.87471E-04	1.15287E-03	8.41500E-04	8.49591E-04
153.0 -	9.66171E-04	8.40761E-04	6.76550E-04	6.40898E-04	6.05069E-04
151.0 -	6.29644E-04	4.96844E-04	4.70969E-04	5.45728E-04	4.77988E-04
149.0 -	4.60599E-04	4.90844E-04	5.95191E-04	4.95521E-04	4.29492E-04
147.0 -	4.97613E-04	3.03660E-04	4.46975E-04	4.11895E-04	3.38805E-04
145.0 -	4.08346E-04	3.25824E-04	5.55803E-04	3.57988E-04	3.38134E-04
143.0 -	2.06091E-04	3.14895E-04	3.93923E-04	2.37760E-04	2.90716E-04
141.0 -	1.78359E-04	1.06591E-04	2.03377E-04	2.64360E-04	1.38372E-04
136.0 -	1.20081E-04	9.62488E-05	2.00346E-04	1.40184E-04	1.37187E-04
131.0 -	3.55880E-04	7.98639E-05	1.13287E-04	9.95042E-05	1.00764E-04
126.0 -	2.58776E-05	9.05660E-05	4.30526E-05	5.46282E-05	4.74582E-05
121.0 -	1.32099E-05	4.97233E-05	5.05439E-05	3.15802E-05	2.32020E-05
116.0 -	1.26209E-05	3.59566E-05	3.35987E-05	5.41621E-05	2.69315E-05
111.0 -	9.01495E-06	8.57073E-06	1.03983E-05	2.44189E-05	1.32933E-05
101.0 -	3.77160E-06	5.52152E-06	7.73236E-06	8.01500E-06	1.76519E-05
91.0 -	5.54765E-06	5.80458E-06	6.43317E-06	1.93433E-06	2.28685E-06

81.0 -	1.31699E-06	6.37680E-06	5.69469E-06	2.26745E-06	1.28420E-06
71.0 -	2.48627E-07	2.83976E-07	1.17389E-05	6.72695E-06	1.28578E-06
61.0 -	3.38726E-07	2.45591E-06	8.93100E-07	6.96278E-07	4.89983E-07
51.0 -	1.40269E-07	1.84228E-07	3.64884E-07	1.56701E-06	1.36679E-07
41.0 -	1.03007E-08	1.26592E-08	1.25250E-08	8.95143E-08	3.26666E-08
31.0 -	6.52920E-07	3.10522E-10	7.82920E-09	2.55029E-08	2.55316E-07
21.0 -	7.08580E-09	0.00000E+00	1.23475E-08	2.17482E-09	1.58658E-09
11. - 0	9.04197E-10	0.00000E+00	8.78672E-08	1.90910E-08	1.61810E-08

Table 2.11 continued: Spatial distribution of energy deposition in the target of an ADS $[MeV/(proton \cdot cm^3)] = [kW/(mA \cdot cm^3)]$

r [cm]:	5 - 6	6 - 7	7 - 7.9	7.9- 9	9 - 10
z [cm]					
195.0 -	3.25092E-22	3.16110E-22	3.06833E-22	2.98872E-22	2.79289E-22
194.5 -	3.39433E-22	3.24829E-22	3.17328E-22	4.39788E-06	8.42677E-04
194.0 -	7.98325E-06	3.39216E-22	3.30038E-22	3.18519E-22	9.06814E-04
193.5 -	3.70897E-22	3.60625E-22	3.40354E-22	3.31614E-22	1.14333E-03
193.0 -	3.81914E-22	3.72630E-22	3.54232E-22	4.36011E-06	9.94902E-04
192.5 -	4.03623E-22	3.85926E-22	3.71973E-22	3.52512E-22	1.05606E-03
192.0 -	4.21452E-22	4.01253E-22	6.09668E-06	3.65655E-22	1.06478E-03
191.5 -	4.46142E-22	4.24964E-22	3.98972E-22	6.10909E-06	8.56710E-04
191.0 -	4.71326E-22	4.42267E-22	4.20229E-22	3.82484E-22	8.25146E-04
190.5 -	4.97317E-22	1.29848E-05	6.19467E-06	1.48163E-03	5.70058E-04
190.0 -	5.25305E-22	1.34224E-05	8.68570E-06	1.47064E-03	5.82049E-04
189.5 -	5.55689E-22	5.98446E-06	4.69594E-22	1.40523E-03	5.03216E-04
189.0 -	5.94228E-22	6.57225E-06	1.06116E-02	9.14297E-04	5.68727E-04
188.5 -	6.40094E-22	5.91458E-22	1.04433E-02	1.14027E-03	5.60544E-04
188.0 -	7.00476E-22	5.51832E-02	9.70273E-03	1.02446E-03	6.49284E-04
187.5 -	8.77833E-06	5.64962E-02	9.68023E-03	1.10771E-03	6.09712E-04
187.0 -	1.06331E-01	5.62215E-02	1.00438E-02	1.42753E-03	7.66004E-04
186.5 -	1.07942E-01	5.78420E-02	1.04000E-02	1.54297E-03	7.90666E-04
186.0 -	1.09559E-01	5.86624E-02	1.07344E-02	1.77564E-03	9.50907E-04

185.5 -	1.12072E-01	5.78335E-02	1.05291E-02	1.99890E-03	1.05912E-03
185.0 -	1.11746E-01	5.61137E-02	1.19477E-02	2.43147E-03	1.13952E-03
184.5 -	1.08378E-01	5.46070E-02	1.17287E-02	2.67273E-03	1.40478E-03
184.0 -	1.06350E-01	5.47226E-02	1.18772E-02	2.61322E-03	1.31299E-03
183.5 -	1.05150E-01	5.54887E-02	1.19665E-02	2.72296E-03	1.65952E-03
183.0 -	1.01815E-01	5.14968E-02	1.23141E-02	3.09828E-03	2.07551E-03
182.5 -	1.00143E-01	5.27625E-02	1.33122E-02	3.51591E-03	2.07536E-03
182.0 -	9.84199E-02	5.09497E-02	1.47286E-02	3.69388E-03	2.02472E-03
181.5 -	9.87022E-02	4.89912E-02	1.44017E-02	4.34222E-03	2.00983E-03
181.0 -	9.47853E-02	4.86515E-02	1.49776E-02	4.24982E-03	2.25760E-03
180.5 -	9.09217E-02	4.84008E-02	1.42500E-02	4.43094E-03	2.21495E-03
180.0 -	9.18000E-02	4.72791E-02	1.53438E-02	4.52648E-03	2.61980E-03
179.5 -	8.79502E-02	4.69303E-02	1.47978E-02	4.41581E-03	2.58299E-03
179.0 -	8.53173E-02	4.53053E-02	1.53400E-02	4.70717E-03	2.48740E-03
178.5 -	8.37022E-02	4.49301E-02	1.50906E-02	4.78280E-03	2.60195E-03
178.0 -	8.34852E-02	4.38062E-02	1.70307E-02	5.34411E-03	2.69462E-03
177.5 -	7.89432E-02	4.37459E-02	1.60149E-02	5.52292E-03	2.59895E-03
177.0 -	7.81066E-02	4.29180E-02	1.53898E-02	5.08485E-03	2.54210E-03
176.5 -	7.57268E-02	4.10293E-02	1.56663E-02	5.26440E-03	3.00555E-03
176.0 -	7.52884E-02	4.00800E-02	1.61927E-02	5.50720E-03	3.05290E-03
175.5 -	7.14510E-02	3.87731E-02	1.63380E-02	5.77978E-03	2.94401E-03
175.0 -	6.78253E-02	3.79736E-02	1.71118E-02	5.94719E-03	2.98272E-03
173.0 -	6.19141E-02	3.54671E-02	1.73433E-02	6.32305E-03	3.03265E-03
171.0 -	5.63875E-02	3.27191E-02	1.70208E-02	6.76109E-03	2.95413E-03
169.0 -	5.17858E-02	3.09015E-02	1.77595E-02	7.40854E-03	3.09308E-03
167.0 -	4.85425E-02	2.92312E-02	1.76623E-02	7.88142E-03	3.25300E-03
165.0 -	4.47179E-02	2.80900E-02	1.87041E-02	8.67359E-03	3.48169E-03
163.0 -	4.44391E-02	2.86961E-02	1.98935E-02	9.69150E-03	3.87535E-03
161.0 -	5.00985E-02	3.19251E-02	2.35861E-02	1.24877E-02	5.01594E-03
159.0 -	3.97204E-02	2.35766E-02	1.19575E-02	4.95904E-03	1.84247E-03
157.0 -	1.98443E-03	1.26710E-03	1.21309E-03	7.99228E-04	6.17260E-04
155.0 -	8.62195E-04	7.91110E-04	1.07047E-03	7.27029E-04	5.41915E-04
153.0 -	6.51939E-04	6.43719E-04	7.72457E-04	5.66202E-04	4.42537E-04
151.0 -	5.19075E-04	4.90972E-04	6.16179E-04	4.58291E-04	4.50090E-04
149.0 -	4.59875E-04	4.14049E-04	4.76912E-04	4.19673E-04	3.65781E-04
147.0 -	2.98725E-04	3.44759E-04	4.82575E-04	3.30045E-04	3.11055E-04
145.0 -	2.80334E-04	3.00844E-04	3.69313E-04	2.81965E-04	2.43391E-04

143.0 -	2.49050E-04	3.05087E-04	3.13503E-04	2.25810E-04	2.72245E-04
141.0 -	2.27166E-04	1.84392E-04	1.67532E-04	1.97562E-04	1.79577E-04
136.0 -	1.29313E-04	1.09512E-04	1.42401E-04	1.09905E-04	1.00083E-04
131.0 -	9.61880E-05	9.24556E-05	8.97556E-05	7.67077E-05	8.16404E-05
126.0 -	5.52620E-05	5.40446E-05	7.67645E-05	5.45704E-05	3.95880E-05
121.0 -	4.50205E-05	3.40094E-05	4.14857E-05	3.54703E-05	3.10624E-05
116.0 -	2.54867E-05	4.71348E-05	1.75084E-05	4.12911E-05	2.71312E-05
111.0 -	1.52133E-05	1.14962E-05	1.70688E-05	3.18403E-05	1.65211E-05
101.0 -	8.59999E-06	5.73668E-06	5.30645E-06	6.93424E-06	1.20300E-05
91.0 -	8.93677E-06	2.58835E-06	4.35384E-06	2.99156E-06	3.13793E-06
81.0 -	4.22398E-06	2.22517E-06	1.05275E-06	1.99094E-06	2.61025E-06
71.0 -	2.82101E-06	6.99328E-07	5.58092E-07	7.41018E-07	8.17466E-07
61.0 -	5.07429E-07	5.91153E-07	4.68122E-07	4.56368E-07	6.80835E-07
51.0 -	1.11366E-07	2.31812E-07	1.83792E-07	4.29788E-07	8.94204E-08
41.0 -	5.48517E-08	4.11272E-07	1.49240E-07	1.09554E-07	1.36444E-07
31.0 -	7.44358E-09	4.20868E-08	6.14312E-09	3.36598E-08	6.73340E-09
21.0 -	2.44142E-08	3.08948E-09	2.98376E-09	1.27466E-07	4.83675E-09
11. - 0	9.42443E-10	2.08509E-08	1.04107E-08	8.96265E-09	1.89331E-08

Table 2.11a: densities of energy deposition contributions from LAHET and from MCNP $[MeV/(proton \cdot cm^3)] = [kW/(mA \cdot cm^3)]$ (mean values are given and statistical errors)

4.0 cm < r < 5.0 cm

z [cm]	MCNP		LAHET		total	
195.0 -	3.30920E-22	.0100	9.84085E-06	1.0000	9.84085E-06	1.0000
194.5 -	3.48052E-22	.0099	0.00000E+00	.0000	3.48052E-22	.0099
194.0 -	3.64906E-22	.0097	0.00000E+00	.0000	3.64906E-22	.0097
193.5 -	3.81929E-22	.0095	0.00000E+00	.0000	3.81929E-22	.0095
193.0 -	4.01574E-22	.0093	0.00000E+00	.0000	4.01574E-22	.0093
192.5 -	4.21020E-22	.0091	0.00000E+00	.0000	4.21020E-22	.0091
192.0 -	4.40252E-22	.0091	0.00000E+00	.0000	4.40252E-22	.0091
191.5 -	4.60856E-22	.0089	1.28595E-05	1.0000	1.28595E-05	1.0000

191.0 -	4.90222E-22	.0089	0.00000E+00	.0000	4.90222E-22	.0089
190.5 -	5.20671E-22	.0087	0.00000E+00	.0000	5.20671E-22	.0087
190.0 -	5.52498E-22	.0086	0.00000E+00	.0000	5.52498E-22	.0086
189.5 -	5.90342E-22	.0085	9.09155E-06	1.0000	9.09155E-06	1.0000
189.0 -	6.24935E-22	.0083	0.00000E+00	.0000	6.24935E-22	.0083
188.5 -	6.77498E-22	.0082	0.00000E+00	.0000	6.77498E-22	.0082
188.0 -	7.42056E-22	.0081	0.00000E+00	.0000	7.42056E-22	.0081
187.5 -	8.21144E-22	.0082	9.50782E-06	1.0000	9.50782E-06	1.0000
187.0 -	9.25727E-22	.0085	8.57999E-06	1.0000	8.57999E-06	1.0000
186.5 -	6.26980E-03	.0825	1.38498E-01	.0150	1.44768E-01	.0179
186.0 -	7.26106E-03	.0775	1.41870E-01	.0140	1.49131E-01	.0171
185.5 -	7.73376E-03	.0753	1.43444E-01	.0140	1.51177E-01	.0171
185.0 -	7.97974E-03	.0696	1.43620E-01	.0140	1.51599E-01	.0169
184.5 -	8.06734E-03	.0696	1.40775E-01	.0140	1.48843E-01	.0170
184.0 -	7.78004E-03	.0693	1.37398E-01	.0130	1.45178E-01	.0160
183.5 -	7.85622E-03	.0674	1.35385E-01	.0130	1.43242E-01	.0160
183.0 -	7.48455E-03	.0628	1.39056E-01	.0140	1.46540E-01	.0165
182.5 -	7.72549E-03	.0644	1.36381E-01	.0140	1.44107E-01	.0167
182.0 -	7.28985E-03	.0633	1.32209E-01	.0140	1.39498E-01	.0166
181.5 -	7.01908E-03	.0610	1.25386E-01	.0130	1.32405E-01	.0155
181.0 -	6.76660E-03	.0633	1.23425E-01	.0140	1.30192E-01	.0166
180.5 -	6.64093E-03	.0769	1.20732E-01	.0130	1.27373E-01	.0163
180.0 -	6.54749E-03	.0774	1.17830E-01	.0130	1.24377E-01	.0164
179.5 -	6.27359E-03	.0596	1.17202E-01	.0140	1.23476E-01	.0163
179.0 -	5.94173E-03	.0635	1.14474E-01	.0140	1.20416E-01	.0164
178.5 -	5.76994E-03	.0634	1.10554E-01	.0130	1.16324E-01	.0155
178.0 -	5.26607E-03	.0689	1.10960E-01	.0140	1.16227E-01	.0165
177.5 -	6.02087E-03	.0835	1.06365E-01	.0130	1.12386E-01	.0168
177.0 -	5.13148E-03	.0638	1.05086E-01	.0140	1.10217E-01	.0163
176.5 -	4.75755E-03	.0662	1.00557E-01	.0130	1.05315E-01	.0154
176.0 -	4.37252E-03	.0628	9.88088E-02	.0130	1.03181E-01	.0151
175.5 -	4.38185E-03	.0651	9.54475E-02	.0130	9.98293E-02	.0153
175.0 -	4.08211E-03	.0421	9.19800E-02	.0100	9.60621E-02	.0114
173.0 -	3.09155E-03	.0391	8.52154E-02	.0100	8.83069E-02	.0110
171.0 -	2.53460E-03	.0284	7.76518E-02	.0100	8.01864E-02	.0106
169.0 -	2.11823E-03	.0268	7.16202E-02	.0100	7.37384E-02	.0105
167.0 -	1.83430E-03	.0263	6.62785E-02	.0110	6.81127E-02	.0114

165.0 -	1.49189E-03	.0158	6.16016E-02	.0120	6.30935E-02	.0121
163.0 -	1.27274E-03	.0243	6.00829E-02	.0120	6.13556E-02	.0123
161.0 -	1.03589E-03	.0380	6.55352E-02	.0130	6.65711E-02	.0134
159.0 -	7.11536E-04	.0193	5.96786E-02	.0150	6.03902E-02	.0151
157.0 -	4.76783E-04	.0234	3.47607E-03	.0440	3.95285E-03	.0415
155.0 -	3.38488E-04	.0259	5.11103E-04	.1370	8.49591E-04	.0927
153.0 -	2.62340E-04	.0298	3.42729E-04	.1480	6.05069E-04	.0968
151.0 -	2.12962E-04	.0338	2.65026E-04	.1960	4.77988E-04	.1237
149.0 -	1.84542E-04	.0395	2.44950E-04	.1680	4.29492E-04	.1128
147.0 -	1.40586E-04	.0405	1.98219E-04	.2170	3.38805E-04	.1438
145.0 -	1.15340E-04	.0448	2.22794E-04	.2200	3.38134E-04	.1602
143.0 -	9.99210E-05	.0497	1.90795E-04	.2350	2.90716E-04	.1713
141.0 -	7.15495E-05	.0407	6.68226E-05	.2110	1.38372E-04	.1229
136.0 -	5.33037E-05	.0491	8.38837E-05	.2240	1.37187E-04	.1560
131.0 -	3.16162E-05	.0577	6.91482E-05	.2690	1.00764E-04	.2027
126.0 -	3.07460E-05	.2667	1.67122E-05	.4210	4.74582E-05	.3210
121.0 -	1.46401E-05	.0816	8.56188E-06	.5290	2.32020E-05	.2467
116.0 -	1.16821E-05	.0995	1.52494E-05	.4980	2.69315E-05	.3251
111.0 -	8.30926E-06	.1132	4.98403E-06	.5150	1.32933E-05	.2638
101.0 -	4.48558E-06	.1257	1.31663E-05	.5230	1.76519E-05	.4220
91.0 -	1.99367E-06	.1409	2.93180E-07	.8110	2.28685E-06	.2268
81.0 -	1.20533E-06	.2399	7.88702E-08	.9270	1.28420E-06	.2821
71.0 -	8.24222E-07	.2567	4.61560E-07	.7320	1.28578E-06	.4273
61.0 -	3.40488E-07	.3685	1.49496E-07	1.0000	4.89983E-07	.5612
51.0 -	1.36679E-07	.4765	0.00000E+00	.0000	1.36679E-07	.4765
41.0 -	3.26666E-08	.6350	0.00000E+00	.0000	3.26666E-08	.6350
31.0 -	4.34921E-08	.6030	2.11824E-07	1.0000	2.55316E-07	.9324
21.0 -	1.58658E-09	.2535	0.00000E+00	.0000	1.58658E-09	.2535
11. - 0	1.61810E-08	.9347	0.00000E+00	.0000	1.61810E-08	.9347

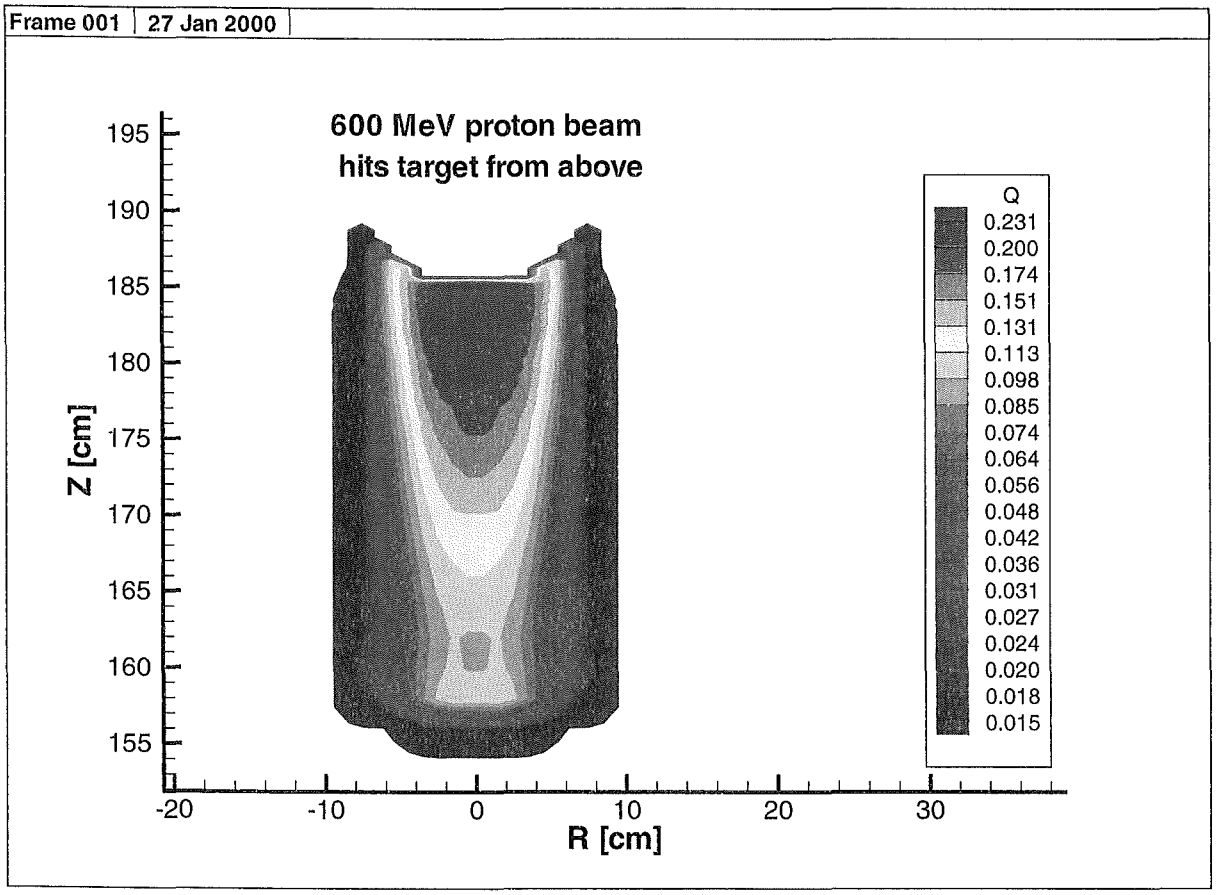

Figure 2.8: Energy $[kW/(mA \cdot cm^3)]$ deposited in a liquid lead target by a 600MeV 1mA proton beam

Chapter 3

Calculation of the Energy Distribution of the Neutron Flux Density for Different Regions of the Liquid Lead Target

In this part of the report we will discuss the calculation of the energy distribution of the neutron flux density in different regions of the target studied above and shown in Fig. 2.1. Neutron flux density spectra are needed e.g.

- for the calculation of reaction rates
- for the condensation of group constants, especially for the calculation of one-group-cross-section for burnup calculations
- for the calculation of radiation damage [19].

Again the calculations have been carried out with the LAHET Code System (LCS) [6]. The primary proton energy was 600MeV, the beam profile was parabolic over the beam radius of 7.5cm.
In the calculations with LCS, neutrons that are slowed down below the cutoff energy E_{cutoff} (input quantity ELON in LAHET) are stored on the so-called NEUTP file and subsequently used as source for the MCNP calculation. The standard value of ELON is 20MeV. Below this energy the nuclear reaction models applied in LAHET are no longer valid for neutrons. In the energy region between $10^{-5}eV$ and 20MeV evaluated neutron nuclear data are available on cross section libraries like ENDF/B or JEF. The nuclear data used in MCNP are based on these libraries. For our calculations with MCNP we have used nuclear data from ENDF/B-VI.
The neutron flux density spectra have been calculated for 83 energy intervals (energy groups) between $10^{-5}eV$ and 600MeV:

- calculation with LAHET for 11 energy intervals above 20MeV up to 600MeV
- calculation with MCNP for 72 energy intervals below 20MeV

The group structure up to 50MeV corresponds to the group structure of the 75 groups constant set, discussed in [26]. Eight additional energy intervals have been chosen above 50MeV, the upper group boundaries are shown in Table 3.1.
The following definitions will be used:

$$\Phi^{LAHET} = \int_{E_{cutoff}}^{E_{max}} \phi(E)dE \tag{3.1}$$

here E_{max} means the maximum energy in the calculation (600MeV in the present investigation), E_{cutoff} has been explained above.
Φ^{LAHET} may also be written as sum over energy intervals:

$$\Phi^{LAHET} = \sum_{g=11}^{1} \phi_g \tag{3.2}$$

where ϕ_g is the neutron flux density for the energy interval g and index 1 is attributed to the interval with the highest neutron energies.
The neutron flux density between the minimum energy E_{min}, used in the calculation and E_{cutoff} is given by:

$$\Phi^{MCNP} = \int_{E_{min}}^{E_{cutoff}} \phi(E)dE \tag{3.3}$$

or for energy intervals (energy groups) g:

$$\Phi^{MCNP} = \sum_{g=83}^{12} \phi_g \tag{3.4}$$

The total flux is then given by:

$$\Phi^{total} = \Phi^{MCNP} + \Phi^{LAHET} \tag{3.5}$$

The fraction of the flux above E_{cutoff} is given by: $\Phi^{LAHET}/\Phi^{total}$ and shown in the figures as contribution from E >20MeV.
The group flux ϕ_g in energy group g is defined by:

$$\phi_g = \int_{E_{g+1}}^{E_g} \phi(E)dE \tag{3.6}$$

and the average value of $\phi(E)$ in energy group g is: $\phi_g(E)$:

$$\phi_g(E) = \frac{\int_{E_{g+1}}^{E_g} \phi(E)dE}{\int_{E_{g+1}}^{E_g} dE} \tag{3.7}$$

Now the relation between functions of energy and functions of lethargy is used

$$F(u) = E \cdot F(E) \tag{3.8}$$

[20] with $u = ln(E_0/E)$ where E_0 usually characterizes the energy of the most energetic neutrons.

The average value of $\phi(u)$ in energy group g, $\phi_g(u)$, is obtained as:

$$\phi_g(u) = \phi_g(E) \ \frac{E_g + E_{g+1}}{2} \tag{3.9}$$

In column 4 of Table 3.1 the group values ϕ_g of the neutron flux densities calculated by LAHET or MCNP, respectively, are given, column 5 gives the estimated relative 1σ errors of the Monte Carlo calculations [9]. Column 6 gives $\phi_g(u)$ as defined in equation 3.9. The number of the energy group, the upper energy boundary of each group and the energy width are given in columns 1, 2 and 3 of Table 3.1.

Figures 3.1, 3.2 and 3.3 show the spectra for the target window (steel HT9), for zone 6 of Fig.2.1 which is the region between the window and the funnel and for zone 15 (liquid lead within the funnel neck).

In the Figures $\phi_g(u)[n/(cm^2 \cdot sec)]$ per proton/sec is shown versus energy.

Table 3.1: Neutron flux density spectrum in the HT9 window of the liquid lead target shown in Fig. 2.1 and 2.4.

g	E_g	ΔE	ϕ_g		$\phi_g(u)$
83	5.0000E-03	5.0000E-03	1.00000E-20	.0000	5.00000E-21
82	1.0000E-02	5.0000E-03	1.00000E-20	.0000	1.50000E-20
81	1.5000E-02	5.0000E-03	1.00000E-20	.0000	2.50000E-20
80	2.0000E-02	5.0000E-03	1.00000E-20	.0000	3.50000E-20
79	2.5000E-02	5.0000E-03	1.00000E-20	.0000	4.50000E-20
78	3.0000E-02	5.0000E-03	1.00000E-20	.0000	5.50000E-20
77	3.5000E-02	5.0000E-03	1.00000E-20	.0000	6.50000E-20
76	4.2000E-02	7.0000E-03	1.00000E-20	.0000	5.50000E-20
75	5.0000E-02	8.0000E-03	1.00000E-20	.0000	5.75000E-20
74	5.8000E-02	8.0000E-03	1.00000E-20	.0000	6.75000E-20
73	6.7000E-02	9.0000E-03	1.00000E-20	.0000	6.94444E-20
72	8.0000E-02	1.3000E-02	1.00000E-20	.0000	5.65385E-20
71	1.0000E-01	2.0000E-02	1.00000E-20	.0000	4.50000E-20

70	1.4000E-01	4.0000E-02	1.00000E-20	.0000	3.00000E-20
69	1.8000E-01	4.0000E-02	1.00000E-20	.0000	4.00000E-20
68	2.2000E-01	4.0000E-02	1.00000E-20	.0000	5.00000E-20
67	2.5000E-01	3.0000E-02	1.00000E-20	.0000	7.83333E-20
66	2.8000E-01	3.0000E-02	1.00000E-20	.0000	8.83333E-20
65	3.0000E-01	2.0000E-02	1.00000E-20	.0000	1.45000E-19
64	3.2000E-01	2.0000E-02	1.00000E-20	.0000	1.55000E-19
63	3.5000E-01	3.0000E-02	1.00000E-20	.0000	1.11667E-19
62	4.0000E-01	5.0000E-02	1.00000E-20	.0000	7.50000E-20
61	5.0000E-01	1.0000E-01	1.00000E-20	.0000	4.50000E-20
60	6.2500E-01	1.2500E-01	1.00000E-20	.0000	4.50000E-20
59	7.8000E-01	1.5500E-01	1.00000E-20	.0000	4.53226E-20
58	8.5000E-01	7.0000E-02	1.00000E-20	.0000	1.16429E-19
57	9.1000E-01	6.0000E-02	1.00000E-20	.0000	1.46667E-19
56	9.5000E-01	4.0000E-02	1.00000E-20	.0000	2.32500E-19
55	9.7200E-01	2.2000E-02	1.00000E-20	.0000	4.36819E-19
54	9.9600E-01	2.4000E-02	1.00000E-20	.0000	4.09998E-19
53	1.0200E+00	2.4000E-02	1.00000E-20	.0000	4.20001E-19
52	1.0450E+00	2.5000E-02	1.00000E-20	.0000	4.13000E-19
51	1.0710E+00	2.6000E-02	1.00000E-20	.0000	4.06921E-19
50	1.0970E+00	2.6000E-02	1.00000E-20	.0000	4.16925E-19
49	1.1230E+00	2.6000E-02	1.00000E-20	.0000	4.26925E-19
48	1.1500E+00	2.7000E-02	1.00000E-20	.0000	4.20925E-19
47	1.3000E+00	1.5000E-01	1.00000E-20	.0000	8.16667E-20
46	1.5000E+00	2.0000E-01	1.00000E-20	.0000	7.00000E-20
45	2.1000E+00	6.0000E-01	1.00000E-20	.0000	3.00000E-20
44	2.6000E+00	5.0000E-01	1.00000E-20	.0000	4.70000E-20
43	3.3000E+00	7.0000E-01	1.00000E-20	.0000	4.21428E-20
42	4.0000E+00	7.0000E-01	1.00000E-20	.0000	5.21429E-20
41	9.8770E+00	5.8770E+00	1.00000E-20	.0000	1.18062E-20
40	1.5968E+01	6.0910E+00	6.14202E-09	1.0000	1.30307E-08
39	2.7700E+01	1.1732E+01	6.62730E-08	.7479	1.23338E-07
38	4.8052E+01	2.0352E+01	7.52354E-08	.5179	1.40017E-07
37	7.5501E+01	2.7449E+01	5.28607E-08	.4737	1.18968E-07
36	1.4873E+02	7.3229E+01	1.51156E-07	.6524	2.31424E-07

35	3.6726E+02	2.1853E+02	1.59380E-06	.1967	1.88163E-06
34	9.0690E+02	5.3964E+02	4.40988E-06	.1138	5.20615E-06
33	1.4251E+03	5.1820E+02	4.83135E-06	.1067	1.08710E-05
32	2.2395E+03	8.1440E+02	9.33893E-06	.0757	2.10114E-05
31	3.5191E+03	1.2796E+03	1.53710E-05	.0644	3.45872E-05
30	5.5300E+03	2.0109E+03	2.78797E-05	.0473	6.27297E-05
29	9.1180E+03	3.5880E+03	3.74938E-05	.0396	7.65342E-05
28	1.5030E+04	5.9120E+03	7.57392E-05	.0297	1.54681E-04
27	2.4780E+04	9.7500E+03	1.77253E-04	.0198	3.61869E-04
26	4.0850E+04	1.6070E+04	2.21773E-04	.0168	4.52861E-04
25	6.7340E+04	2.6490E+04	3.93860E-04	.0131	8.04298E-04
24	1.1100E+05	4.3660E+04	6.00879E-04	.0108	1.22722E-03
23	1.8300E+05	7.2000E+04	9.88038E-04	.0085	2.01724E-03
22	3.0250E+05	1.1950E+05	1.43080E-03	.0070	2.90650E-03
21	5.0000E+05	1.9750E+05	1.93082E-03	.0061	3.92274E-03
20	8.2100E+05	3.2100E+05	2.66402E-03	.0053	5.48157E-03
19	1.3530E+06	5.3200E+05	2.48086E-03	.0055	5.06898E-03
18	2.2310E+06	8.7800E+05	2.11348E-03	.0059	4.31362E-03
17	3.6790E+06	1.4480E+06	1.34771E-03	.0072	2.75033E-03
16	6.0655E+06	2.3865E+06	6.01708E-04	.0100	1.22844E-03
15	1.0000E+07	3.9345E+06	3.21122E-04	.0131	6.55609E-04
14	1.3800E+07	3.8000E+06	1.24542E-04	.0202	3.90013E-04
13	1.5000E+07	1.2000E+06	2.71125E-05	.0412	3.25350E-04
12	2.0000E+07	5.0000E+06	7.83528E-05	.0249	2.74235E-04
11	2.7100E+07	7.1000E+06	7.02474E-05	.0267	2.33004E-04
10	3.6800E+07	9.7000E+06	6.24228E-05	.0282	2.05609E-04
9	5.0000E+07	1.3200E+07	5.36223E-05	.0309	1.76303E-04
8	6.0000E+07	1.0000E+07	2.48213E-05	.0442	1.36517E-04
7	1.0000E+08	4.0000E+07	5.25111E-05	.0306	1.05022E-04
6	1.5000E+08	5.0000E+07	2.08481E-05	.0478	5.21203E-05
5	2.0000E+08	5.0000E+07	6.94603E-06	.0755	2.43111E-05
4	3.0000E+08	1.0000E+08	4.54719E-06	.0924	1.13680E-05
3	4.0000E+08	1.0000E+08	1.02933E-06	.1249	3.60265E-06
2	5.0000E+08	1.0000E+08	3.80439E-07	.1270	1.71198E-06
1	6.0000E+08	1.0000E+08	3.91868E-07	.1178	2.15527E-06

Φ^{LAHET}, Φ^{MCNP} and Φ^{total} defined in formulas (3.1) to (3.5) take the following values $\Phi^{LAHET} = 2.97768 \cdot 10^{-4}$, $\Phi^{MCNP} = 1.56793 \cdot 10^{-2}$, $\Phi^{total} = 1.59771 \cdot 10^{-2}$. The above values are given in $[n/(cm^2 \cdot sec)]$ and are normalized to a proton current of 1proton/sec. The fraction of the neutron flux density due to neutrons above 20MeV is $\Phi^{LAHET}/\Phi^{total} = 1.86372 \cdot 10^{-2}$.

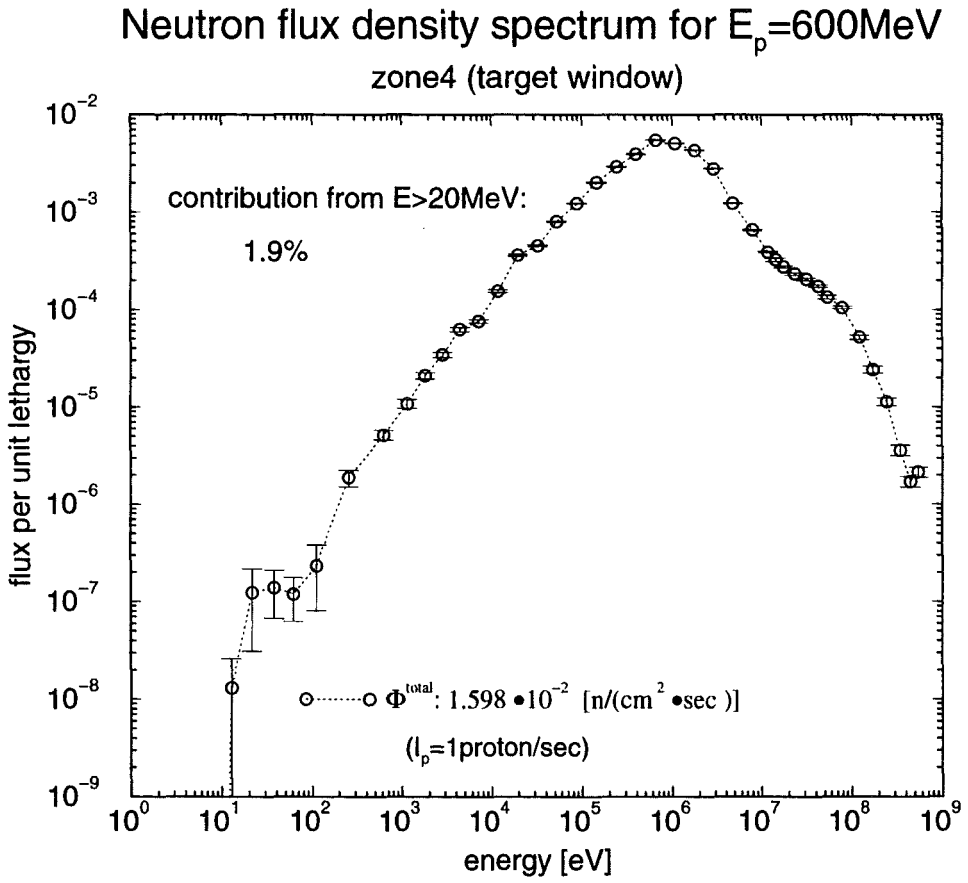

Figure 3.1: Flux per unit lethargy in the beam window plotted versus energy. $\phi_g(u)[n/(cm^2 \cdot sec)]$ for a proton current $I_p = 1\text{proton/sec}$

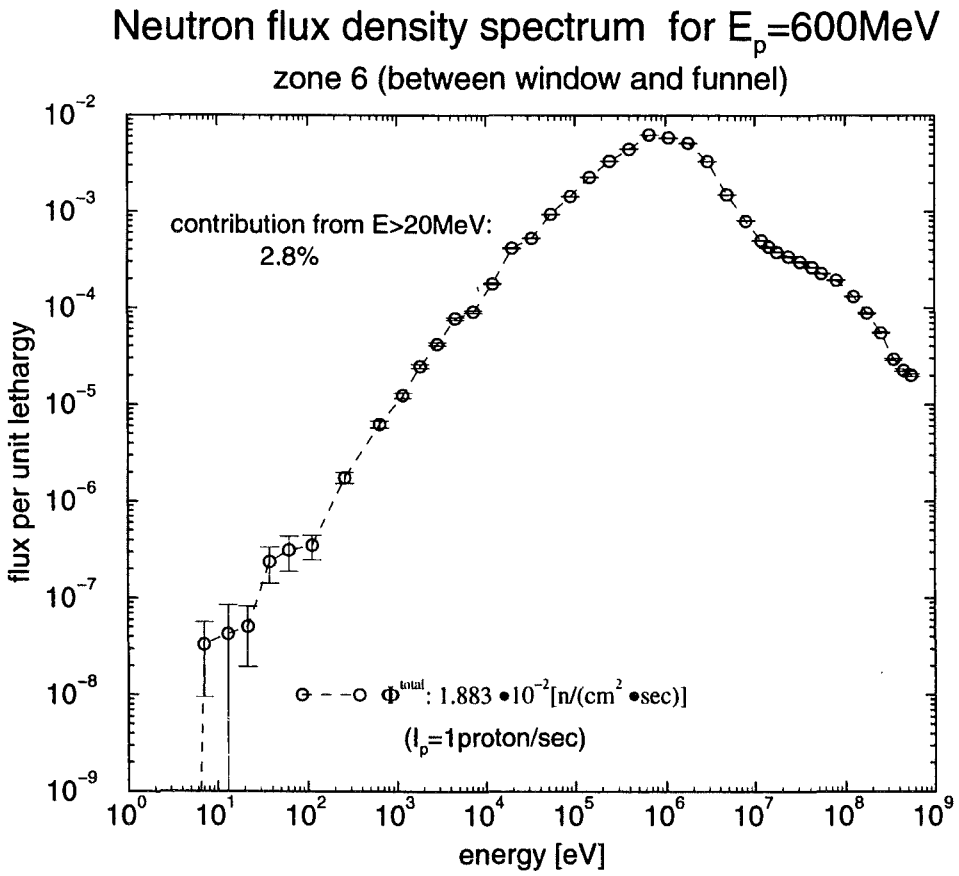

Figure 3.2: Flux per unit lethargy between beam window and funnel (zone 6 in Fig. 2.1)

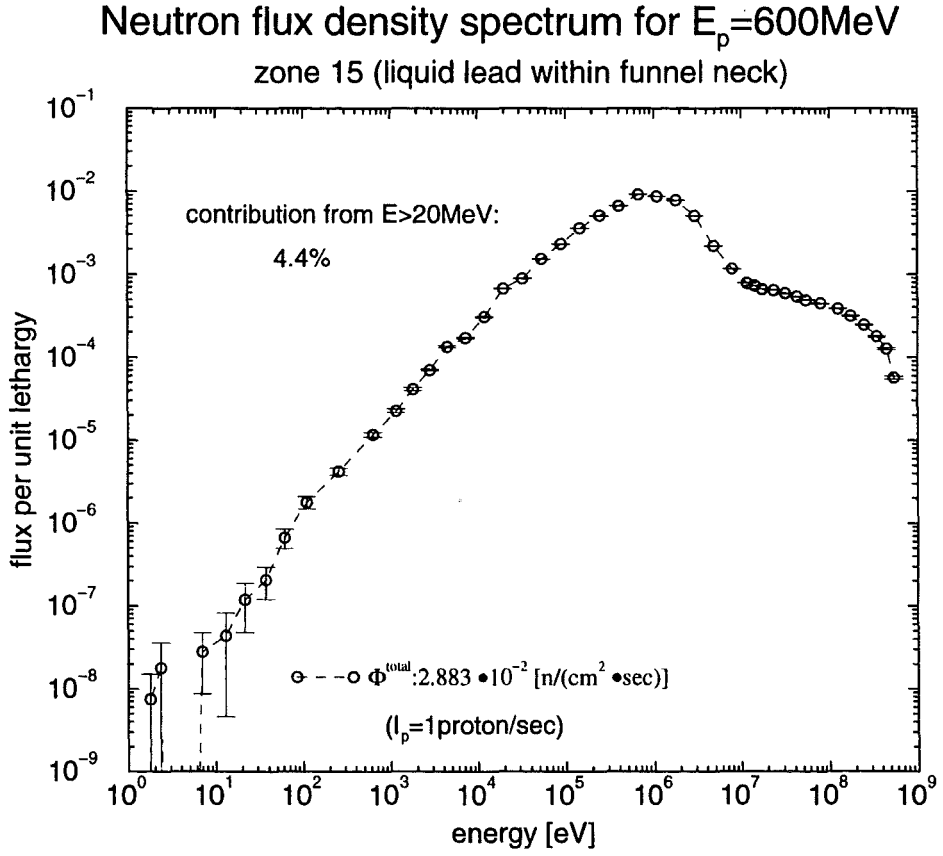

Figure 3.3: Flux per unit lethargy in the funnel neck (zone 15 in Fig. 2.1)

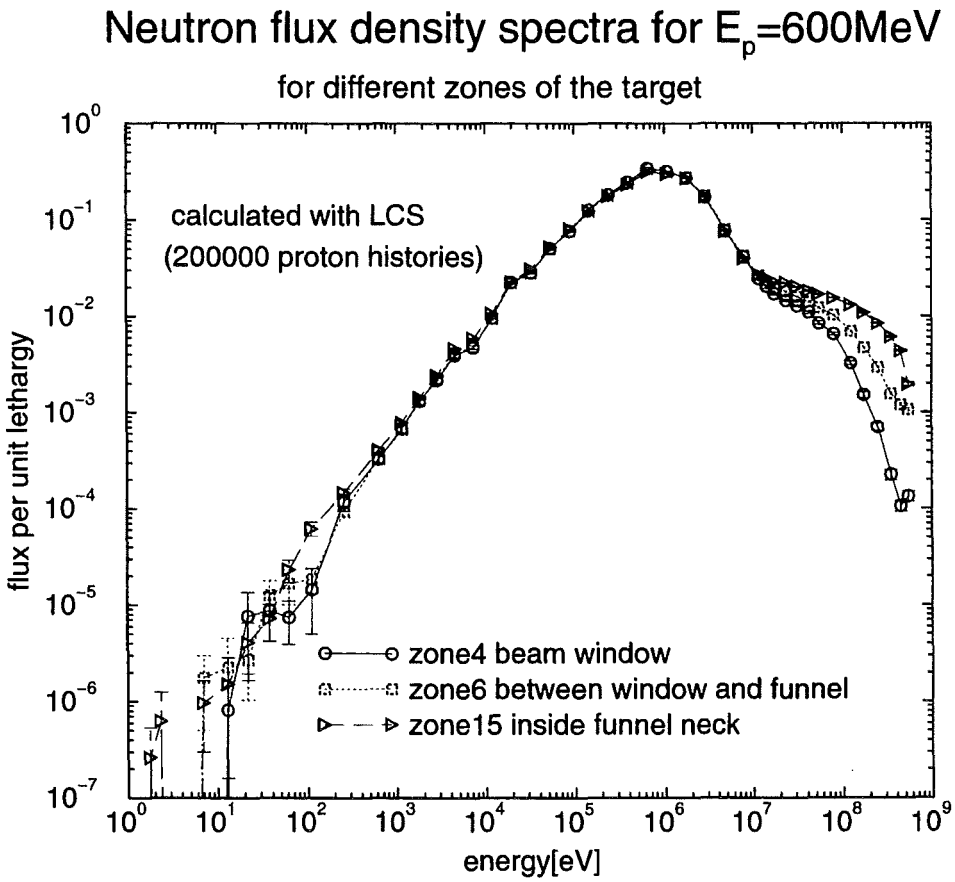

Figure 3.4: Flux per unit lethargy normalised to $\int_{E_{min}}^{E_{max}} \phi(E)dE = 1$ for the beam window (zone 4) and zones 6 and 15 (see Fig. 2.1)

Chapter 4

Experience with MCNPX

The results discussed in the previous sections have been obtained with the **L**AHET **C**ode **S**ystem (LCS), version 2.70 [6]. In these calculations the spallation processes (intranuclear cascade, preequilibrium, evaporation and high energy fission) are simulated in the Monte Carlo code LAHET. Neutrons with energy $E_n \leq 20$MeV and photons that are produced in the spallation process are used as source for a subsequent Monte Carlo calculation with MCNP. MCNP uses data from evaluated nuclear data libraries. For the calculation several user-defined input files are needed, which partly contain the same information. Results, e.g. neutron flux densities and neutron flux density spectra, energy deposition, ... have to be calculated as the sum of the results of LAHET and MCNP with user supplied programs. Moreover, the transfer of the source of low energy neutrons and of γ's from the LAHET code into the MCNP code via the NEUTP-, GAMTP- and RSSA-files requires additional program calls in a shell script and additional attention to partial results.
The MCNPX code system [18] that is currently developed at the Los Alamos National Laboratory requires only **one** user-defined input file. Moreover additional nuclear physics models for the simulation of the spallation process have been implemented and new options for the analysis of the results, e.g. the calculation of recoil energy and damage energy spectra. [21].
For our calculations we used MCNPX version 2.1.5.
MCNPX is still being tested. FZK is beta-tester for MCNPX.

4.1 Application of MCNPX for the calculation of the energy deposition in target zones

To get acquainted with MCNPX and to support the testing, we used the code to calculate energy depositions for the different zones of the target given in Fig. 2.1. In order to keep the source specification relatively simple these calculations have been carried out for a parallel proton beam **uniformly** distributed over a circle of radius r=7.5cm. The input

file for the MCNPX-calculation is given in Appendix C.2.

The results of our study are given in Table 4.1. The Table shows the results of the Monte Carlo codes LCS and MCNPX (mean values and statistical errors) and the deviations relative to the results of LCS.
In all zones except in zone 13 (see Fig. 2.1) the energy densities calculated with LCS are larger than the results from MCNPX.
Deviations $\geq 15\%$ are found in (see Fig. 2.1 zone 12 (-18%) and in zone 17 (-40%). Zone 17 has a rather large **vertical** distance from the proton source (more than 150 cm) and the energy density in zone 17 is rather small $((< 1. \cdot 10^{-7}))[kW/(mA \cdot cm^3)]$. Zone 12 (target container, inner radius 31.94cm) is in large **radial** distance from the proton source. The energy density in zone 12 is about $2. \cdot 10^{-5}[kW/(mA \cdot cm^3)]$. The average energy density deposited in the window (zone 4) is about $3 \cdot 10^{-2} kW/(mA \cdot cm^3)$. In the window the relative deviation between the two calculations is about 11 %. In zone 6 (between window and funnel) the relative deviation is about 6 % and in the lead region within the funnel neck (zone 15) a relative deviation of about 5 % is found.
In all calculations discussed so far in this report the default values defined in the LCS system are used for the description of the nuclear reactions involved in the spallation process (intranuclear cascade, preequilibrium, evaporation and high energy fission). However the parameter IPREQ has been set equal to 1 that means that the preequilibrium model is used following the intranuclear cascade.
The default values defined in MCNPX correspond to those which we used in the LAHET input with one exception: the default value of IEXISA is set to 1 in MCNPX instead of IEXISA=0 in LAHET [6].

- For IEXISA=0: only the Bertini model is used for the simulation of the intranuclear cascade
- For IEXISA=1: the Bertini model is used for nucleons and pions and the ISABEL model (see [6, 7] and references given there) is used for other particle types

For the calculations described in this section we used IEXISA=1 in the MCNPX-calculations and in the LAHET-calculations, that means that the **same** physics options are employed in MCNPX and in the LAHET Code System (LCS) [6].
The Monte Carlo calculations described in this section have been carried out for 100.000 proton histories.

In a further calculation with MCNPX we used the option to take into account only *neutron* elastic scattering (IELAS=1) instead of the default option (IELAS=2) that takes into account elastic scattering of *neutrons and protons.* The difference for the energy deposition in the zones of the target is less than 4 % except in zones 13 and 17 (see Fig. 2.1). Zones 13 and 17, however, are in large distance from the proton source nd the energy deposition in these zones is very low (see Table 4.1).

For the results shown in the Table 4.1, zones 1 and 2 of the target layout (see Fig. 2.1) contained ^4He of particle number density $2.69 \cdot 10^{-20}$ $[10^{24}/cm^3]$. This particle number density is equal to 10^{-15} times the particle number density of ^4He (density $\rho = 0.1785 \cdot 10^{-3} g/cm^3$ for $0°C$ and 1atm). The multiplication with 10^{-15} has been carried out in order to simulate the vacuum in zones 1 and 2.

Table 4.1: Comparison of results of MCNPX and LCS for the energy deposition in the zones of the liquid lead target (Fig. 2.1)
the energy deposition is given in $[MeV/(proton \cdot cm^3)] = [kW/(mA \cdot cm^3)]$
calculations are for a 600MeV parallel proton beam uniformly distributed over a circle with radius 7.5cm.

zone	MCNPX		LCS		deviation relative to LCS [%]
1	1.43304E-21	.0026	2.52890E-07	.3430	-100.0000
2	2.46347E-21	.0056	2.81515E-06	.1791	-100.0000
3	4.41678E-04	.0357	5.05002E-04	.0752	-12.5393
4	2.97780E-02	.0066	3.33060E-02	.0342	-10.5925
5	1.03133E-04	.0162	1.09001E-04	.0597	-5.3837
6	2.41004E-02	.0020	2.61141E-02	.0152	-7.7110
7	2.04178E-03	.0115	2.27459E-03	.0208	-10.2353
8	6.76759E-05	.0237	7.48020E-05	.0868	-9.5265
9	2.12038E-05	.0117	2.25584E-05	.0430	-6.0051
10	1.29293E-04	.0089	1.37980E-04	.0200	-6.2957
11	2.12670E-02	.0068	2.24104E-02	.0112	-5.1022
12	1.74126E-05	.0233	2.12571E-05	.0416	-18.0857
13	9.41497E-09	.2409	8.58850E-09	.1954	9.6230
14	4.19844E-04	.0051	4.22585E-04	.0080	-.6487
15	3.93267E-02	.0025	4.10857E-02	.0090	-4.2814
16	1.11449E-05	.0153	1.29740E-05	.0238	-14.0980
17	4.69882E-08	.3507	7.93604E-08	.4530	-40.7914
18	0.00000E+00	.0000	0.00000E+00	.0000	.0000
19	0.00000E+00	.0000	0.00000E+00	.0000	.0000
20	0.00000E+00	.0000	0.00000E+00	.0000	.0000

The results shown in Table 4.1 above were obtained from calculations with 'diluted' ^4He in zones 1 and 2 and with stainless steel 1.4970 in zones 3, 4, 7, 8, 11, 12 and 13 (see Fig. 2.1). The average energy depositions are given and the statistical errors.

4.2 Comparison of Neutron Spectra calculated with MCNPX and with the LAHET Code System

For a second test we calculated the neutron flux spectrum in the window with the LAHET code system and with MCNPX. The source definition and the choice of the nuclear physics input parameters were the same as for the calculation of the energy deposition described before. The result is shown in the following Fig. 4.2. The agreement is very satisfactory, deviations are mainly found for energies below about 250eV; at these low energies the statistical errors in the Monte Carlo calculations carried out with LCS or MCNPX, respectively, are very large.

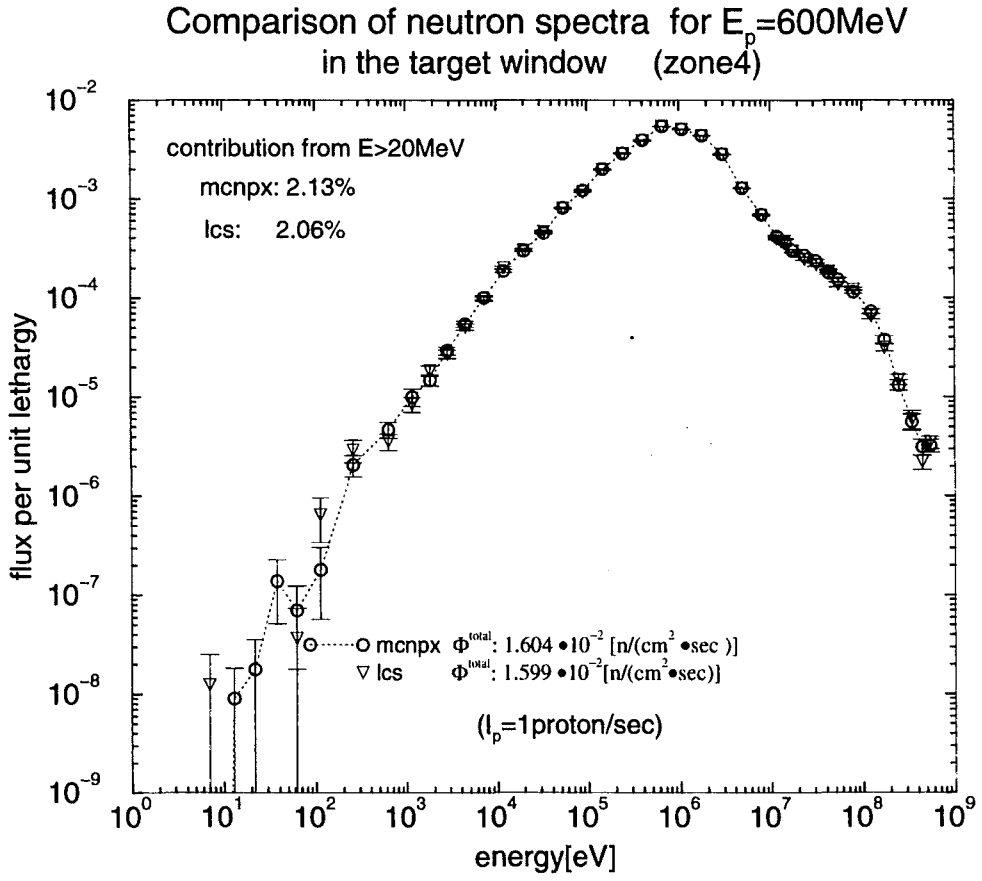

Figure 4.1: Flux per unit lethargy; comparison of results obtained from MCNPX with results of the LAHET Code System

Chapter 5

Spallation Products in a Pb/Bi Target

A high energy particle (e.g. proton) that hits a target, initiates a sequence of nuclear reactions: intranuclear cascade, preequilibrium, evaporation and/or fission and deexcitation (by γ emission) of the residual nuclei. The entire process is called spallation. A schemetical view of the spallation process is given in Fig. 5.1 taken from [18]. The reaction times for nuclear reactions are between 10^{-22} sec and 10^{-14} sec depending on the energy of the incoming particle and on the corresponding reaction type [16, 12]. Reaction times of about 10^{-22} sec are typical for direct reactions, e.g. the intranuclear cascade, reaction times of about 10^{-14} sec are typical for the compoud nucleus reactions in the evaporation- and fission-stage of the spallation process.

In this chapter we investigate the *reaction products* (spallation products) at the end of the spallation process and after different stages of this process.

The spallation products have been calculated with LAHET/HTAPE for a Pb/Bi-target. The geometry of the target is shown in Fig. 2.1. The Pb/Bi-composition was chosen as 45.5w% Pb and 55.5w% Bi, the density $\rho = 10.36 g/cm^3$ corresponds to T= 300°C. For the material of the beam window and the structural material in zones 3, 7, 8, 11, 12, and 13 (see Fig. 2.1) we use steel HT9.

The following assumptions were applied for the proton beam parameters: the energy of the proton beam is 570MeV; the beam has a 2-dimensional Gaussian distribution with σ_x=2.12cm, σ_y=3.58cm.

The material composition of the Pb/Bi zones and the details of the proton beam correspond to the specifications given for the MEGAPIE (MEGAwatt PIlot Experiment) [23]. The geometry of the target however is taken over from the investigations discussed earlier in this report. (The present investigation is a first step of our contribution to the neutron physics work in support of MEGAPIE).

For the calculations with LAHET the parameters, that define the nuclear models used, have been set to their default values with the exception of IPREQ. IPREQ=1 has been applied, which means that a preequilibrium phase is assumed to follow the intranuclear cascade.

In the calculations with LAHET 500.000 proton histories have been taken into account. The following HTAPE edit options [6] have been applied:

- IOPT=8: depending on the suboption KOPT, the edit is given for the final residual nuclei (KOPT=0 or 1), for the residuals after the cascade phase and before evaporation (KOPT=2 or 3), or for the nuclei immediately preceding fission (KOPT=4 or 5), see Fig. 5.1 and [6]. Results in the edit are provided as residual masses versus Z and N, versus Z only, versus N only, and versus A. 'Tally units are dimensionless (particle weight producing a given nuclide per source particle)'.

  (IOPT=5 provides residual nuclei and their mean excitation energies as function of the atomic mass number A. Results are given after the intranuclear cascade (before evaporation and/or fission) and after evaporation and/or fission).

- IOPT=3: particle production spectra. We calculated the *total* production (sum over energies) for each particle (neutron, proton, deuteron, triton, ^3He, α-particles and π-mesons). The code performs separate edits for cascade and evaporation phase production. In addition, total nucleon production from either phase is edited. 'Tally option 3 represents the weight of particles emitted in a given bin per source particle. As such, it is a dimensionless quantity'.

5.1 Results of the calculations with LAHET/HTAPE

The results for the residual nuclei are shown in Tables 5.1a-c and in Table 5.2.
Tables 5.1 give a listing of residual nuclei per proton as function of charge number Z. The mean values are given and the corresponding statistical errors:
In Table 5.1a results of the *final residual nuclei* are shown, that means for the nuclei which are left after the entire reaction process: intranuclear cascade, preequilibrium, evaporation and/or fission and final deexcitation (emission of γ's). In a thick target the nucleons produced during the reaction may interact with another nucleus of the target and produce additional residual nuclei. Table 5.1b is a listing of the residual nuclei after the intranuclear cascade and before evaporation, Table 5.1c lists the residual nuclei immediately preceding fission.
The total number of residual nuclei after the cascade phase and before evaporation is 2.37023 (.0013), where the value given in parenthesis is the statistical error. The number of nuclei immediately preceding fission is calculated to be $4.80856 \cdot 10^{-2}$ (.0063), that means that only about 2% of the nuclei resulting from the intranuclear cascade will

undergo high energy fission. The fission-evaporation ratio however is a still unresolved question [22] within the simulation of the spallation process.
In Table 5.2 results for the *final residual nuclei* are shown as *function of Z and A*.
Please note: The LAHET/HTAPE results presented here do not take into account the radioactive decay of the nuclides; to do this, the application of a decay formalism is necessary. This will be done in a later step of our investigations.
Table 5.3 lists the total number of each particle (nucleon, meson, deuteron, triton, ^{3}He, α-particle) produced in the target

Table 5.1a: Spallation products (per proton) in a Pb/Bi target
final residual nuclei as a function of Z
Proton beam: 2d Gaussian distribution
($\sigma_x = 2.12cm$, $\sigma_y = 3.58cm$), E_p =570MeV

Z		mean value of number of nuclei	statistical error	Z		mean value of number of nuclei	statistical error
2	He	4.00000E-06	.7071	3	Li	8.98000E-05	.1491
4	Be	6.40000E-05	.1768	5	B	1.10000E-04	.1348
6	C	1.84000E-04	.1042	7	N	3.00000E-05	.2582
8	O	3.00000E-05	.2582	9	F	2.80000E-05	.2673
10	Ne	6.60000E-05	.1741	11	Na	4.80000E-05	.2041
12	Mg	1.62000E-04	.1111	13	Al	2.74000E-04	.0854
14	Si	2.92000E-04	.0827	15	P	2.70000E-04	.0861
16	S	4.66000E-04	.0655	17	Cl	6.92000E-04	.0537
18	Ar	1.05800E-03	.0435	19	K	1.38000E-03	.0380
20	Ca	3.09055E-03	.0254	21	Sc	3.55171E-03	.0237
22	Ti	7.68583E-03	.0162	23	V	1.41236E-02	.0120
24	Cr	2.69969E-02	.0087	25	Mn	4.58402E-02	.0067
26	Fe	4.75394E-02	.0068	27	Co	1.65600E-03	.0347
28	Ni	1.49600E-03	.0365	29	Cu	1.65400E-03	.0348
30	Zn	2.01580E-03	.0315	31	Ga	2.06180E-03	.0311
32	Ge	2.54900E-03	.0280	33	As	2.63980E-03	.0275
34	Se	3.04320E-03	.0256	35	Br	3.27980E-03	.0247

36	Kr	3.77580E-03	.0230	37	Rb	3.84740E-03	.0228
38	Sr	4.18000E-03	.0219	39	Y	4.10760E-03	.0221
40	Zr	4.77940E-03	.0205	41	Nb	4.35000E-03	.0222
42	Mo	5.12540E-03	.0217	43	Tc	4.20800E-03	.0218
44	Ru	4.09580E-03	.0221	45	Rh	4.03760E-03	.0222
46	Pd	3.83580E-03	.0228	47	Ag	3.26940E-03	.0248
48	Cd	3.40320E-03	.0242	49	In	2.78380E-03	.0268
50	Sn	2.52340E-03	.0281	51	Sb	2.26580E-03	.0297
52	Te	2.06580E-03	.0311	53	I	1.94000E-03	.0321
54	Xe	1.26780E-03	.0397	55	Cs	1.19600E-03	.0409
56	Ba	1.04400E-03	.0437	57	La	7.76000E-04	.0507
58	Ce	7.64000E-04	.0511	59	Pr	5.58000E-04	.0599
60	Nd	5.42000E-04	.0607	61	Pm	3.35800E-04	.0771
62	Sm	2.92000E-04	.0827	63	Eu	2.44000E-04	.0905
64	Gd	1.84000E-04	.1042	65	Tb	1.12000E-04	.1336
66	Dy	1.24000E-04	.1270	67	Ho	1.20000E-04	.1291
68	Er	1.50000E-04	.1155	69	Tm	2.36000E-04	.0921
70	Yb	4.28000E-04	.0683	71	Lu	1.09000E-03	.0428
72	Hf	1.70800E-03	.0342	73	Ta	3.41600E-03	.0242
74	W	4.94800E-03	.0201	75	Re	8.68580E-03	.0151
76	Os	1.64312E-02	.0109	77	Ir	2.52812E-02	.0088
78	Pt	4.40268E-02	.0066	79	Au	3.72830E-02	.0072
80	Hg	1.08770E-01	.0042	81	Tl	2.64086E-01	.0028
82	Pb	8.64347E-01	.0018	83	Bi	7.32896E-01	.0020
84	Po	5.73906E-02	.0058	85	At	1.21800E-04	.1280

mean weight of residual nuclei per incident proton: 2.41792 (.0013)

Table 5.1b: Spallation products (per proton) in a Pb/Bi target
residual nuclei after the intranuclear cascade and before evaporation as function of Z
Proton beam: 2d Gaussian distribution
($\sigma_x = 2.12cm$, $\sigma_y = 3.58cm$), E_p =570MeV

Z		mean value of number of nuclei	statistical error	Z		mean value of number of nuclei	statistical error
3	Li	2.00000E-06	1.0000	4	Be	3.20000E-05	.2500
5	B	1.32000E-04	.1231	6	C	3.96000E-04	.0711
7	N	1.60000E-05	.3535	11	Na	4.00000E-06	.7071
12	Mg	4.00000E-05	.2236	13	Al	1.40000E-04	.1195
14	Si	3.20000E-04	.0790	15	P	1.60000E-05	.3535
18	Ar	2.00000E-06	1.0000	19	K	2.00000E-05	.3162
20	Ca	1.44000E-04	.1179	21	Sc	4.22000E-04	.0688
22	Ti	2.14200E-03	.0306	23	V	6.86683E-03	.0171
24	Cr	2.08790E-02	.0098	25	Mn	3.42073E-02	.0077
26	Fe	7.93276E-02	.0051	27	Co	4.26980E-03	.0217
28	Ni	2.00000E-05	.3162	37	Rb	4.00000E-06	.7071
38	Sr	6.00000E-06	.5773	39	Y	1.40000E-05	.3779
40	Zr	8.18000E-05	.1562	41	Nb	2.62000E-04	.0874
42	Mo	7.58000E-04	.0514	43	Tc	6.80000E-05	.1715
44	Ru	2.00000E-06	1.0000	64	Gd	8.20000E-05	.1562
65	Tb	2.80000E-05	.2672	66	Dy	1.80000E-05	.3333
67	Ho	1.00000E-05	.4472	68	Er	1.60000E-05	.3536
69	Tm	1.00000E-05	.4472	70	Yb	1.20000E-05	.4082
71	Lu	2.00000E-05	.3162	72	Hf	3.60000E-05	.2357
73	Ta	5.98000E-05	.1826	74	W	2.00000E-05	.3162
75	Re	1.40000E-05	.3780	76	Os	1.04000E-04	.1387
77	Ir	1.94000E-03	.0321	78	Pt	1.95520E-02	.0101
79	Au	2.13760E-02	.0096	80	Hg	8.58684E-02	.0048

81	Tl	2.65929E-01	.0027	82	Pb	9.14959E-01	.0015
83	Bi	8.20049E-01	.0017	84	Po	8.87040E-02	.0047
85	At	8.33800E-04	.0490				

mean weight of residual nuclei per incident proton: 2.37023 (.0013)

Table 5.1c: Spallation products (per proton) in a Pb/Bi target
nuclides immediately preceding fission as function of Z
Proton beam: 2d Gaussian distribution
($\sigma_x = 2.12cm$, $\sigma_y = 3.58cm$), E_p =570MeV

Z		mean value of number of nuclei	statistical error	Z		mean value of number of nuclei	statistical error
71	Lu	8.00000E-06	.5000	72	Hf	1.00000E-05	.4472
73	Ta	1.60000E-05	.3536	74	W	2.40000E-05	.2887
75	Re	3.60000E-05	.2357	76	Os	6.40000E-05	.1768
77	Ir	1.86000E-04	.1037	78	Pt	5.82000E-04	.0586
79	Au	8.18000E-04	.0494	80	Hg	3.35380E-03	.0244
81	Tl	5.17940E-03	.0196	82	Pb	1.05326E-02	.0138
83	Bi	1.51486E-02	.0115	84	Po	1.19492E-02	.0129
85	At	1.78000E-04	.1060				

mean weight of residual nuclei per incident proton: $4.80856 \cdot 10^{-2}$ (.0063)

In Table 5.2 the spallation products are given per isotope. The total number of different final residual nuclei is calculated to be 1765.
The result for the total (statistical) weight of all residual nuclei (spallation products) is 2.41791 (.0056)
In Tables 5.2 only those spallation products are included whose fraction of the total statistical weight of all spallation products exceeds 0.00005. This reduced number of spallation products is 535, the sum of their statistical weights is 2.38425 (.0055).

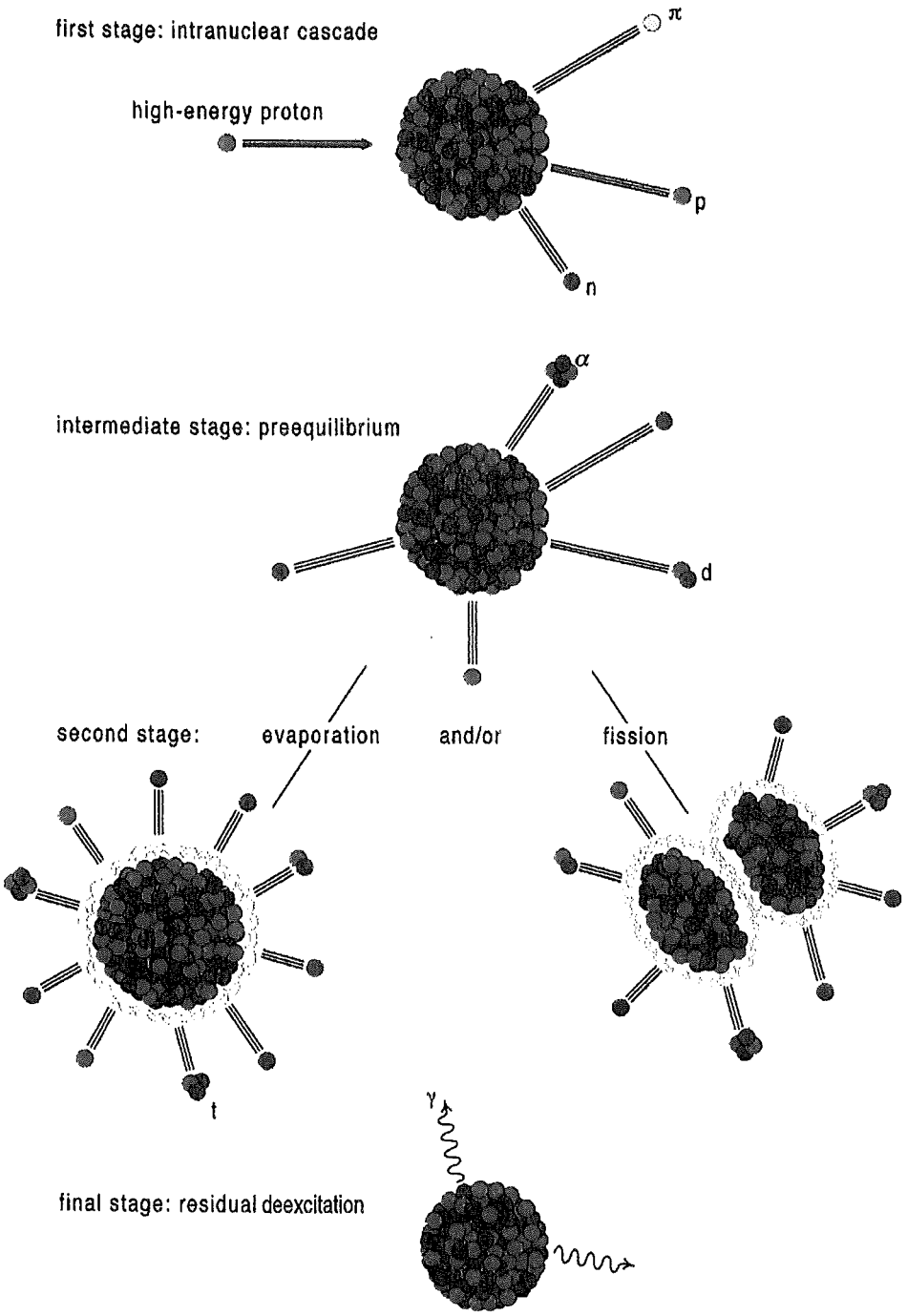

Figure 5.1: Schematic view of the interactions involved in the spallation process taken from [18]

Table 5.2: Spallation products (per proton) in a Pb/Bi target
final residual nuclei as function Z and A
Proton beam: 2d Gaussian distribution (σ_x=2.12cm, σ_y=3.58cm), E_p = 570MeV

Z (symbol)	A	mean weight	error	Z (symbol)	A	mean weight	error
13 (Al)	27	1.60000E-04	.1118	16 (S)	34	1.90000E-04	.1026
17 (Cl)	35	1.50000E-04	.1155	17 (Cl)	36	2.58000E-04	.0880
17 (Cl)	37	1.40000E-04	.1195	18 (Ar)	37	2.06000E-04	.0985
18 (Ar)	38	5.02000E-04	.0631	19 (K)	39	3.16000E-04	.0795
19 (K)	40	4.00000E-04	.0707	19 (K)	41	3.00000E-04	.0816
20 (Ca)	41	3.88000E-04	.0718	20 (Ca)	42	8.43800E-04	.0487
20 (Ca)	43	7.72000E-04	.0509	20 (Ca)	44	5.54989E-04	.0600
20 (Ca)	45	1.23764E-04	.1270	21 (Sc)	44	8.03600E-04	.0499
21 (Sc)	45	1.19160E-03	.0410	21 (Sc)	46	5.93600E-04	.0580
21 (Sc)	47	4.33311E-04	.0679	21 (Sc)	48	1.44000E-04	.1195
22 (Ti)	45	2.20000E-04	.0953	22 (Ti)	46	1.92180E-03	.0322
22 (Ti)	47	2.09304E-03	.0310	22 (Ti)	48	2.02959E-03	.0314
22 (Ti)	49	5.74000E-04	.0590	22 (Ti)	50	4.75800E-04	.0648
23 (V)	47	2.40000E-04	.0913	23 (V)	48	2.12760E-03	.0307
23 (V)	49	3.84680E-03	.0229	23 (V)	50	3.81919E-03	.0229
23 (V)	51	3.24200E-03	.0249	23 (V)	52	4.26000E-04	.0685
24 (Cr)	49	4.80000E-04	.0645	24 (Cr)	50	4.68138E-03	.0208
24 (Cr)	51	7.75376E-03	.0162	24 (Cr)	52	9.87380E-03	.0143
24 (Cr)	53	2.39000E-03	.0289	24 (Cr)	54	1.16200E-03	.0415
24 (Cr)	55	1.60000E-04	.1132	25 (Mn)	51	4.22000E-04	.0688
25 (Mn)	52	3.63157E-03	.0236	25 (Mn)	53	1.12591E-02	.0134
25 (Mn)	54	1.48306E-02	.0117	25 (Mn)	55	1.39489E-02	.0120
25 (Mn)	56	1.11400E-03	.0423	25 (Mn)	57	1.56000E-04	.1132
26 (Fe)	53	7.12000E-04	.0531	26 (Fe)	54	9.46140E-03	.0146
26 (Fe)	55	2.02910E-02	.0101	26 (Fe)	56	1.57790E-02	.0115
26 (Fe)	57	4.04000E-04	.0703	27 (Co)	55	1.24000E-04	.1270
27 (Co)	56	2.08000E-04	.0980	27 (Co)	59	1.22000E-04	.1280
27 (Co)	63	1.52000E-04	.1147				

Table 5.2 continued: Spallation products (per proton) in a Pb/Bi target
Proton beam: 2d Gaussian distribution (σ_x=2.12cm, σ_y=3.58cm), $E_p = 570$MeV

Z (symbol)	A	mean weight	error	Z (symbol)	A	mean weight	error
28 (Ni)	62	1.40000E-04	.1195	28 (Ni)	64	1.54000E-04	.1140
28 (Ni)	66	1.38000E-04	.1204	28 (Ni)	68	1.22000E-04	.1280
29 (Cu)	63	1.40000E-04	.1195	29 (Cu)	64	1.26000E-04	.1260
29 (Cu)	65	1.66000E-04	.1098	29 (Cu)	67	1.54000E-04	.1140
29 (Cu)	68	1.38000E-04	.1204	29 (Cu)	69	1.64000E-04	.1104
29 (Cu)	71	1.48000E-04	.1162	30 (Zn)	66	2.22000E-04	.0949
30 (Zn)	68	1.50000E-04	.1155	30 (Zn)	69	1.36000E-04	.1213
30 (Zn)	70	2.04000E-04	.0990	30 (Zn)	72	2.12000E-04	.0971
30 (Zn)	74	1.56000E-04	.1132	31 (Ga)	68	1.38000E-04	.1204
31 (Ga)	69	1.80000E-04	.1054	31 (Ga)	70	1.70000E-04	.1085
31 (Ga)	71	2.00000E-04	.1000	31 (Ga)	72	1.44000E-04	.1178
31 (Ga)	73	1.80000E-04	.1054	31 (Ga)	74	1.42000E-04	.1187
31 (Ga)	75	1.75800E-04	.1066	31 (Ga)	77	1.40000E-04	.1195
32 (Ge)	70	2.09800E-04	.0976	32 (Ge)	71	1.58000E-04	.1125
32 (Ge)	72	2.30000E-04	.0932	32 (Ge)	73	1.80000E-04	.1054
32 (Ge)	74	2.52000E-04	.0891	32 (Ge)	75	1.68000E-04	.1091
32 (Ge)	76	2.44000E-04	.0905	32 (Ge)	77	1.70000E-04	.1085
32 (Ge)	78	1.64000E-04	.1104	32 (Ge)	80	1.42000E-04	.1187
33 (As)	72	1.44000E-04	.1178	33 (As)	73	1.94000E-04	.1015
33 (As)	74	2.02000E-04	.0995	33 (As)	75	2.70000E-04	.0861
33 (As)	76	1.58000E-04	.1125	33 (As)	77	2.98000E-04	.0819
33 (As)	78	1.84000E-04	.1042	33 (As)	79	2.50000E-04	.0894
33 (As)	80	1.48000E-04	.1162	33 (As)	81	1.54000E-04	.1140
33 (As)	83	1.34000E-04	.1222	34 (Se)	74	1.94000E-04	.1015
34 (Se)	75	1.46000E-04	.1170	34 (Se)	76	3.02000E-04	.0814
34 (Se)	77	1.90000E-04	.1026	34 (Se)	78	2.99800E-04	.0816
34 (Se)	79	2.42000E-04	.0909	34 (Se)	80	3.05800E-04	.0808
34 (Se)	81	1.87800E-04	.1031	34 (Se)	82	2.32000E-04	.0928
34 (Se)	83	1.71800E-04	.1078	34 (Se)	84	2.36000E-04	.0920

Table 5.2 continued: Spallation products (per proton) in a Pb/Bi target
Proton beam: 2d Gaussian distribution (σ_x=2.12cm, σ_y=3.58cm), E_p = 570MeV

Z (symbol)	A	mean weight	error	Z (symbol)	A	mean weight	error
35 (Br)	76	1.38000E-04	.1204	35 (Br)	77	1.56000E-04	.1132
35 (Br)	78	1.70000E-04	.1085	35 (Br)	79	2.82000E-04	.0842
35 (Br)	80	2.08000E-04	.0980	35 (Br)	81	3.06000E-04	.0808
35 (Br)	82	2.42000E-04	.0909	35 (Br)	83	3.84000E-04	.0722
35 (Br)	84	3.14000E-04	.0798	35 (Br)	85	2.82000E-04	.0842
35 (Br)	86	1.84000E-04	.1042	35 (Br)	87	1.26000E-04	.1260
36 (Kr)	78	1.42000E-04	.1187	36 (Kr)	79	1.90000E-04	.1026
36 (Kr)	80	2.64000E-04	.0870	36 (Kr)	81	2.56000E-04	.0884
36 (Kr)	82	3.84000E-04	.0725	36 (Kr)	83	2.72000E-04	.0857
36 (Kr)	84	4.04000E-04	.0703	36 (Kr)	85	2.82000E-04	.0842
36 (Kr)	86	4.20000E-04	.0690	36 (Kr)	87	2.26000E-04	.0941
36 (Kr)	88	2.52000E-04	.0891	36 (Kr)	89	1.56000E-04	.1132
37 (Rb)	81	1.74000E-04	.1072	37 (Rb)	82	2.14000E-04	.0967
37 (Rb)	83	2.80000E-04	.0845	37 (Rb)	84	2.62000E-04	.0874
37 (Rb)	85	3.94000E-04	.0712	37 (Rb)	86	3.56000E-04	.0749
37 (Rb)	87	4.47800E-04	.0668	37 (Rb)	88	3.07800E-04	.0806
37 (Rb)	89	3.33800E-04	.0774	37 (Rb)	90	1.96000E-04	.1010
37 (Rb)	91	2.18000E-04	.0958	37 (Rb)	92	1.54000E-04	.1140
38 (Sr)	83	1.72000E-04	.1078	38 (Sr)	84	3.02000E-04	.0814
38 (Sr)	85	2.58000E-04	.0880	38 (Sr)	86	4.28000E-04	.0683
38 (Sr)	87	3.76000E-04	.0729	38 (Sr)	88	4.82000E-04	.0644
38 (Sr)	89	2.98000E-04	.0819	38 (Sr)	90	3.60000E-04	.0745
38 (Sr)	91	2.48000E-04	.0898	38 (Sr)	92	3.06000E-04	.0808
38 (Sr)	93	1.50000E-04	.1155	38 (Sr)	94	2.00000E-04	.1000
39 (Y)	85	1.22000E-04	.1280	39 (Y)	86	1.66000E-04	.1098
39 (Y)	87	2.74000E-04	.0854	39 (Y)	88	3.21800E-04	.0788
39 (Y)	89	4.66000E-04	.0655	39 (Y)	90	3.46000E-04	.0760
39 (Y)	91	4.32000E-04	.0680	39 (Y)	92	3.32000E-04	.0776
39 (Y)	93	3.34000E-04	.0774	39 (Y)	94	2.59800E-04	.0877
39 (Y)	95	2.52000E-04	.0891	39 (Y)	96	1.64000E-04	.1104
39 (Y)	97	1.58000E-04	.1125	39 (Y)	99	1.26000E-04	.1260

Table 5.2 continued: Spallation products (per proton) in a Pb/Bi target
Proton beam: 2d Gaussian distribution (σ_x=2.12cm, σ_y=3.58cm), E_p = 570MeV

Z (symbol)	A	mean weight	error	Z (symbol)	A	mean weight	error
40 (Zr)	87	1.32000E-04	.1231	40 (Zr)	88	2.80000E-04	.0845
40 (Zr)	89	2.93800E-04	.0825	40 (Zr)	90	5.13800E-04	.0624
40 (Zr)	91	3.90000E-04	.0723	40 (Zr)	92	4.60000E-04	.0659
40 (Zr)	93	3.72000E-04	.0733	40 (Zr)	94	4.46000E-04	.0672
40 (Zr)	95	3.44000E-04	.0767	40 (Zr)	96	3.21800E-04	.0788
40 (Zr)	97	2.40000E-04	.0913	40 (Zr)	98	2.34000E-04	.0924
40 (Zr)	100	1.42000E-04	.1187	41 (Nb)	90	1.36000E-04	.1213
41 (Nb)	91	3.22000E-04	.0788	41 (Nb)	92	2.68000E-04	.0864
41 (Nb)	93	3.56000E-04	.0749	41 (Nb)	94	4.10000E-04	.0708
41 (Nb)	95	4.08000E-04	.0703	41 (Nb)	96	4.38000E-04	.0682
41 (Nb)	97	3.86000E-04	.0727	41 (Nb)	98	3.12000E-04	.0811
41 (Nb)	99	2.94000E-04	.0825	41 (Nb)	100	1.74000E-04	.1072
41 (Nb)	101	2.00000E-04	.1000	41 (Nb)	103	1.30000E-04	.1240
42 (Mo)	92	2.48000E-04	.0898	42 (Mo)	93	2.34000E-04	.0924
42 (Mo)	94	4.49800E-04	.0667	42 (Mo)	95	4.60000E-04	.0659
42 (Mo)	96	6.24000E-04	.0566	42 (Mo)	97	4.38000E-04	.0679
42 (Mo)	98	5.63800E-04	.0604	42 (Mo)	99	2.74000E-04	.0867
42 (Mo)	100	4.08000E-04	.0710	42 (Mo)	101	2.54000E-04	.0901
42 (Mo)	102	2.94000E-04	.0830	42 (Mo)	103	1.66000E-04	.1098
42 (Mo)	104	1.75800E-04	.1066	43 (Tc)	95	1.90000E-04	.1026
43 (Tc)	96	1.96000E-04	.1010	43 (Tc)	97	3.28000E-04	.0781
43 (Tc)	98	3.10000E-04	.0803	43 (Tc)	99	4.16000E-04	.0693
43 (Tc)	100	3.02000E-04	.0814	43 (Tc)	101	4.34000E-04	.0679
43 (Tc)	102	2.86000E-04	.0836	43 (Tc)	103	3.46000E-04	.0760
43 (Tc)	104	2.32000E-04	.0928	43 (Tc)	105	3.08000E-04	.0806
43 (Tc)	107	1.58000E-04	.1125	43 (Tc)	109	1.26000E-04	.1260

Table 5.2 continued: Spallation products (per proton) in a Pb/Bi target
Proton beam: 2d Gaussian distribution (σ_x=2.12cm, σ_y=3.58cm), E_p = 570MeV

Z (symbol)	A	mean weight	error	Z (symbol)	A	mean weight	error
44 (Ru)	96	1.24000E-04	.1270	44 (Ru)	97	1.42000E-04	.1187
44 (Ru)	98	2.60000E-04	.0877	44 (Ru)	99	2.40000E-04	.0913
44 (Ru)	100	4.08000E-04	.0700	44 (Ru)	101	3.32000E-04	.0776
44 (Ru)	102	4.13800E-04	.0695	44 (Ru)	103	3.08000E-04	.0806
44 (Ru)	104	4.06000E-04	.0702	44 (Ru)	105	2.42000E-04	.0909
44 (Ru)	106	2.88000E-04	.0833	44 (Ru)	107	1.50000E-04	.1155
44 (Ru)	108	2.16000E-04	.0962	45 (Rh)	99	1.42000E-04	.1187
45 (Rh)	100	1.60000E-04	.1118	45 (Rh)	101	3.22000E-04	.0788
45 (Rh)	102	2.90000E-04	.0830	45 (Rh)	103	3.50000E-04	.0756
45 (Rh)	104	3.02000E-04	.0814	45 (Rh)	105	4.33600E-04	.0679
45 (Rh)	106	3.50000E-04	.0756	45 (Rh)	107	3.68000E-04	.0737
45 (Rh)	108	2.22000E-04	.0949	45 (Rh)	109	2.44000E-04	.0905
45 (Rh)	110	1.66000E-04	.1098	45 (Rh)	111	1.54000E-04	.1140
46 (Pd)	102	1.94000E-04	.1015	46 (Pd)	103	2.06000E-04	.0985
46 (Pd)	104	2.47800E-04	.0898	46 (Pd)	105	2.90000E-04	.0830
46 (Pd)	106	3.78000E-04	.0727	46 (Pd)	107	2.82000E-04	.0842
46 (Pd)	108	3.86000E-04	.0720	46 (Pd)	109	2.68000E-04	.0864
46 (Pd)	110	3.12000E-04	.0801	46 (Pd)	111	1.94000E-04	.1015
46 (Pd)	112	2.18000E-04	.0958	46 (Pd)	113	1.24000E-04	.1270
46 (Pd)	114	1.44000E-04	.1178	47 (Ag)	105	2.04000E-04	.0990
47 (Ag)	106	1.68000E-04	.1091	47 (Ag)	107	3.04000E-04	.0811
47 (Ag)	108	2.40000E-04	.0913	47 (Ag)	109	3.89600E-04	.0716
47 (Ag)	110	2.62000E-04	.0874	47 (Ag)	111	2.55800E-04	.0884
47 (Ag)	112	2.02000E-04	.0995	47 (Ag)	113	2.32000E-04	.0928
47 (Ag)	114	1.78000E-04	.1060	47 (Ag)	115	1.64000E-04	.1104
48 (Cd)	106	1.22000E-04	.1280	48 (Cd)	107	1.67800E-04	.1091
48 (Cd)	108	2.36000E-04	.0920	48 (Cd)	109	2.22000E-04	.0949
48 (Cd)	110	3.28000E-04	.0781	48 (Cd)	111	2.42000E-04	.0909
48 (Cd)	112	3.33800E-04	.0774	48 (Cd)	113	2.58000E-04	.0880
48 (Cd)	114	3.07600E-04	.0806	48 (Cd)	115	1.78000E-04	.1060
48 (Cd)	116	2.58000E-04	.0880	48 (Cd)	117	1.42000E-04	.1187
48 (Cd)	118	1.42000E-04	.1187				

Table 5.2 continued: Spallation products (per proton) in a Pb/Bi target
Proton beam: 2d Gaussian distribution (σ_x=2.12cm, σ_y=3.58cm), E_p = 570MeV

Z (symbol)	A	mean weight	error	Z (symbol)	A	mean weight	error
49 (In)	110	1.44000E-04	.1178	49 (In)	111	1.86000E-04	.1037
49 (In) •	112	2.32000E-04	.0928	49 (In)	113	2.48000E-04	.0898
49 (In)	114	2.56000E-04	.0884	49 (In)	115	2.76000E-04	.0851
49 (In)	116	1.76000E-04	.1066	49 (In)	117	2.04000E-04	.0990
49 (In)	118	1.84000E-04	.1042	49 (In)	119	1.56000E-04	.1132
50 (Sn)	112	1.76000E-04	.1066	50 (Sn)	113	1.43800E-04	.1179
50 (Sn)	114	2.30000E-04	.0932	50 (Sn)	115	1.98000E-04	.1005
50 (Sn)	116	2.43800E-04	.0905	50 (Sn)	117	1.70000E-04	.1085
50 (Sn)	118	2.28000E-04	.0936	50 (Sn)	119	1.47800E-04	.1162
50 (Sn)	120	1.86000E-04	.1037	50 (Sn)	121	1.38000E-04	.1204
51 (Sb)	115	1.46000E-04	.1170	51 (Sb)	116	1.52000E-04	.1147
51 (Sb)	117	1.96000E-04	.1010	51 (Sb)	118	1.68000E-04	.1091
51 (Sb)	119	2.36000E-04	.0920	51 (Sb)	120	1.78000E-04	.1060
51 (Sb)	121	2.32000E-04	.0928	51 (Sb)	122	1.44000E-04	.1178
51 (Sb)	123	1.84000E-04	.1042	52 (Te)	118	1.86000E-04	.1037
52 (Te)	120	2.10000E-04	.0976	52 (Te)	121	1.44000E-04	.1178
52 (Te)	122	1.94000E-04	.1015	52 (Te)	123	1.56000E-04	.1132
52 (Te)	124	1.92000E-04	.1021	52 (Te)	125	1.35800E-04	.1213
52 (Te)	126	1.34000E-04	.1222	53 (I)	120	1.26000E-04	.1260
53 (I)	121	1.58000E-04	.1125	53 (I)	122	1.46000E-04	.1170
53 (I)	123	1.74000E-04	.1072	53 (I)	124	1.78000E-04	.1060
53 (I)	125	2.34000E-04	.0924	53 (I)	126	1.22000E-04	.1280
53 (I)	127	1.52000E-04	.1147	53 (I)	128	1.22000E-04	.1280
53 (I)	129	1.24000E-04	.1270	54 (Xe)	124	1.28000E-04	.1250
54 (Xe)	126	1.46000E-04	.1170	54 (Xe)	128	1.46000E-04	.1170
55 (Cs)	129	1.22000E-04	.1280	71 (Lu)	166	1.42000E-04	.1187
71 (Lu)	168	1.28000E-04	.1250	71 (Lu)	169	1.52000E-04	.1147

Table 5.2 continued: Spallation products (per proton) in a Pb/Bi target
Proton beam: 2d Gaussian distribution (σ_x=2.12cm, σ_y=3.58cm), E_p = 570MeV

Z (symbol)	A	mean weight	error	Z (symbol)	A	mean weight	error
72 (Hf)	166	1.68000E-04	.1091	72 (Hf)	167	2.38000E-04	.0917
72 (Hf)	168	3.22000E-04	.0788	72 (Hf)	169	2.14000E-04	.0967
72 (Hf)	170	1.96000E-04	.1010	72 (Hf)	171	1.38000E-04	.1204
72 (Hf)	172	1.44000E-04	.1178	73 (Ta)	168	1.58000E-04	.1125
73 (Ta)	169	3.74000E-04	.0731	73 (Ta)	170	3.94000E-04	.0712
73 (Ta)	171	6.02000E-04	.0576	73 (Ta)	172	4.78000E-04	.0647
73 (Ta)	173	5.16000E-04	.0622	73 (Ta)	174	3.08000E-04	.0806
73 (Ta)	175	2.58000E-04	.0880	74 (W)	171	2.88000E-04	.0833
74 (W)	172	6.50000E-04	.0555	74 (W)	173	7.58000E-04	.0513
74 (W)	174	1.02800E-03	.0441	74 (W)	175	6.68000E-04	.0547
74 (W)	176	6.02000E-04	.0576	74 (W)	177	3.36000E-04	.0771
74 (W)	178	2.54000E-04	.0887	74 (W)	179	1.60000E-04	.1118
75 (Re)	173	2.98000E-04	.0819	75 (Re)	174	5.74000E-04	.0590
75 (Re)	175	1.12200E-03	.0422	75 (Re)	176	1.26000E-03	.0398
75 (Re)	177	1.61200E-03	.0352	75 (Re)	178	1.18600E-03	.0410
75 (Re)	179	1.07380E-03	.0431	75 (Re)	180	5.96000E-04	.0579
75 (Re)	181	4.78000E-04	.0647	75 (Re)	182	1.50000E-04	.1155
75 (Re)	183	1.54000E-04	.1140	76 (Os)	175	3.08000E-04	.0806
76 (Os)	176	8.96000E-04	.0472	76 (Os)	177	1.15600E-03	.0416
76 (Os)	178	2.48800E-03	.0283	76 (Os)	179	2.22200E-03	.0300
76 (Os)	180	2.71400E-03	.0271	76 (Os)	181	2.02780E-03	.0314
76 (Os)	182	1.96800E-03	.0318	76 (Os)	183	1.04180E-03	.0438
76 (Os)	184	6.88000E-04	.0539	76 (Os)	185	4.49600E-04	.0667
76 (Os)	186	2.46000E-04	.0902	77 (Ir)	177	2.24000E-04	.0945
77 (Ir)	178	5.42000E-04	.0607	77 (Ir)	179	1.21600E-03	.0405
77 (Ir)	180	2.00000E-03	.0316	77 (Ir)	181	3.42980E-03	.0241
77 (Ir)	182	3.07600E-03	.0255	77 (Ir)	183	4.17800E-03	.0218
77 (Ir)	184	3.01580E-03	.0257	77 (Ir)	185	3.22000E-03	.0249
77 (Ir)	186	1.19600E-03	.0409	77 (Ir)	187	1.69800E-03	.0343
77 (Ir)	188	6.94000E-04	.0537	77 (Ir)	189	3.83800E-04	.0722
77 (Ir)	190	1.74000E-04	.1072				

Table 5.2 continued: Spallation products (per proton) in a Pb/Bi target
Proton beam: 2d Gaussian distribution (σ_x=2.12cm, σ_y=3.58cm), E_p = 570MeV

Z (symbol)	A	mean weight	error	Z (symbol)	A	mean weight	error
78 (Pt)	180	4.78000E-04	.0647	78 (Pt)	181	9.64000E-04	.0455
78 (Pt)	182	2.47800E-03	.0284	78 (Pt)	183	3.41800E-03	.0241
78 (Pt)	184	5.89400E-03	.0184	78 (Pt)	185	5.27000E-03	.0194
78 (Pt)	186	7.36740E-03	.0164	78 (Pt)	187	5.62380E-03	.0188
78 (Pt)	188	3.53600E-03	.0237	78 (Pt)	189	3.59980E-03	.0235
78 (Pt)	190	2.58800E-03	.0278	78 (Pt)	191	1.08780E-03	.0429
78 (Pt)	192	7.42000E-04	.0520	78 (Pt)	193	2.98000E-04	.0819
78 (Pt)	194	2.54000E-04	.0887	79 (Au)	183	2.14000E-04	.0967
79 (Au)	184	6.24000E-04	.0566	79 (Au)	185	1.83600E-03	.0330
79 (Au)	186	2.24600E-03	.0298	79 (Au)	187	3.64400E-03	.0234
79 (Au)	188	3.92760E-03	.0225	79 (Au)	189	4.97160E-03	.0200
79 (Au)	190	2.34000E-03	.0292	79 (Au)	191	4.43980E-03	.0212
79 (Au)	192	3.01320E-03	.0257	79 (Au)	193	2.67500E-03	.0273
79 (Au)	194	1.65800E-03	.0347	79 (Au)	195	1.53580E-03	.0361
79 (Au)	196	9.48000E-04	.0459	79 (Au)	197	8.80000E-04	.0477
79 (Au)	198	5.80000E-04	.0587	79 (Au)	199	5.30000E-04	.0614
79 (Au)	200	3.60000E-04	.0745	79 (Au)	201	3.28000E-04	.0781
79 (Au)	202	1.86000E-04	.1037	79 (Au)	203	1.80000E-04	.1054
80 (Hg)	184	1.70000E-04	.1085	80 (Hg)	185	4.94000E-04	.0636
80 (Hg)	186	1.63200E-03	.0350	80 (Hg)	187	2.39380E-03	.0289
80 (Hg)	188	4.87340E-03	.0202	80 (Hg)	189	5.65160E-03	.0188
80 (Hg)	190	8.91380E-03	.0149	80 (Hg)	191	8.59520E-03	.0152
80 (Hg)	192	6.71520E-03	.0172	80 (Hg)	193	9.32620E-03	.0146
80 (Hg)	194	1.04072E-02	.0138	80 (Hg)	195	7.66598E-03	.0161
80 (Hg)	196	7.92840E-03	.0159	80 (Hg)	197	5.30180E-03	.0194
80 (Hg)	198	6.13340E-03	.0180	80 (Hg)	199	4.06380E-03	.0222
80 (Hg)	200	4.49920E-03	.0211	80 (Hg)	201	3.31580E-03	.0245
80 (Hg)	202	3.47980E-03	.0240	80 (Hg)	203	2.43800E-03	.0286
80 (Hg)	204	2.62340E-03	.0276	80 (Hg)	205	1.26380E-03	.0398
80 (Hg)	206	7.94000E-04	.0502				

Table 5.2 continued: Spallation products (per proton) in a Pb/Bi target
Proton beam: 2d Gaussian distribution (σ_x=2.12cm, σ_y=3.58cm), E_p = 570MeV

Z (symbol)	A	mean weight	error	Z (symbol)	A	mean weight	error
81 (Tl)	187	1.88000E-04	.1031	81 (Tl)	188	4.80000E-04	.0645
81 (Tl)	189	1.23560E-03	.0402	81 (Tl)	190	1.75360E-03	.0337
81 (Tl)	191	3.61580E-03	.0235	81 (Tl)	192	4.90320E-03	.0201
81 (Tl)	193	9.00660E-03	.0149	81 (Tl)	194	4.67740E-03	.0206
81 (Tl)	195	1.48645E-02	.0116	81 (Tl)	196	1.30715E-02	.0123
81 (Tl)	197	1.69618E-02	.0108	81 (Tl)	198	1.47842E-02	.0116
81 (Tl)	199	1.87558E-02	.0103	81 (Tl)	200	1.52306E-02	.0115
81 (Tl)	201	1.95652E-02	.0101	81 (Tl)	202	1.80796E-02	.0105
81 (Tl)	203	2.19284E-02	.0096	81 (Tl)	204	2.06286E-02	.0099
81 (Tl)	205	2.67314E-02	.0087	81 (Tl)	206	2.12262E-02	.0097
81 (Tl)	207	1.62560E-02	.0111	82 (Pb)	190	2.82000E-04	.0842
82 (Pb)	191	4.70000E-04	.0652	82 (Pb)	192	1.61000E-03	.0352
82 (Pb)	193	2.83400E-03	.0265	82 (Pb)	194	6.33740E-03	.0177
82 (Pb)	195	8.46900E-03	.0153	82 (Pb)	196	7.95820E-03	.0158
82 (Pb)	197	1.58090E-02	.0112	82 (Pb)	198	2.48546E-02	.0090
82 (Pb)	199	2.59498E-02	.0088	82 (Pb)	200	3.82954E-02	.0073
82 (Pb)	201	4.03132E-02	.0071	82 (Pb)	202	6.53732E-02	.0056
82 (Pb)	203	7.32354E-02	.0053	82 (Pb)	204	1.21473E-01	.0042
82 (Pb)	205	1.20196E-01	.0042	82 (Pb)	206	1.50559E-01	.0038
82 (Pb)	207	8.37442E-02	.0050	82 (Pb)	208	7.26694E-02	.0054
82 (Pb)	209	3.82600E-03	.0229	83 (Bi)	194	3.75800E-04	.0729
83 (Bi)	195	1.18400E-03	.0411	83 (Bi)	196	2.27380E-03	.0296
83 (Bi)	197	4.38780E-03	.0213	83 (Bi)	198	5.97580E-03	.0183
83 (Bi)	199	8.06800E-03	.0157	83 (Bi)	200	1.23474E-02	.0127
83 (Bi)	201	2.16052E-02	.0096	83 (Bi)	202	2.50772E-02	.0090
83 (Bi)	203	4.20508E-02	.0069	83 (Bi)	204	4.75050E-02	.0066
83 (Bi)	205	8.29994E-02	.0050	83 (Bi)	206	1.14320E-01	.0043
83 (Bi)	207	1.88666E-01	.0035	83 (Bi)	208	1.01185E-01	.0046
83 (Bi)	209	7.47924E-02	.0056				

Table 5.2 continued: Spallation products (per proton) in a Pb/Bi target
Proton beam: 2d Gaussian distribution (σ_x=2.12cm, σ_y=3.58cm), E_p = 570MeV

Z (symbol)	A	mean weight	error	Z (symbol)	A	mean weight	error
84 (Po)	196	1.84000E-04	.1042	84 (Po)	197	4.38000E-04	.0676
84 (Po)	198	1.01400E-03	.0444	84 (Po)	199	1.37400E-03	.0381
84 (Po)	200	2.36400E-03	.0291	84 (Po)	201	3.05000E-03	.0256
84 (Po)	202	5.11360E-03	.0197	84 (Po)	203	5.63000E-03	.0188
84 (Po)	204	7.85180E-03	.0159	84 (Po)	205	7.34740E-03	.0165
84 (Po)	206	9.08600E-03	.0148	84 (Po)	207	7.29780E-03	.0165
84 (Po)	208	5.85200E-03	.0185	84 (Po)	209	7.58000E-04	.0513

The results of HTAPE are residual nuclides per proton.
The weight in grammes of a nuclide or element produced in 1sec by a proton beam of 1mA, $w(N^{HTAPE})$, is obtained from
$w(N^{HTAPE}) = N^{HTAPE} \cdot A \cdot 1.036402 \cdot 10^{-8}$ [g]
where N^{HTAPE} is the number of nuclides per proton given in the output of HTAPE and A is the mass number

5.2 Nucleons, deuterons, tritons, ^{3}He, α-particles and π-mesons

In the following we give the number of particles produced per proton in the Pb/Bi target described above. The number of nucleons, deuterons, tritons, ^{3}He and α-particles produced in the target is given per primary proton, the mean values of the numbers of particles are given and the statistical errors.

Table 5.3: Particle production in the Pb/Bi target
(nucleons, deuterons, tritons, ^{3}He,
α-particles and π-mesons)

particle	number of particles per proton	
	mean value	statistical error
protons	2.012	(.002)
neutrons	13.15	(.001)
deuteron	$8.982 \cdot 10^{-2}$	(.005)
triton	$4.633 \cdot 10^{-2}$	(.007)
^{3}He	$2.462 \cdot 10^{-3}$	(.037)
α-particles	$2.029 \cdot 10^{-1}$	(.004)
π^+	$2.381 \cdot 10^{-2}$	(.009)
π^0	$2.814 \cdot 10^{-2}$	(.008)
π^-	$1.485 \cdot 10^{-2}$	(.012)

In the following table we give the production of nucleons in the **different zones of the target** shown in Fig. 2.1. This information may be of interest for the choice of the dimensions (radius, height) of the target to be used for the MEGAPIE project.

Table 5.4: Nucleons produced (per proton) in the zones of the Pb/Bi-target. Proton beam: 2d Gaussian distribution (σ_x=2.12cm, σ_y=3.58cm), E_p = 570MeV

zone	volume cm^3	protons	neutrons
3	$3.71336 \cdot 10^2$	$4.872 \cdot 10^{-3}$ (.048)	$6.812 \cdot 10^{-3}$ (.036)
4	$1.53338 \cdot 10^2$	$4.976 \cdot 10^{-2}$ (.018)	$5.490 \cdot 10^{-2}$ (.014)
5	$1.14505 \cdot 10^4$	$1.048 \cdot 10^{-2}$ (.023)	$9.544 \cdot 10^{-2}$ (.015)
6	$4.48594 \cdot 10^3$	$5.295 \cdot 10^{-1}$ (.003)	$2.921 \cdot 10^{0}$ (.003)
7	$9.81105 \cdot 10^2$	$1.990 \cdot 10^{-2}$ (.032)	$3.545 \cdot 10^{-2}$ (.014)
8	$1.95093 \cdot 10^3$	$1.631 \cdot 10^{-3}$ (.121)	$4.503 \cdot 10^{-3}$ (.033)
9	$4.44142 \cdot 10^4$	$3.263 \cdot 10^{-3}$ (.027)	$6.635 \cdot 10^{-2}$ (.013)
10	$3.73077 \cdot 10^4$	$1.983 \cdot 10^{-2}$ (.012)	$3.315 \cdot 10^{-1}$ (.006)
11	$1.68515 \cdot 10^3$	$1.322 \cdot 10^{-1}$ (.011)	$2.160 \cdot 10^{-1}$ (.006)
12	$2.21765 \cdot 10^4$	$1.272 \cdot 10^{-2}$ (.048)	$2.790 \cdot 10^{-2}$ (.014)
13	$3.91863 \cdot 10^3$	$2.000 \cdot 10^{-6}$ (1.00)	$1.200 \cdot 10^{-5}$ (.745)
14	$1.20355 \cdot 10^5$	$2.130 \cdot 10^{-1}$ (.004)	$2.755 \cdot 10^{0}$ (.003)
15	$6.15752 \cdot 10^3$	$9.701 \cdot 10^{-1}$ (.002)	$6.088 \cdot 10^{0}$ (.002)
16	$3.47608 \cdot 10^5$	$4.435 \cdot 10^{-2}$ (.009)	$5.429 \cdot 10^{-1}$ (.007)
17	$6.82438 \cdot 10^4$	$9.200 \cdot 10^{-5}$ (.211)	$9.160 \cdot 10^{-4}$ (.165)

5.3 Calculations with MCNP

In order to get an idea of the contribution of nuclides produced by reactions with neutrons of energy E_n $\leq$**20MeV**, we also carried out an MCNP calculation using the neutron source provided by LAHET. We evaluated the (n,γ)-reaction rate of $^{83}_{209}Bi$ in zones 5,6,9, 10, 14, 15, 16 and 17 of the target shown in Fig. 2.1 in order to get the contribution of $^{83}_{210}Bi$. The (n,γ)-reaction rate of $^{82}_{208}Pb$ and the (n,2n)-reaction rates of ^{209}Bi and of ^{206}Pb were evaluated for the same zones. Table 5.5 gives the production of $^{83}_{210}Bi$, $^{82}_{209}Pb$, $^{83}_{208}Bi$ and $^{82}_{205}Pb$ due to the reactions named above.

Examples for the production of nuclides in reactions initiated by neutrons with energy $E_n \leq$ 20MeV:
mean values and statistical errors are given

Table 5.5: Production of $^{83}_{210}$Bi, $^{82}_{209}$Pb,
$^{83}_{208}$Bi and $^{82}_{205}$Pb in the Pb/Bi target
by neutrons with ($E_n \leq 20$MeV)
mean values are given for the number of nuclides and the statistical errors

Isotope	number of nuclides per proton	
	mean value	statistical error
$^{83}_{210}Bi$	$2.231 \cdot 10^{-3}$	.0027
$^{82}_{209}Pb$	$2.666 \cdot 10^{-4}$	.0040
$^{83}_{208}Bi$	$1.165 \cdot 10^{-2}$	.0044
$^{82}_{205}Pb$	$2.021 \cdot 10^{-3}$	.0046

The total volume of the target is $6.79112 \cdot 10^5 cm^3$, the total weight is $6.87436 \cdot 10^3$kg. The volume taken by Pb/Bi is $6.40023 \cdot 10^5 cm^3$, the weight of the Pb/Bi in the target is $6.63175 \cdot 10^3$kg.

Appendix A

Calculation of Neutron Flux Density Spectra for Different Regions of an Accelerator-Driven System (ADS)

In this part of the report we will discuss the calculation of neutron flux density spectra in different regions (target, inner core region, outer core region, radial blanket) of the accelerator-driven reactor defined in the ADS neutronic benchmark, that was coordinated by the IAEA [3]. The layout of the reactor is given in in Fig. A.1 [2], [22]. Neutron flux density spectra are needed e.g.

- for the calculation of reaction rates
- for the condensation of group constants, especially for the calculation of one group cross sections for burnup calculations
- for the calculation of radiation damage [19].

Again the calculations have been carried out with LCS, [6]. The primary proton energy was 1GeV, the beam profile was parabolic over the beam radius of 10cm.
In the calculations with LCS neutrons that are slowed down below 20MeV are stored on the so called NEUTP file (see [6]) and used as source for the MCNP calculation.
The neutron flux density spectra have been calculated for a 84 energy groups structure, 9 energy groups above 50MeV up to 1GeV and 75 energy groups below 50MeV. The energy group structure below 50MeV is the one of the 75 groups constant set [26] and is also used in section C.2 and in chapter 3. The upper group boundaries of the 84 energy groups structure are shown in columns 2 of Tables A.1-A.4.
Fig. A.2 and Table A.1 show the spectra for the target, in Fig. A.3 and Table A.2 the spectra are given for the inner core region, in Fig. A.4 and Table A.3 for the outer core region. The spectra for the radial blanket are shown in Fig. A.5 and Table A.4.
In the Figures $\phi(u)[n/(cm^2 \cdot sec)]$ is shown versus energy. In order to facilitate comparison of different spectra the following normalization has been chosen for the plots of the spectra:

$$\int_{E_{min}}^{E_{max}} \phi(E)dE \;=\; 1 = \int_{u_{min}}^{u_{max}} \phi(u)du$$

where E_{max} = 1GeV, E_0=1GeV,
and $u_{min} = ln(E_0/E_{max})$ and $u_{max} = ln(E_0/E_{min})$

integral over the group fluxes below 20MeV:

$$\Phi^{MCNP} = \int_{E_{min}}^{E_{cutoff}} \phi(E)dE$$

or as sum over energy groups:

$$\Phi^{MCNP} = \sum_{g=84}^{13} \phi_g$$

integral over the group fluxes above 20MeV:

$$\Phi^{LAHET} = \int_{E_{cutoff}}^{E_{max}} \phi(E)dE$$

or as sum over energy groups:

$$\Phi^{LAHET} = \sum_{g=12}^{1} \phi_g$$

$$\Phi^{total} = \Phi^{MCNP} + \Phi^{LAHET}$$

fraction of flux above E_{cutoff} (E_{cutoff} is 20MeV in the standard case):
$\Phi^{LAHET}/\Phi^{total}$

In the following, volume averaged neutron flux densities are given for the different regions of the reactor shown in Fig. A.1. The neutron flux densities are normalized to a proton current of 1proton/sec. ($6.2418 \cdot 10^{15}$ protons/sec are necessary for a proton current of 1mA).

For the target:
$\Phi^{MCNP} = 8.53197 \cdot 10^{-2}[\frac{n}{cm^2 \cdot sec}]$ for a proton current of 1proton/sec
$\Phi^{LAHET} = 1.69114 \cdot 10^{-3}[\frac{n}{cm^2 \cdot sec}]$ for a proton current of 1proton/sec
$\Phi^{total} = 8.70108 \cdot 10^{-2}[\frac{n}{cm^2 \cdot sec}]$ for a proton current of 1proton/sec
$\Phi^{LAHET}/\Phi^{total} = 1.944 \cdot 10^{-2}$

For the inner core region:
$\Phi^{MCNP} = 1.80567 \cdot 10^{-2}[\frac{n}{cm^2 \cdot sec}]$ for a proton current of 1proton/sec
$\Phi^{LAHET} = 5.17561 \cdot 10^{-6}[\frac{n}{cm^2 \cdot sec}]$ for a proton current of 1proton/sec
$\Phi^{total} = 1.8061876 \cdot 10^{-2}[\frac{n}{cm^2 \cdot sec}]$ for a proton current of 1proton/sec

$\Phi^{LAHET}/\Phi^{total} = 2.865 \cdot 10^{-4}$

For the outer core region:

$\Phi^{MCNP} = 5.96187 \cdot 10^{-3}[\frac{n}{cm^2 \cdot sec}]$ for a proton current of 1proton/sec

$\Phi^{LAHET} = 1.53543 \cdot 10^{-7}[\frac{n}{cm^2 \cdot sec}]$ for a proton current of 1proton/sec

$\Phi^{total} = 5.96202 \cdot 10^{-3}[\frac{n}{cm^2 \cdot sec}]$ for a proton current of 1proton/sec

$\Phi^{LAHET}/\Phi^{total} = 2.575 \cdot 10^{-5}$

For the radial blanket:

$\Phi^{MCNP} = 1.73602 \cdot 10^{-3}[\frac{n}{cm^2 \cdot sec}]$ for a proton current of 1proton/sec

$\Phi^{LAHET} = 9.85819 \cdot 10^{-9}[\frac{n}{cm^2 \cdot sec}]$ for a proton current of 1proton/sec

$\Phi^{total} = 1.73603 \cdot 10^{-3}[\frac{n}{cm^2 \cdot sec}]$ for a proton current of 1proton/sec

$\Phi^{LAHET}/\Phi^{total} = 5.679 \cdot 10^{-6}$

The fraction $\Phi^{LAHET}/\Phi^{total}$ is decreasing with increasing distance from the neutron source. $\Phi^{LAHET}/\Phi^{total}$ is $1.94 \cdot 10^{-2}$ in the target, $2.87 \cdot 10^{-4}$ in the inner core region, $2.58 \cdot 10^{-5}$ in the outer core region and $5.68 \cdot 10^{-6}$ in the radial blanket.

The decrease of the fraction of the neutron flux density above 20MeV ($\Phi^{LAHET}/\Phi^{total}$) with increasing distance from the neutron source may also be observed in Fig. A.4. In Fig. A.4 $\phi(u)$ is shown versus energy for the inner and the outer core regions. The fluxes are normalized to $\int_{u_{min}}^{u_{max}} \phi(u)du = 1$. It is seen in the figure that $\Phi^{LAHET}/\Phi^{total}$ is larger by about a factor of 10 for the inner core region than for the outer core region.

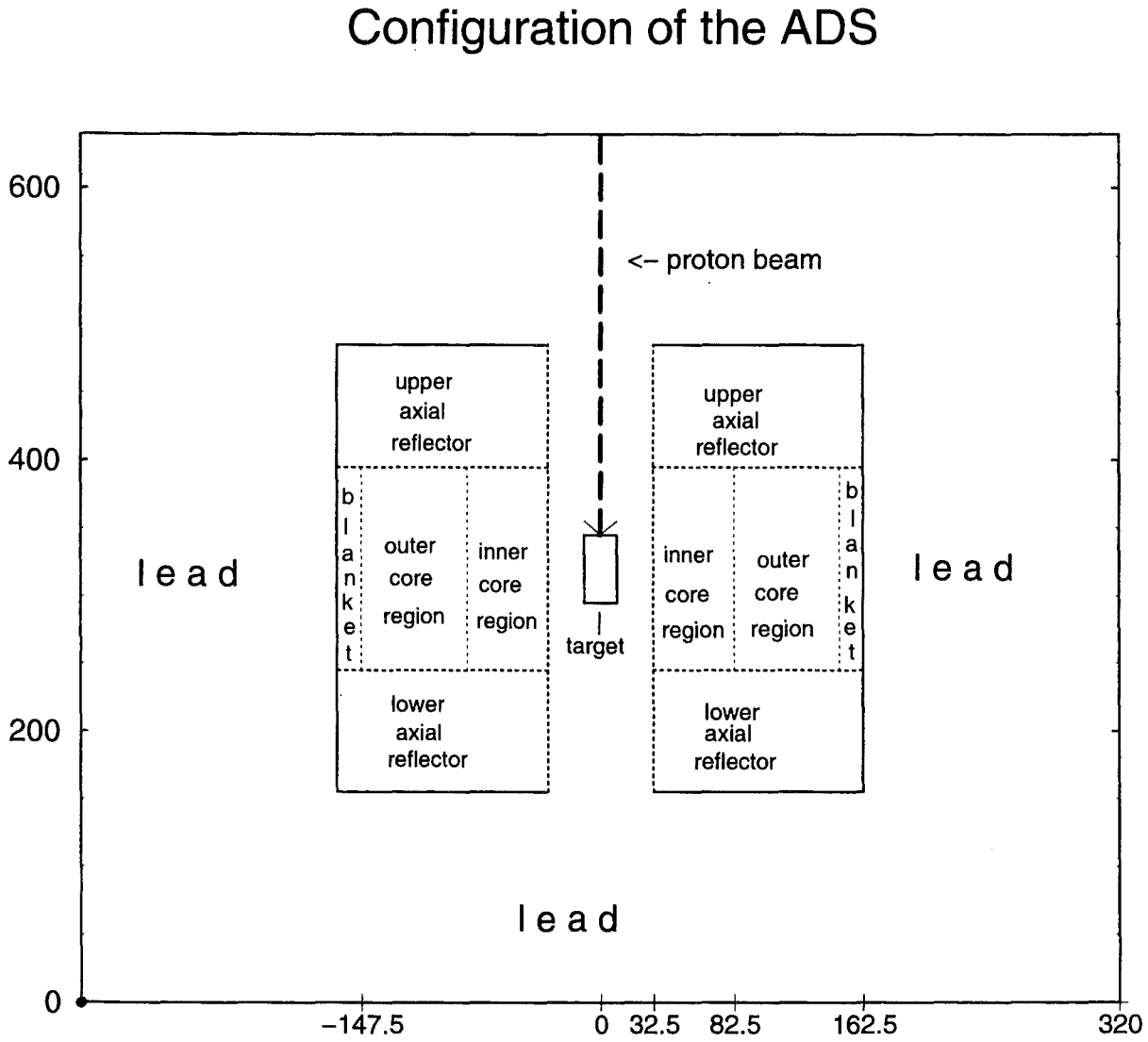

Figure A.1: Layout of the IAEA-ADS benchmark reactor

A.1 Tables of the neutron flux density spectra in target, core-regions and radial blanket of the ADS neutronic benchmark reactor

In the following the neutron flux density spectra in the target and in the core- and blanket regions of the ADS neutronic benchmark reactor are given as tables.
In columns 1 to 3 of the Tables (A.1, A.2, A.3, A.4) the group numbers, g, the upper energy of the group, E_g, and the energy width ΔE are given, columns 4 and 5 give the group fluxes ϕ_g calculated by the MCNP and LAHET codes and the the statistical errors of the Monte Carlo calculations. $\phi(u)$ is calculated from ϕ_g according to formulas 3.7 and 3.9 and is shown in columns 6 of the tables.

Table A.1: Neutron flux density spectra in the target of the IAEA-ADS neutronic benchmark

g	E_g	ΔE	ϕ_g	statistical error	$\phi_g(u)$
84	5.0000E-03	4.9900E-03	1.14928E-19	.0000	5.74641E-20
83	1.0000E-02	5.0000E-03	1.14928E-19	.0000	1.72392E-19
82	1.5000E-02	5.0000E-03	1.14928E-19	.0000	2.87321E-19
81	2.0000E-02	5.0000E-03	1.14928E-19	.0000	4.02249E-19
80	2.5000E-02	5.0000E-03	1.14928E-19	.0000	5.17177E-19
79	3.0000E-02	5.0000E-03	2.36161E-08	1.0000	1.29889E-07
78	3.5000E-02	5.0000E-03	5.44993E-08	1.0000	3.54245E-07
77	4.2000E-02	7.0000E-03	9.72863E-08	1.0000	5.35075E-07
76	5.0000E-02	8.0000E-03	4.85600E-08	1.0000	2.79220E-07
75	5.8000E-02	8.0000E-03	1.93841E-07	.9448	1.30843E-06
74	6.7000E-02	9.0000E-03	3.78724E-07	.9679	2.63003E-06
73	8.0000E-02	1.3000E-02	5.37817E-07	.5773	3.04074E-06
72	1.0000E-01	2.0000E-02	1.23614E-06	.4905	5.56265E-06
71	1.4000E-01	4.0000E-02	5.29616E-07	.5762	1.58885E-06
70	1.8000E-01	4.0000E-02	5.29672E-07	.5368	2.11869E-06
69	2.2000E-01	4.0000E-02	1.44110E-06	.4110	7.20548E-06
68	2.5000E-01	3.0000E-02	1.76045E-06	.3943	1.37902E-05
67	2.8000E-01	3.0000E-02	1.65683E-06	.4108	1.46353E-05
66	3.0000E-01	2.0000E-02	3.65186E-07	.5318	5.29519E-06
65	3.2000E-01	2.0000E-02	6.89301E-07	.5158	1.06842E-05

64	3.5000E-01	3.0000E-02	8.66032E-07	.4596	9.67069E-06
63	4.0000E-01	5.0000E-02	1.43218E-06	.4612	1.07413E-05
62	5.0000E-01	1.0000E-01	3.36483E-06	.3978	1.51418E-05
61	6.2500E-01	1.2500E-01	3.46261E-06	.3006	1.55818E-05
60	7.8000E-01	1.5500E-01	4.52024E-06	.2785	2.04869E-05
59	8.5000E-01	7.0000E-02	8.48100E-07	.3643	9.87431E-06
58	9.1000E-01	6.0000E-02	6.68765E-07	.2849	9.80855E-06
57	9.5000E-01	4.0000E-02	1.78000E-06	.3114	4.13849E-05
56	9.7200E-01	2.2000E-02	5.26496E-07	.3979	2.29984E-05
55	9.9600E-01	2.4000E-02	4.11969E-07	.3659	1.68907E-05
54	1.0200E+00	2.4000E-02	8.91543E-07	.3906	3.74449E-05
53	1.0450E+00	2.5000E-02	3.90997E-07	.4864	1.61482E-05
52	1.0710E+00	2.6000E-02	8.91575E-07	.3632	3.62801E-05
51	1.0970E+00	2.6000E-02	8.45590E-07	.3740	3.52547E-05
50	1.1230E+00	2.6000E-02	1.29594E-06	.3795	5.53270E-05
49	1.1500E+00	2.7000E-02	1.23217E-06	.4186	5.18650E-05
48	1.3000E+00	1.5000E-01	3.97796E-06	.2495	3.24867E-05
47	1.5000E+00	2.0000E-01	5.79346E-06	.2162	4.05542E-05
46	2.1000E+00	6.0000E-01	1.57194E-05	.1802	4.71583E-05
45	2.6000E+00	5.0000E-01	7.45551E-06	.2276	3.50409E-05
44	3.3000E+00	7.0000E-01	9.32841E-06	.1883	3.93126E-05
43	4.0000E+00	7.0000E-01	1.22856E-05	.1597	6.40606E-05
42	9.8770E+00	5.8770E+00	1.08608E-04	.0816	1.28225E-04
41	1.5968E+01	6.0910E+00	1.08735E-04	.0754	2.30690E-04
40	2.7700E+01	1.1732E+01	1.90211E-04	.0563	3.53994E-04
39	4.8052E+01	2.0352E+01	3.35995E-04	.0428	6.25302E-04
38	7.5501E+01	2.7449E+01	4.80608E-04	.0354	1.08165E-03
37	1.4873E+02	7.3229E+01	1.23605E-03	.0240	1.89243E-03
36	3.6726E+02	2.1853E+02	3.51584E-03	.0157	4.15077E-03
35	9.0690E+02	5.3964E+02	7.69289E-03	.0110	9.08196E-03
34	1.4251E+03	5.1820E+02	6.29330E-03	.0103	1.41605E-02
33	2.2395E+03	8.1440E+02	8.61348E-03	.0092	1.93793E-02
32	3.5191E+03	1.2796E+03	1.16981E-02	.0081	2.63225E-02
31	5.5300E+03	2.0109E+03	1.62622E-02	.0073	3.65902E-02
30	9.1180E+03	3.5880E+03	2.31478E-02	.0067	4.72504E-02
29	1.5030E+04	5.9120E+03	2.96689E-02	.0062	6.05925E-02
28	2.4780E+04	9.7500E+03	3.65730E-02	.0059	7.46652E-02
27	4.0850E+04	1.6070E+04	4.93093E-02	.0054	1.00690E-01
26	6.7340E+04	2.6490E+04	5.40089E-02	.0053	1.10291E-01
25	1.1100E+05	4.3660E+04	6.42887E-02	.0051	1.31301E-01
24	1.8300E+05	7.2000E+04	7.81407E-02	.0048	1.59537E-01
23	3.0250E+05	1.1950E+05	9.63377E-02	.0045	1.95698E-01

22	5.0000E+05	1.9750E+05	1.05195E-01	.0044	2.13720E-01
21	8.2100E+05	3.2100E+05	1.22716E-01	.0042	2.52504E-01
20	1.3530E+06	5.3200E+05	9.48501E-02	.0043	1.93801E-01
19	2.2310E+06	8.7800E+05	8.03234E-02	.0043	1.63940E-01
18	3.6790E+06	1.4480E+06	4.80107E-02	.0048	9.79776E-02
17	6.0655E+06	2.3865E+06	2.04824E-02	.0055	4.18166E-02
16	1.0000E+07	3.9345E+06	1.15671E-02	.0065	2.36155E-02
15	1.3800E+07	3.8000E+06	4.94425E-03	.0088	1.54833E-02
14	1.5000E+07	1.2000E+06	1.12271E-03	.0165	1.34725E-02
13	2.0000E+07	5.0000E+06	3.25407E-03	.0101	1.13892E-02
12	2.7100E+07	7.1000E+06	3.11294E-03	.0088	1.03253E-02
11	3.6800E+07	9.7000E+06	2.77377E-03	.0094	9.13629E-03
10	5.0000E+07	1.3200E+07	2.54418E-03	.0098	8.36496E-03
9	6.0000E+07	1.0000E+07	1.36317E-03	.0132	7.49742E-03
8	1.0000E+08	4.0000E+07	3.39395E-03	.0087	6.78791E-03
7	1.5000E+08	5.0000E+07	2.15076E-03	.0110	5.37689E-03
6	2.0000E+08	5.0000E+07	1.21427E-03	.0149	4.24996E-03
5	3.0000E+08	1.0000E+08	1.27673E-03	.0152	3.19182E-03
4	4.0000E+08	1.0000E+08	6.39849E-04	.0228	2.23947E-03
3	5.0000E+08	1.0000E+08	3.55140E-04	.0314	1.59813E-03
2	7.5000E+08	2.5000E+08	4.53206E-04	.0296	1.13301E-03
1	1.0000E+09	2.5000E+08	1.58032E-04	.0541	5.53112E-04

$\Phi^{MCNP} = 8.53197 \cdot 10^{-2} n/(cm^2 \cdot sec)$ for a proton current of 1proton/sec
$\Phi^{LAHET} = 1.69114 \cdot 10^{-3} n/(cm^2 \cdot sec)$ for a proton current of 1proton/sec
$\Phi^{total} = 8.70108 \cdot 10^{-2} n/(cm^2 \cdot sec)$ for a proton current of 1proton/sec
$\Phi^{LAHET}/\Phi^{total} = 1.94360 \cdot 10^{-2}$

Table A.2: Neutron flux density spectra in the inner core region of the IAEA-ADS neutronic benchmark

g	E_g	ΔE	ϕ_g	statistical error	$\phi_g(u)$
84	5.0000E-03	4.9900E-03	5.53652E-19	.0000	2.76826E-19
83	1.0000E-02	5.0000E-03	5.53652E-19	.0000	8.30478E-19
82	1.5000E-02	5.0000E-03	5.53652E-19	.0000	1.38413E-18
81	2.0000E-02	5.0000E-03	5.53652E-19	.0000	1.93778E-18

80	2.5000E-02	5.0000E-03	5.53652E-19	.0000	2.49144E-18
79	3.0000E-02	5.0000E-03	2.42732E-09	.8173	1.33502E-08
78	3.5000E-02	5.0000E-03	1.95978E-10	.8605	1.27386E-09
77	4.2000E-02	7.0000E-03	5.23036E-09	.8846	2.87670E-08
76	5.0000E-02	8.0000E-03	1.01828E-08	.6600	5.85513E-08
75	5.8000E-02	8.0000E-03	1.59622E-08	.5991	1.07745E-07
74	6.7000E-02	9.0000E-03	1.50530E-08	.5339	1.04535E-07
73	8.0000E-02	1.3000E-02	1.74208E-08	.5056	9.84944E-08
72	1.0000E-01	2.0000E-02	7.92659E-08	.2931	3.56696E-07
71	1.4000E-01	4.0000E-02	1.71910E-07	.2166	5.15731E-07
70	1.8000E-01	4.0000E-02	2.61475E-07	.2319	1.04590E-06
69	2.2000E-01	4.0000E-02	2.82467E-07	.1945	1.41234E-06
68	2.5000E-01	3.0000E-02	3.21682E-07	.1732	2.51984E-06
67	2.8000E-01	3.0000E-02	3.43902E-07	.1727	3.03780E-06
66	3.0000E-01	2.0000E-02	2.56404E-07	.1729	3.71785E-06
65	3.2000E-01	2.0000E-02	2.78474E-07	.1958	4.31636E-06
64	3.5000E-01	3.0000E-02	3.85318E-07	.1917	4.30272E-06
63	4.0000E-01	5.0000E-02	5.81490E-07	.1433	4.36117E-06
62	5.0000E-01	1.0000E-01	1.22057E-06	.1052	5.49257E-06
61	6.2500E-01	1.2500E-01	1.44498E-06	.0985	6.50240E-06
60	7.8000E-01	1.5500E-01	2.01109E-06	.0880	9.11479E-06
59	8.5000E-01	7.0000E-02	7.96351E-07	.1316	9.27181E-06
58	9.1000E-01	6.0000E-02	5.54837E-07	.1329	8.13761E-06
57	9.5000E-01	4.0000E-02	3.74648E-07	.1681	8.71057E-06
56	9.7200E-01	2.2000E-02	2.21149E-07	.2191	9.66022E-06
55	9.9600E-01	2.4000E-02	2.10762E-07	.1601	8.64121E-06
54	1.0200E+00	2.4000E-02	1.90774E-07	.1815	8.01254E-06
53	1.0450E+00	2.5000E-02	2.52086E-07	.1930	1.04111E-05
52	1.0710E+00	2.6000E-02	1.71381E-07	.1859	6.97387E-06
51	1.0970E+00	2.6000E-02	1.63487E-07	.1758	6.81619E-06
50	1.1230E+00	2.6000E-02	2.54244E-07	.1765	1.08543E-05
49	1.1500E+00	2.7000E-02	2.42101E-07	.1727	1.01906E-05
48	1.3000E+00	1.5000E-01	8.48450E-07	.1171	6.92901E-06
47	1.5000E+00	2.0000E-01	7.93046E-07	.1029	5.55132E-06
46	2.1000E+00	6.0000E-01	2.02375E-06	.0613	6.07126E-06
45	2.6000E+00	5.0000E-01	4.42109E-06	.0545	2.07791E-05
44	3.3000E+00	7.0000E-01	8.94137E-06	.0511	3.76815E-05
43	4.0000E+00	7.0000E-01	7.17124E-06	.0502	3.73929E-05
42	9.8770E+00	5.8770E+00	4.33561E-05	.0289	5.11871E-05
41	1.5968E+01	6.0910E+00	2.85706E-05	.0321	6.06145E-05
40	2.7700E+01	1.1732E+01	4.71330E-05	.0246	8.77176E-05
39	4.8052E+01	2.0352E+01	1.17128E-04	.0212	2.17981E-04

38	7.5501E+01	2.7449E+01	1.17809E-04	.0187	2.65141E-04
37	1.4873E+02	7.3229E+01	4.04387E-04	.0139	6.19127E-04
36	3.6726E+02	2.1853E+02	1.45160E-03	.0106	1.71375E-03
35	9.0690E+02	5.3964E+02	4.76613E-03	.0092	5.62673E-03
34	1.4251E+03	5.1820E+02	5.05667E-03	.0088	1.13780E-02
33	2.2395E+03	8.1440E+02	8.45012E-03	.0087	1.90117E-02
32	3.5191E+03	1.2796E+03	1.31342E-02	.0086	2.95541E-02
31	5.5300E+03	2.0109E+03	2.06624E-02	.0086	4.64906E-02
30	9.1180E+03	3.5880E+03	3.39042E-02	.0085	6.92068E-02
29	1.5030E+04	5.9120E+03	4.91962E-02	.0085	1.00473E-01
28	2.4780E+04	9.7500E+03	7.03819E-02	.0085	1.43687E-01
27	4.0850E+04	1.6070E+04	6.93998E-02	.0085	1.41715E-01
26	6.7340E+04	2.6490E+04	9.30690E-02	.0085	1.90055E-01
25	1.1100E+05	4.3660E+04	1.05517E-01	.0086	2.15504E-01
24	1.8300E+05	7.2000E+04	1.17543E-01	.0086	2.39983E-01
23	3.0250E+05	1.1950E+05	1.14011E-01	.0086	2.31599E-01
22	5.0000E+05	1.9750E+05	8.82267E-02	.0086	1.79245E-01
21	8.2100E+05	3.2100E+05	1.00872E-01	.0087	2.07558E-01
20	1.3530E+06	5.3200E+05	4.32370E-02	.0088	8.83433E-02
19	2.2310E+06	8.7800E+05	3.30625E-02	.0090	6.74805E-02
18	3.6790E+06	1.4480E+06	1.94156E-02	.0091	3.96224E-02
17	6.0655E+06	2.3865E+06	6.11354E-03	.0094	1.24813E-02
16	1.0000E+07	3.9345E+06	1.28941E-03	.0105	2.63248E-03
15	1.3800E+07	3.8000E+06	1.07574E-04	.0247	3.36877E-04
14	1.5000E+07	1.2000E+06	1.36789E-05	.0776	1.64146E-04
13	2.0000E+07	5.0000E+06	3.96116E-05	.0465	1.38640E-04
12	2.7100E+07	7.1000E+06	5.51862E-05	.0163	1.83047E-04
11	3.6800E+07	9.7000E+06	4.87464E-05	.0175	1.60562E-04
10	5.0000E+07	1.3200E+07	4.32467E-05	.0189	1.42190E-04
9	6.0000E+07	1.0000E+07	2.35562E-05	.0255	1.29559E-04
8	1.0000E+08	4.0000E+07	5.62925E-05	.0171	1.12585E-04
7	1.5000E+08	5.0000E+07	3.03898E-05	.0236	7.59744E-05
6	2.0000E+08	5.0000E+07	1.52578E-05	.0340	5.34024E-05
5	3.0000E+08	1.0000E+08	9.76577E-06	.0422	2.44144E-05
4	4.0000E+08	1.0000E+08	2.68898E-06	.0794	9.41144E-06
3	5.0000E+08	1.0000E+08	1.04275E-06	.1310	4.69236E-06
2	7.5000E+08	2.5000E+08	3.49637E-07	.1876	8.74091E-07
1	1.0000E+09	2.5000E+08	2.59994E-08	.6369	9.09978E-08

$\Phi^{MCNP} = 1.80567 \cdot 10^{-2} n/(cm^2 \cdot sec)$ for a proton current of 1proton/sec

$\Phi^{LAHET} = 5.17561 \cdot 10^{-3} n/(cm^2 \cdot sec)$ for a proton current of 1proton/sec

$\Phi^{total} = 1.80619 \cdot 10^{-2} n/(cm^2 \cdot sec)$ for a proton current of 1proton/sec
$\Phi^{LAHET}/\Phi total = 2.86549 \cdot 10^{-4}$

Table A.3: Neutron flux density spectra in the outer core region of the IAEA-ADS neutronic benchmark

g	E_g	ΔE	ϕ_g	statistical error	$\phi_g(u)$
84	5.0000E-03	4.9900E-03	1.67728E-18	.0000	8.38641E-19
83	1.0000E-02	5.0000E-03	8.65698E-10	.7985	1.29855E-09
82	1.5000E-02	5.0000E-03	5.34488E-09	.4420	1.33622E-08
81	2.0000E-02	5.0000E-03	3.21468E-09	.5156	1.12514E-08
80	2.5000E-02	5.0000E-03	3.07786E-09	.5352	1.38504E-08
79	3.0000E-02	5.0000E-03	1.81068E-09	.5326	9.95873E-09
78	3.5000E-02	5.0000E-03	2.68466E-09	.5247	1.74503E-08
77	4.2000E-02	7.0000E-03	1.45169E-08	.3491	7.98430E-08
76	5.0000E-02	8.0000E-03	1.22729E-08	.2600	7.05693E-08
75	5.8000E-02	8.0000E-03	2.20861E-08	.2409	1.49081E-07
74	6.7000E-02	9.0000E-03	3.07297E-08	.2378	2.13400E-07
73	8.0000E-02	1.3000E-02	6.36604E-08	.1732	3.59926E-07
72	1.0000E-01	2.0000E-02	1.09690E-07	.1382	4.93605E-07
71	1.4000E-01	4.0000E-02	4.09507E-07	.0828	1.22852E-06
70	1.8000E-01	4.0000E-02	5.05446E-07	.0744	2.02178E-06
69	2.2000E-01	4.0000E-02	6.56995E-07	.0680	3.28498E-06
68	2.5000E-01	3.0000E-02	5.63418E-07	.0720	4.41344E-06
67	2.8000E-01	3.0000E-02	5.84183E-07	.0671	5.16028E-06
66	3.0000E-01	2.0000E-02	4.14260E-07	.0798	6.00677E-06
65	3.2000E-01	2.0000E-02	4.24052E-07	.0729	6.57282E-06
64	3.5000E-01	3.0000E-02	7.08451E-07	.0638	7.91103E-06
63	4.0000E-01	5.0000E-02	1.18010E-06	.0535	8.85076E-06
62	5.0000E-01	1.0000E-01	2.71183E-06	.0393	1.22032E-05
61	6.2500E-01	1.2500E-01	3.40624E-06	.0349	1.53281E-05
60	7.8000E-01	1.5500E-01	4.31385E-06	.0321	1.95515E-05
59	8.5000E-01	7.0000E-02	1.82450E-06	.0419	2.12424E-05
58	9.1000E-01	6.0000E-02	1.34705E-06	.0467	1.97567E-05
57	9.5000E-01	4.0000E-02	8.62357E-07	.0525	2.00498E-05
56	9.7200E-01	2.2000E-02	4.48204E-07	.0682	1.95784E-05
55	9.9600E-01	2.4000E-02	5.31643E-07	.0612	2.17973E-05

54	1.0200E+00	2.4000E-02	5.06383E-07	.0687	2.12682E-05
53	1.0450E+00	2.5000E-02	4.45523E-07	.0684	1.84001E-05
52	1.0710E+00	2.6000E-02	5.08958E-07	.0656	2.07106E-05
51	1.0970E+00	2.6000E-02	4.51971E-07	.0661	1.88438E-05
50	1.1230E+00	2.6000E-02	4.32882E-07	.0686	1.84808E-05
49	1.1500E+00	2.7000E-02	4.26115E-07	.0665	1.79363E-05
48	1.3000E+00	1.5000E-01	1.97346E-06	.0384	1.61166E-05
47	1.5000E+00	2.0000E-01	1.89595E-06	.0373	1.32716E-05
46	2.1000E+00	6.0000E-01	4.08719E-06	.0225	1.22616E-05
45	2.6000E+00	5.0000E-01	8.15327E-06	.0217	3.83204E-05
44	3.3000E+00	7.0000E-01	1.55145E-05	.0200	6.53826E-05
43	4.0000E+00	7.0000E-01	1.15329E-05	.0199	6.01360E-05
42	9.8770E+00	5.8770E+00	6.53037E-05	.0125	7.70988E-05
41	1.5968E+01	6.0910E+00	3.62323E-05	.0145	7.68695E-05
40	2.7700E+01	1.1732E+01	5.34792E-05	.0117	9.95281E-05
39	4.8052E+01	2.0352E+01	1.28400E-04	.0104	2.38957E-04
38	7.5501E+01	2.7449E+01	1.09667E-04	.0100	2.46816E-04
37	1.4873E+02	7.3229E+01	3.44224E-04	.0079	5.27015E-04
36	3.6726E+02	2.1853E+02	1.20531E-03	.0061	1.42298E-03
35	9.0690E+02	5.3964E+02	4.17737E-03	.0053	4.93166E-03
34	1.4251E+03	5.1820E+02	4.64656E-03	.0051	1.04552E-02
33	2.2395E+03	8.1440E+02	7.93086E-03	.0050	1.78435E-02
32	3.5191E+03	1.2796E+03	1.25761E-02	.0050	2.82981E-02
31	5.5300E+03	2.0109E+03	2.01442E-02	.0050	4.53246E-02
30	9.1180E+03	3.5880E+03	3.36795E-02	.0050	6.87482E-02
29	1.5030E+04	5.9120E+03	4.95781E-02	.0050	1.01253E-01
28	2.4780E+04	9.7500E+03	7.08781E-02	.0050	1.44700E-01
27	4.0850E+04	1.6070E+04	6.99980E-02	.0050	1.42936E-01
26	6.7340E+04	2.6490E+04	9.46286E-02	.0050	1.93240E-01
25	1.1100E+05	4.3660E+04	1.07080E-01	.0050	2.18698E-01
24	1.8300E+05	7.2000E+04	1.17672E-01	.0051	2.40246E-01
23	3.0250E+05	1.1950E+05	1.11721E-01	.0051	2.26949E-01
22	5.0000E+05	1.9750E+05	8.49242E-02	.0051	1.72536E-01
21	8.2100E+05	3.2100E+05	1.00564E-01	.0052	2.06923E-01
20	1.3530E+06	5.3200E+05	4.31778E-02	.0052	8.82223E-02
19	2.2310E+06	8.7800E+05	3.44460E-02	.0052	7.03044E-02
18	3.6790E+06	1.4480E+06	2.16123E-02	.0053	4.41052E-02
17	6.0655E+06	2.3865E+06	7.02637E-03	.0053	1.43450E-02
16	1.0000E+07	3.9345E+06	1.42442E-03	.0058	2.90813E-03
15	1.3800E+07	3.8000E+06	7.30854E-05	.0130	2.28873E-04
14	1.5000E+07	1.2000E+06	3.02052E-06	.0637	3.62462E-05
13	2.0000E+07	5.0000E+06	4.16632E-06	.0710	1.45821E-05

12	2.7100E+07	7.1000E+06	4.74597E-06	.0594	1.57419E-05
11	3.6800E+07	9.7000E+06	3.62452E-06	.0706	1.19385E-05
10	5.0000E+07	1.3200E+07	4.15553E-06	.0679	1.36629E-05
9	6.0000E+07	1.0000E+07	2.41990E-06	.0894	1.33094E-05
8	1.0000E+08	4.0000E+07	5.91878E-06	.0609	1.18376E-05
7	1.5000E+08	5.0000E+07	3.00070E-06	.0827	7.50174E-06
6	2.0000E+08	5.0000E+07	1.14270E-06	.1212	3.99944E-06
5	3.0000E+08	1.0000E+08	6.12343E-07	.2023	1.53086E-06
4	4.0000E+08	1.0000E+08	8.24152E-08	.4112	2.88453E-07
3	5.0000E+08	1.0000E+08	5.05998E-08	.7149	2.27699E-07
2	7.5000E+08	2.5000E+08	2.38081E-17	.0000	5.95202E-17
1	1.0000E+09	2.5000E+08	2.38081E-17	.0000	8.33282E-17

$\Phi^{MCNP} = 5.96187 \cdot 10^{-3} n/(cm^2 \cdot sec)$ for a proton current of 1proton/sec
$\Phi^{LAHET} = 1.53543 \cdot 10^{-7} n/(cm^2 \cdot sec)$ for a proton current of 1proton/sec
$\Phi^{total} = 5.96202 \cdot 10^{-3} n/(cm^2 \cdot sec)$ for a proton current of 1proton/sec
$\Phi^{LAHET}/\Phi total = 2.57534 \cdot 10^{-5}$

Table A.4: Neutron flux density spectra in the radial blanket of the IAEA-ADS neutronic benchmark

g	E_g	ΔE	ϕ_g	statistical error	$\phi_g(u)$
84	5.0000E-03	4.9900E-03	8.53280E-08	.3619	4.26640E-08
83	1.0000E-02	5.0000E-03	4.70380E-07	.2484	7.05570E-07
82	1.5000E-02	5.0000E-03	9.42875E-07	.1756	2.35719E-06
81	2.0000E-02	5.0000E-03	1.29858E-06	.1494	4.54502E-06
80	2.5000E-02	5.0000E-03	2.21956E-06	.1250	9.98801E-06
79	3.0000E-02	5.0000E-03	2.68991E-06	.0996	1.47945E-05
78	3.5000E-02	5.0000E-03	3.76786E-06	.0988	2.44911E-05
77	4.2000E-02	7.0000E-03	6.15387E-06	.0762	3.38463E-05
76	5.0000E-02	8.0000E-03	8.45970E-06	.0657	4.86433E-05
75	5.8000E-02	8.0000E-03	1.15912E-05	.0559	7.82403E-05
74	6.7000E-02	9.0000E-03	1.46652E-05	.0549	1.01842E-04
73	8.0000E-02	1.3000E-02	2.49952E-05	.0458	1.41319E-04
72	1.0000E-01	2.0000E-02	4.37763E-05	.0385	1.96993E-04
71	1.4000E-01	4.0000E-02	1.04162E-04	.0292	3.12487E-04
70	1.8000E-01	4.0000E-02	1.14287E-04	.0263	4.57146E-04

69	2.2000E-01	4.0000E-02	1.24306E-04	.0247	6.21530E-04
68	2.5000E-01	3.0000E-02	9.35042E-05	.0254	7.32449E-04
67	2.8000E-01	3.0000E-02	9.21217E-05	.0245	8.13742E-04
66	3.0000E-01	2.0000E-02	6.23129E-05	.0270	9.03536E-04
65	3.2000E-01	2.0000E-02	6.14488E-05	.0262	9.52458E-04
64	3.5000E-01	3.0000E-02	9.07986E-05	.0238	1.01392E-03
63	4.0000E-01	5.0000E-02	1.53672E-04	.0210	1.15254E-03
62	5.0000E-01	1.0000E-01	2.98089E-04	.0177	1.34140E-03
61	6.2500E-01	1.2500E-01	3.49318E-04	.0162	1.57193E-03
60	7.8000E-01	1.5500E-01	4.07030E-04	.0152	1.84476E-03
59	8.5000E-01	7.0000E-02	1.73582E-04	.0181	2.02099E-03
58	9.1000E-01	6.0000E-02	1.42530E-04	.0185	2.09044E-03
57	9.5000E-01	4.0000E-02	9.46735E-05	.0205	2.20116E-03
56	9.7200E-01	2.2000E-02	5.01513E-05	.0246	2.19070E-03
55	9.9600E-01	2.4000E-02	5.40390E-05	.0240	2.21559E-03
54	1.0200E+00	2.4000E-02	5.32573E-05	.0245	2.23681E-03
53	1.0450E+00	2.5000E-02	5.49230E-05	.0243	2.26832E-03
52	1.0710E+00	2.6000E-02	5.72604E-05	.0235	2.33004E-03
51	1.0970E+00	2.6000E-02	5.63201E-05	.0239	2.34812E-03
50	1.1230E+00	2.6000E-02	5.61165E-05	.0237	2.39575E-03
49	1.1500E+00	2.7000E-02	5.69342E-05	.0230	2.39650E-03
48	1.3000E+00	1.5000E-01	3.02438E-04	.0150	2.46991E-03
47	1.5000E+00	2.0000E-01	3.64980E-04	.0141	2.55486E-03
46	2.1000E+00	6.0000E-01	9.51021E-04	.0115	2.85306E-03
45	2.6000E+00	5.0000E-01	6.76734E-04	.0119	3.18065E-03
44	3.3000E+00	7.0000E-01	8.01835E-04	.0113	3.37916E-03
43	4.0000E+00	7.0000E-01	6.65023E-04	.0116	3.46762E-03
42	9.8770E+00	5.8770E+00	3.15897E-03	.0093	3.72954E-03
41	1.5968E+01	6.0910E+00	1.45056E-03	.0107	3.07747E-03
40	2.7700E+01	1.1732E+01	1.56486E-03	.0092	2.91231E-03
39	4.8052E+01	2.0352E+01	2.85978E-03	.0088	5.32219E-03
38	7.5501E+01	2.7449E+01	2.06529E-03	.0087	4.64812E-03
37	1.4873E+02	7.3229E+01	4.57988E-03	.0076	7.01191E-03
36	3.6726E+02	2.1853E+02	9.36332E-03	.0066	1.10543E-02
35	9.0690E+02	5.3964E+02	1.78240E-02	.0060	2.10424E-02
34	1.4251E+03	5.1820E+02	1.38897E-02	.0058	3.12532E-02
33	2.2395E+03	8.1440E+02	1.93096E-02	.0056	4.34443E-02
32	3.5191E+03	1.2796E+03	2.56820E-02	.0054	5.77886E-02
31	5.5300E+03	2.0109E+03	3.54595E-02	.0054	7.97844E-02
30	9.1180E+03	3.5880E+03	5.18094E-02	.0053	1.05756E-01
29	1.5030E+04	5.9120E+03	6.77857E-02	.0053	1.38438E-01
28	2.4780E+04	9.7500E+03	8.75745E-02	.0052	1.78787E-01

27	4.0850E+04	1.6070E+04	8.00770E-02	.0052	1.63517E-01
26	6.7340E+04	2.6490E+04	9.91158E-02	.0052	2.02404E-01
25	1.1100E+05	4.3660E+04	1.03286E-01	.0053	2.10948E-01
24	1.8300E+05	7.2000E+04	1.04177E-01	.0053	2.12695E-01
23	3.0250E+05	1.1950E+05	9.03078E-02	.0053	1.83449E-01
22	5.0000E+05	1.9750E+05	6.32034E-02	.0054	1.28407E-01
21	8.2100E+05	3.2100E+05	6.39459E-02	.0055	1.31577E-01
20	1.3530E+06	5.3200E+05	2.04900E-02	.0058	4.18659E-02
19	2.2310E+06	8.7800E+05	1.43968E-02	.0060	2.93838E-02
18	3.6790E+06	1.4480E+06	7.48858E-03	.0065	1.52823E-02
17	6.0655E+06	2.3865E+06	2.01426E-03	.0083	4.11229E-03
16	1.0000E+07	3.9345E+06	4.07588E-04	.0144	8.32139E-04
15	1.3800E+07	3.8000E+06	1.84578E-05	.0614	5.78021E-05
14	1.5000E+07	1.2000E+06	1.25346E-06	.3020	1.50416E-05
13	2.0000E+07	5.0000E+06	8.19289E-07	.3726	2.86751E-06
12	2.7100E+07	7.1000E+06	1.35118E-06	.2690	4.48174E-06
11	3.6800E+07	9.7000E+06	5.75953E-07	.4210	1.89708E-06
10	5.0000E+07	1.3200E+07	7.90688E-07	.3167	2.59969E-06
9	6.0000E+07	1.0000E+07	7.77229E-07	.3592	4.27476E-06
8	1.0000E+08	4.0000E+07	1.29957E-06	.2563	2.59913E-06
7	1.5000E+08	5.0000E+07	3.38430E-07	.5215	8.46076E-07
6	2.0000E+08	5.0000E+07	2.18562E-07	.7088	7.64968E-07
5	3.0000E+08	1.0000E+08	3.26969E-07	.5628	8.17422E-07
4	4.0000E+08	1.0000E+08	2.62875E-16	.0000	9.20062E-16
3	5.0000E+08	1.0000E+08	2.62875E-16	.0000	1.18294E-15
2	7.5000E+08	2.5000E+08	2.62875E-16	.0000	6.57187E-16
1	1.0000E+09	2.5000E+08	2.62875E-16	.0000	9.20062E-16

$\Phi^{MCNP} = 1.73602 \cdot 10^{-3} n/(cm^2 \cdot sec)$ for a proton current of 1proton/sec
$\Phi^{LAHET} = 9.85819 \cdot 10^{-9} n/(cm^2 \cdot sec)$ for a proton current of 1proton/sec
$\Phi^{total} = 1.73603 \cdot 10^{-3} n/(cm^2 \cdot sec)$ for a proton current of 1proton/sec
$\Phi^{LAHET}/\Phi total = 5.67858 \cdot 10^{-6}$

A.2 Figures of the neutron flux density in different zones of the IAEA-ADS neutronic benchmark reactor

The Figures A.2,..., A.5 show the energy dependence of the neutron fluxes in the target, the inner core region, the outer core region and in the radial blanket. In the Figures the lethargy dependent fluxes, $\phi(u)$ are shown as function of energy. The fluxes are normalized to:

$$\int_{u_{min}}^{u_{max}} \phi(u)du = 1$$

Most of the results have been obtained with the modules LAHET and MCNP of the LAHET Code System [6]. In some cases, Figures A.6, A.7 and A.9, results from TWODANT [25] calculations are shown. These calculations have been carried out in S_8/P_3 approximation.

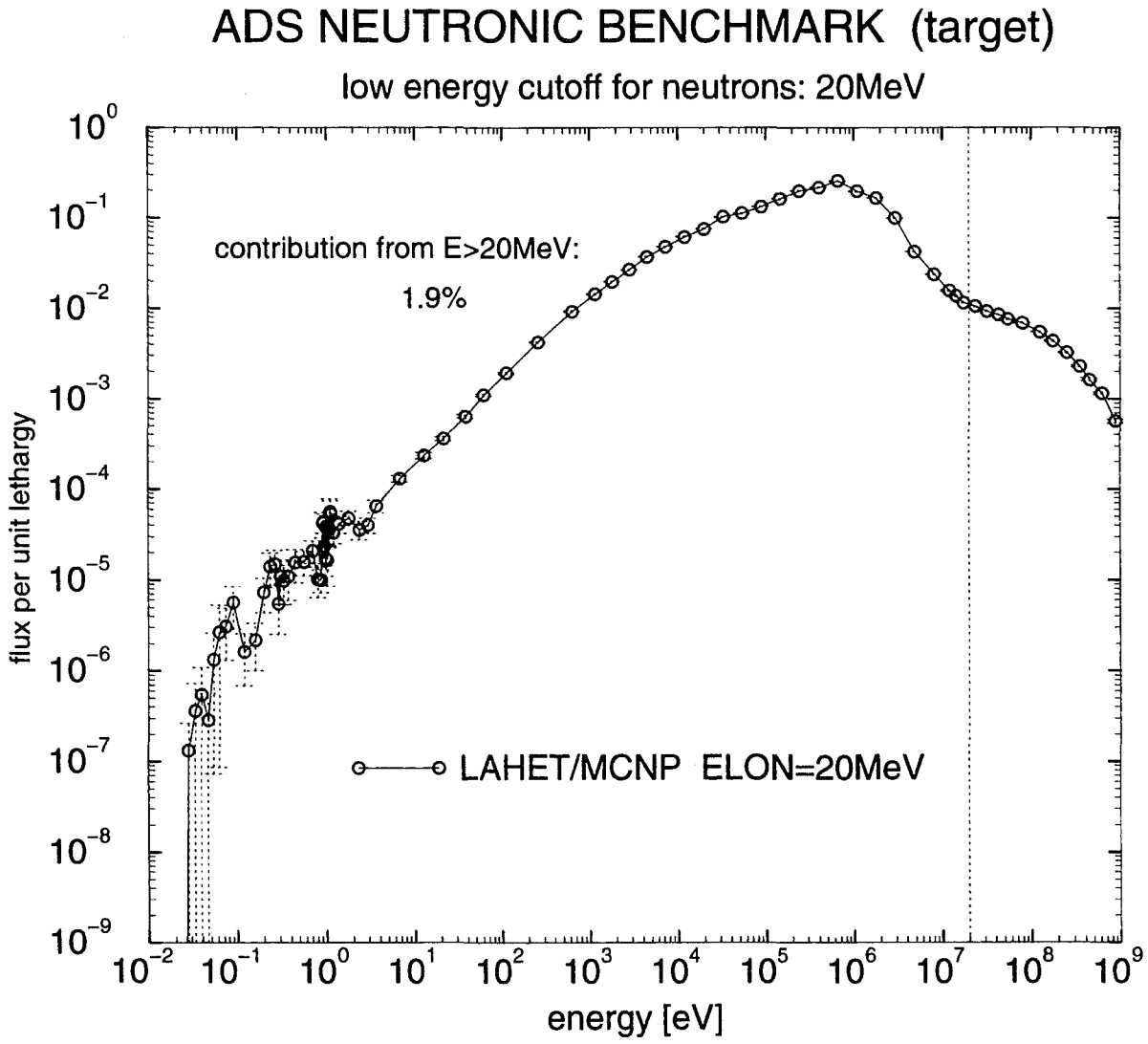

Figure A.2: Flux per unit lethargy in the **target** of the ADS benchmark reactor. $\phi(u)[n/(cm^2 \cdot sec)]$ versus energy, $\int_{u_{min}}^{u_{max}} \phi(u)du = 1$, (total flux for a proton current of 10mA and 1GeV: $5.431 \cdot 10^{15}[n/(cm^2 \cdot sec)]$)

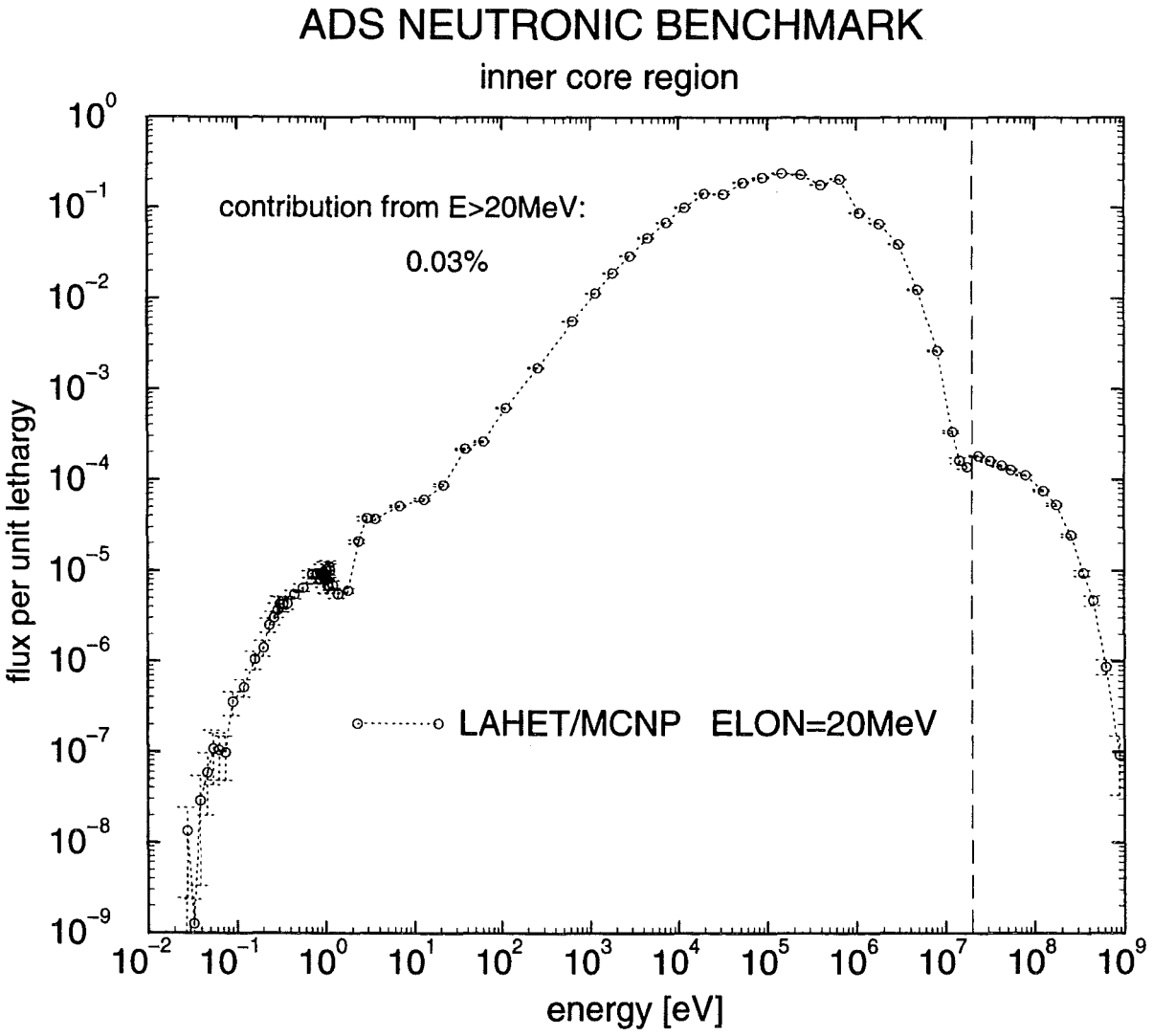

Figure A.3: Flux per unit lethargy in the **inner core region** of the ADS benchmark reactor. $\phi(u)[n/(cm^2 \cdot sec)]$ versus energy, $\int_{u_{min}}^{u_{max}} \phi(u)du = 1$, (total flux for a proton current of 10mA and 1GeV: $1.127 \cdot 10^{15}[n/(cm^2 \cdot sec)]$)

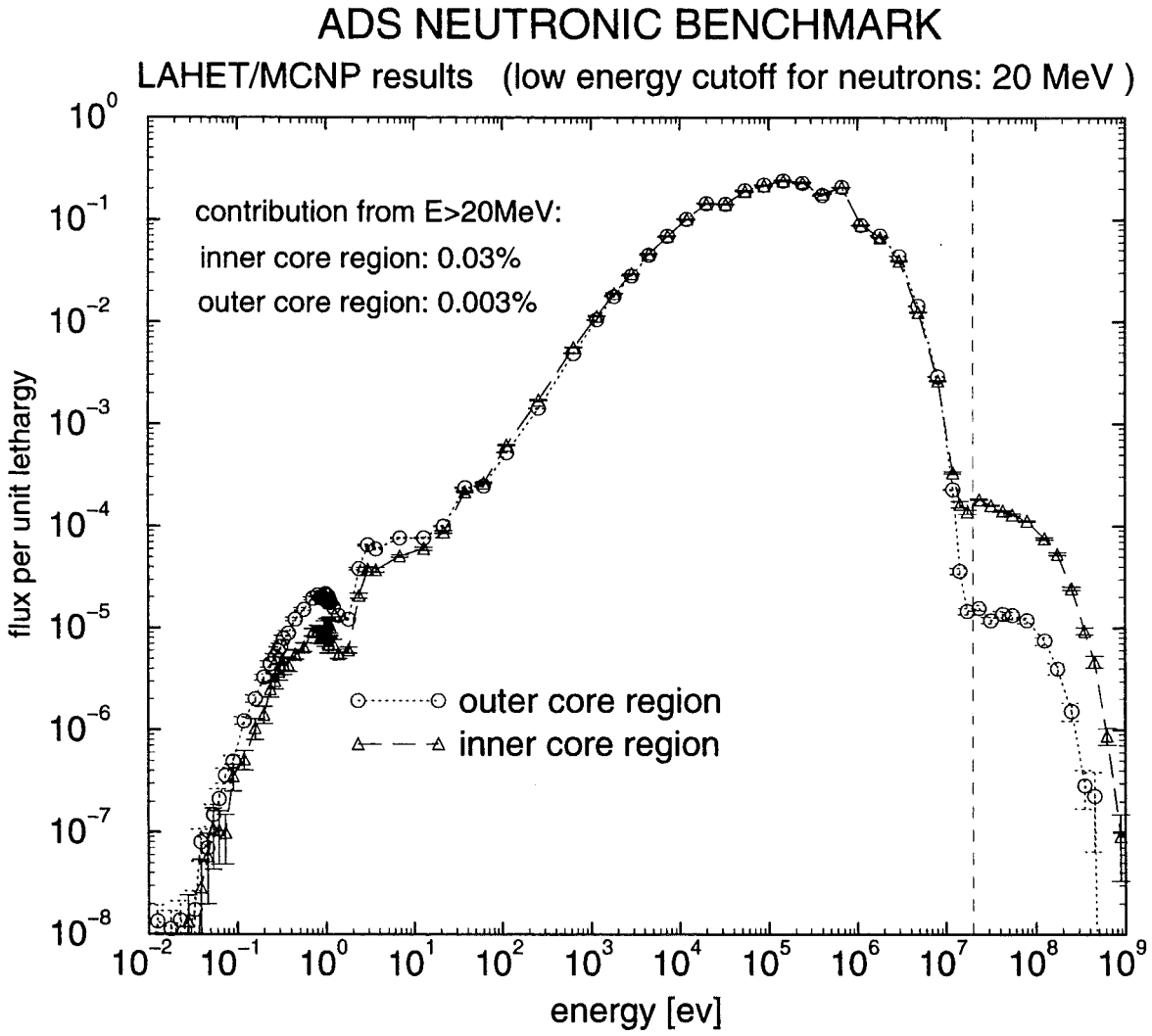

Figure A.4: Flux per unit lethargy in the **inner and outer core region** of an ADS. $\phi(u)[n/(cm^2 \cdot sec)]$ versus energy, $\int_{u_{min}}^{u_{max}} \phi(u)du = 1$. (total flux for a proton current of 10mA and 1GeV: inner core region: $1.127 \cdot 10^{15}[n/(cm^2 \cdot sec)]$; outer core region: $3.721 \cdot 10^{14}[n/(cm^2 \cdot sec)]$)

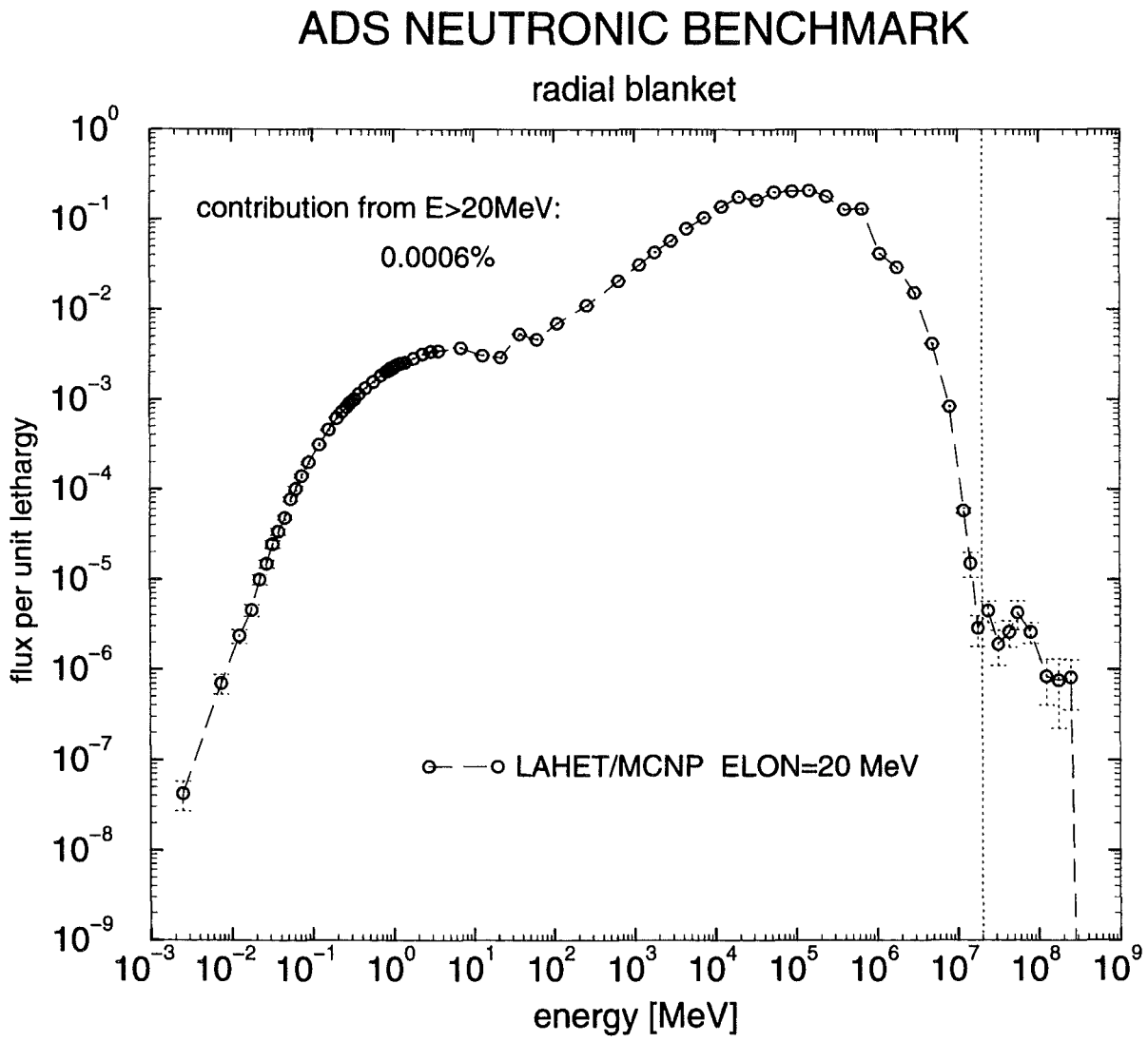

Figure A.5: Flux per unit lethargy in the **radial blanket** of the ADS benchmark reactor. $\phi(u)[n/(cm^2 \cdot sec)]$ versus energy, $\int_{u_{min}}^{u_{max}} \phi(u)du = 1$. (total flux for a proton current of 10mA and 1GeV: $1.084 \cdot 10^{14}[n/(cm^2 \cdot sec)]$)

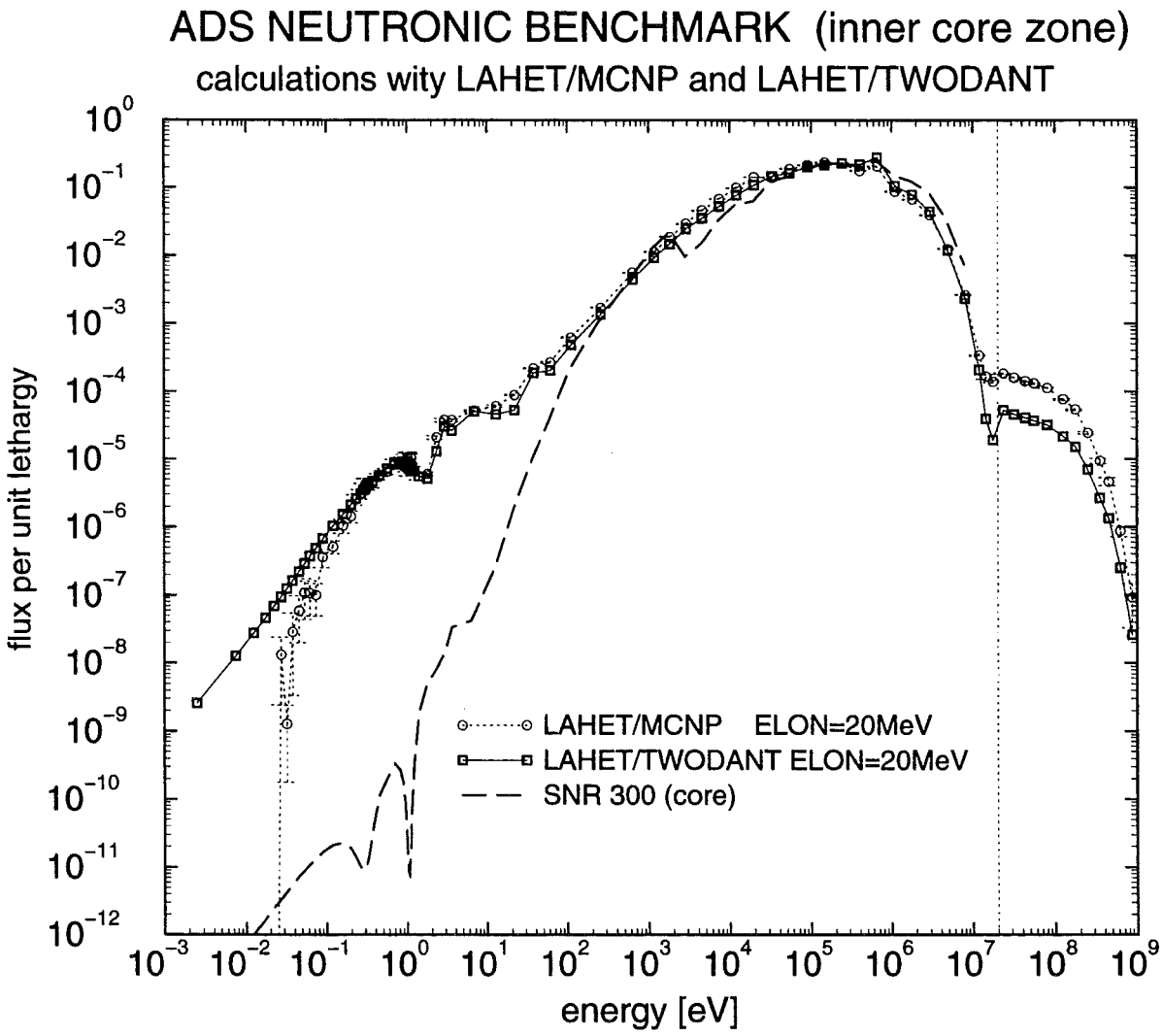

Figure A.6: Flux per unit lethargy **calculated by LAHET/MCNP** and **LAHET/TWODANT** in the inner core region of the ADS benchmark reactor. $\phi(u)[n/(cm^2 \cdot sec)]$ versus energy, $\int_{u_{min}}^{u_{max}} \phi(u)du = 1$. **The same U^{233}-enrichment (8.7216 at%) is used for the calculation with LAHET/MCNP and LAHET/TWODANT**. The SNR 300 core spectrum is shown for comparison

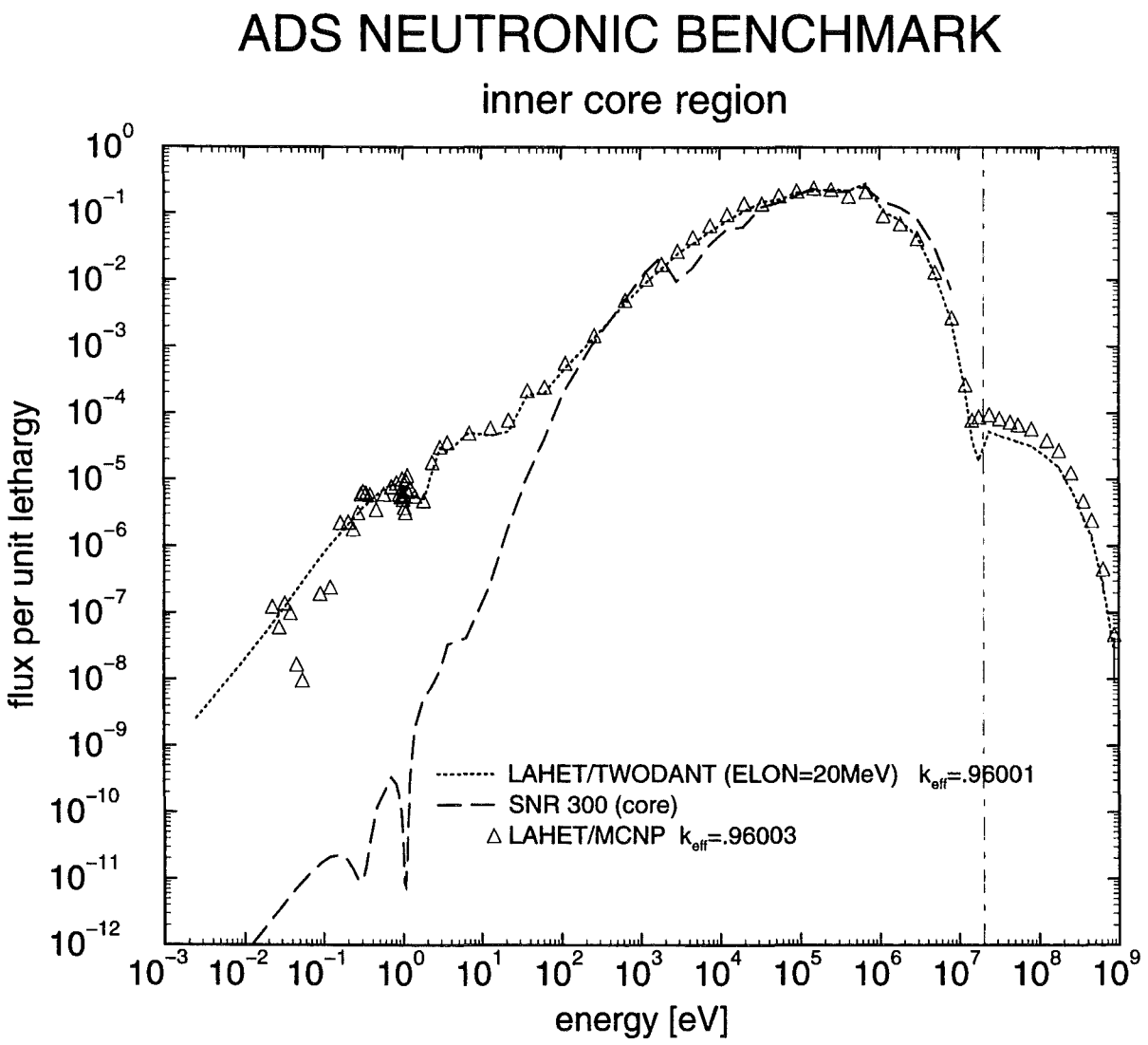

Figure A.7: Flux per unit lethargy calculated with **LAHET/MCNP and with LAHET/TWODANT** for the inner core region of the ADS benchmark reactor $\phi(u)[n/(cm^2 \cdot sec)]$ versus energy, $\int_{u_{min}}^{u_{max}} \phi(u)du = 1$. **Calculations with LAHET/MCNP and LAHET/TWODANT are both carried out for** $k_{eff} = 0.9600$. The SNR 300 core spectrum is shown for comparison

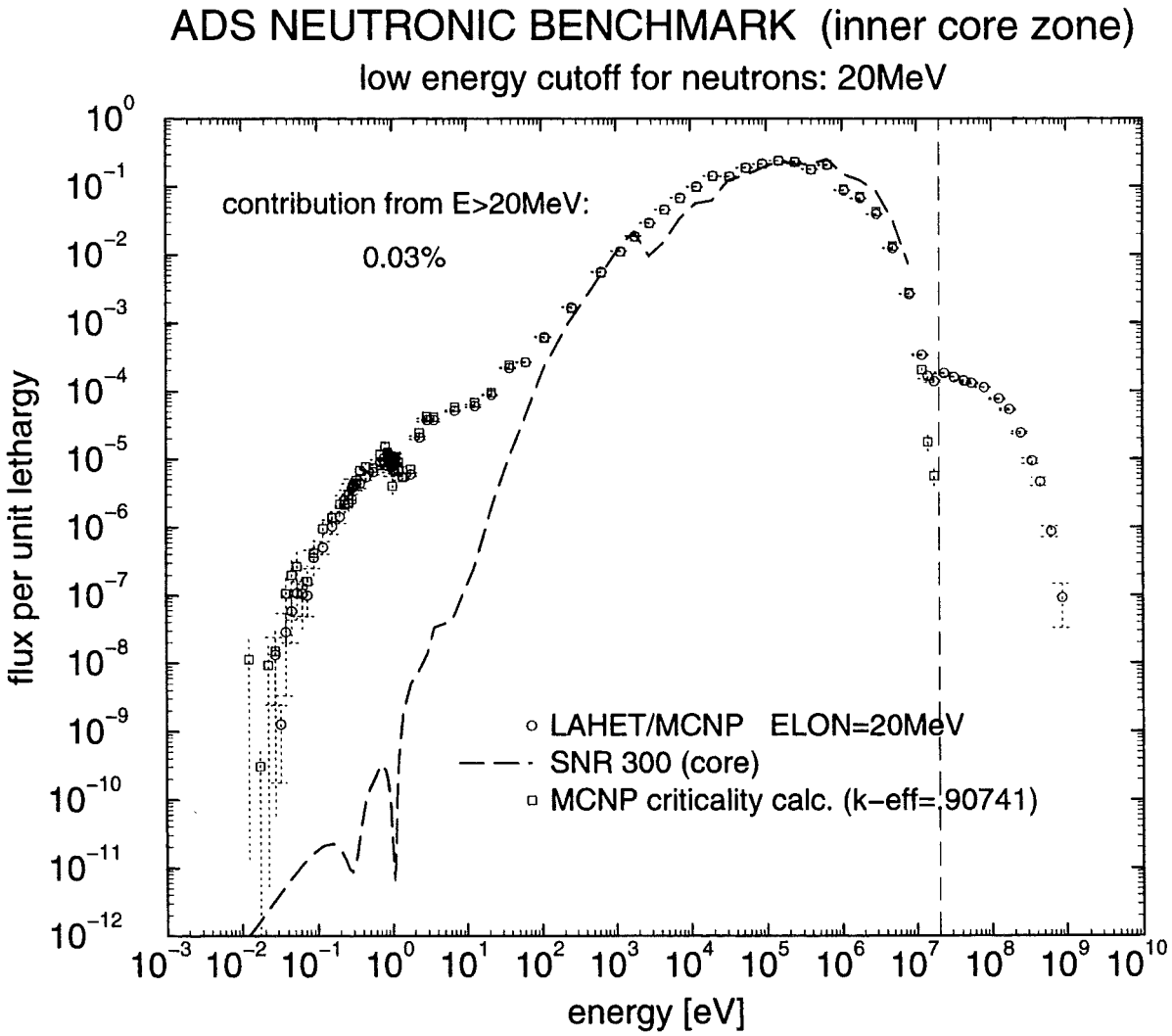

Figure A.8: Comparison of external source calculation and criticality calculation for the inner core region of the ADS benchmark reactor. $\phi(u)[n/(cm^2 \cdot sec)]$ versus energy, $\int_{u_{min}}^{u_{max}} \phi(u)du = 1$. The SNR 300 core spectrum is shown for comparison

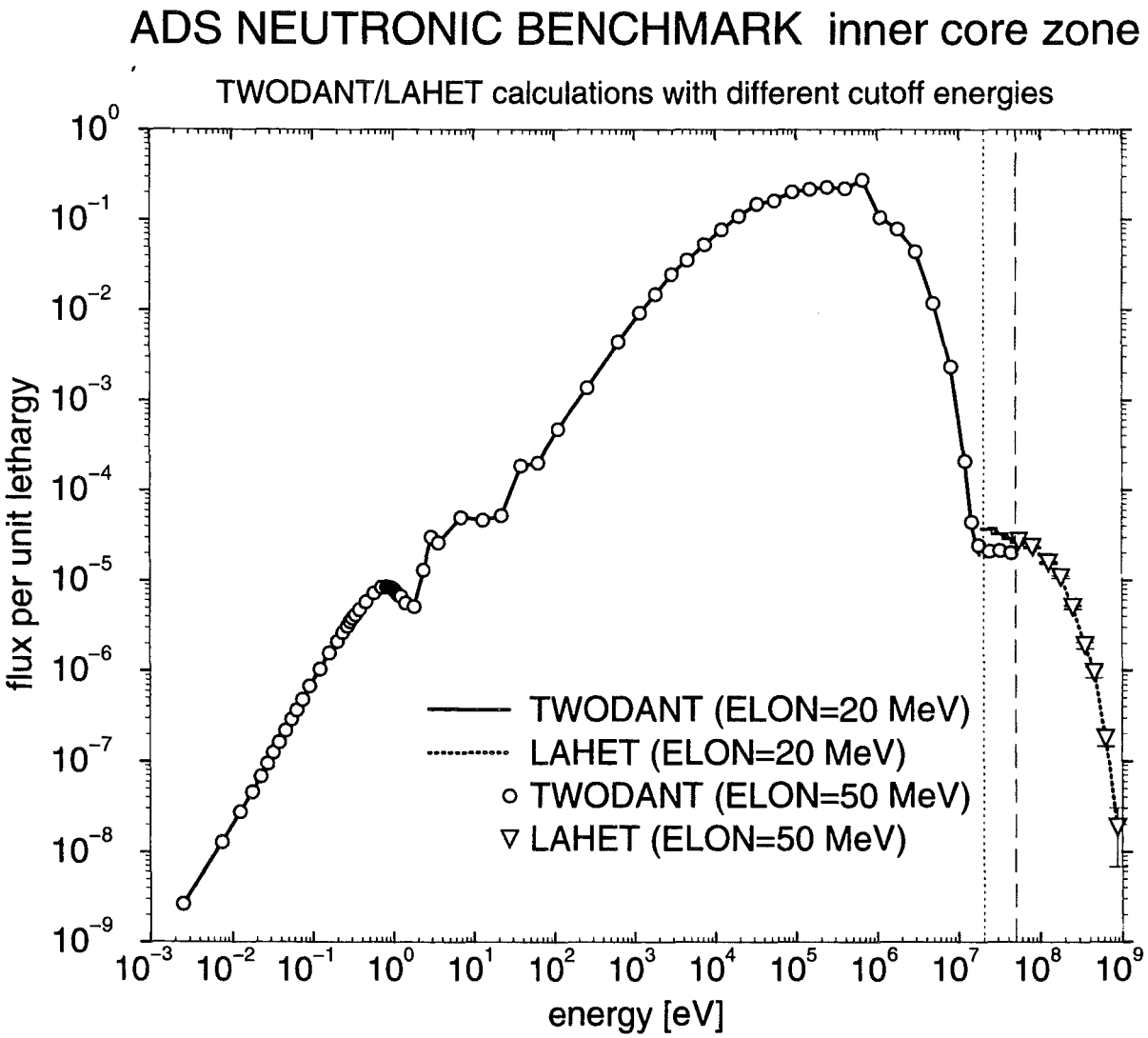

Figure A.9: Flux per unit lethargy in the inner core region of the ADS benchmark reactor calculated with **LAHET/TWODANT for different neutron cutoff energies.** $\phi(u)[n/(cm^2 \cdot sec)]$ versus energy, $\int_{u_{min}}^{u_{max}} \phi(u)du = 1$

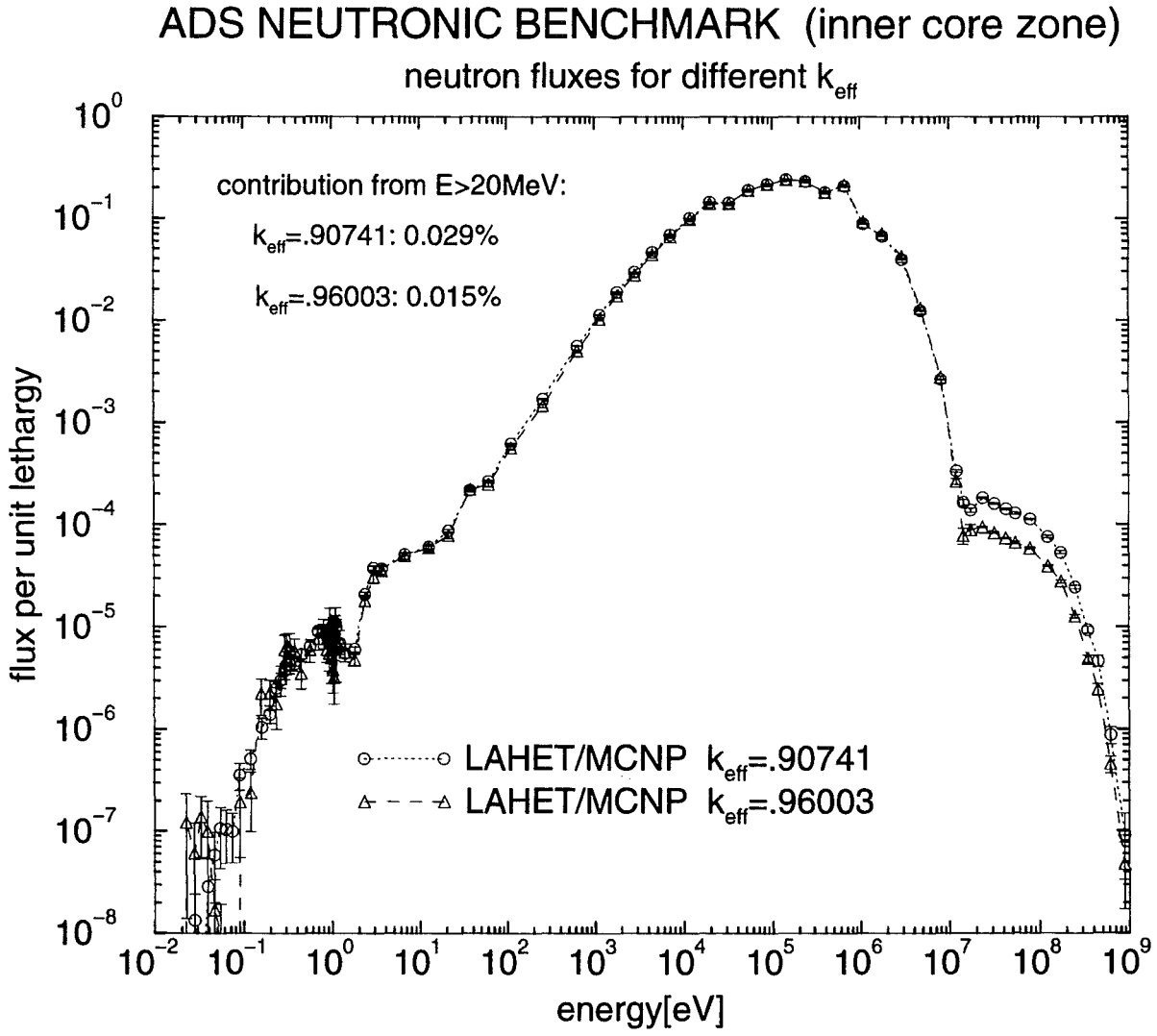

Figure A.10: Flux per unit lethargy in the inner core region of the ADS neutronic benchmark reactor for different values of k_{eff}. $\phi(u)[n/(cm^2 \cdot sec)]$ versus energy, $\int_{u_{min}}^{u_{max}} \phi(u)du = 1$. For $k_{eff} = .90741 : \Phi^{total} = 1.127 \cdot 10^{15}[n/(cm^2 \cdot \text{sec})]$, for $k_{eff} = .96003 : \Phi^{total} = 2.170 \cdot 10^{15}[n/(cm^2 \cdot \text{sec})]$ for a proton current of 10mA and 1GeV

Most of the LCS results shown in this section have been obtained for a fuel composition resulting in $k_{eff} = 0.90741$ in a criticality calculation with MCNP. In order to study the influence of a larger criticality factor, k_{eff}, on the neutron flux density spectra we increased the ^{233}U enrichment in the fuel until achieving $k_{eff} = 0.96$.

Figure A.10 shows the neutron flux density spectra, normalized to $\sum_{g=1}^{84} \phi_g = 1$. It is seen that for the larger value of k_{eff} the contribution of neutrons with $E_n > 20$MeV is smaller than for the lower value of k_{eff}. The neutrons with $E_n > 20$MeV are part of the external source. If k_{eff} is larger (0.96 instead of 0.91), less external neutrons are needed to maintain the specified power level, that means the contribution of neutrons with $E_n > 20$MeV to the total neutron flux density : $\int_{u_{cutoff}}^{u_{max}} \phi(u)du / \int_{u_{min}}^{umax} \phi(u)du$, ($u_{cutoff}$ characterizes the lethargy corresponding to $E_n = 2$MeV) is smaller for $k_{eff} = 0.96$ than for $k_{eff} = 0.91$: it is 0.015 % of Φ^{total} for $k_{eff} = 0.96$ and 0.029 % of Φ^{total} for $k_{eff} = 0.91$, i.e. this fraction changes by a factor of about 2.

A.3 Contributions of neutrons with $E_n > 20$MeV to neutron fluxes and reaction rates

In a further investigation we used the 75 groups constant set with neutron energies up to 50MeV [26] to calculate the contribution of neutrons of energy E_n >20MeV

- to the energy integral of the neutron flux density: $\int_{10^{-5}eV}^{50MeV} \phi(E)dE$ $(=\Phi^{total})$
- to the fission rate $\int_{10^{-5}eV}^{50MeV} \Sigma_{fiss}(E) \cdot \phi(E)dE$ $(=(\Sigma_{fiss}\phi)^{total})$
- to $\int_{10^{-5}eV}^{50MeV} \nu(E) \cdot \Sigma_{fiss}(E)dE$ $(=(\nu\Sigma_{fiss}\phi)^{total})$.

The transport calculations have been carried out with TWODANT [25] in S_8/P_3 approximation. The results are listed in Tables A.5-A.17.
In the tables Φ^{total} , $(\Sigma_{fiss}\phi)^{total}$ and $(\nu\Sigma_{fiss}\phi)^{total}$ are directly taken from the output of TWODANT. TWODANT provides volume integrated results per source neutron.
In order to get the *neutron flux density* produced by a proton current of 10mA the TWODANT results have to be multiplied by $26.759 \cdot 6.24181 \cdot 10^{16}$ and divided by the volume $[cm^3]$ of the reactor region, for which the results have been calculated. (26.759 neutrons with energy $E_n \leq$ 50MeV are produced in the ADS neutronic benchmark reactor by a proton of 1GeV, a proton current of 10mA corresponds to $6.24181 \cdot 10^{16}$ protons/sec). The volume of the inner core region is $1.3548 \cdot 10^6 cm^3$, that means, the neutron flux calculated by TWODANT for the inner core region has to be multiplied by $1.2328 \cdot 10^{12}$ in order to obtain the neutron flux density produced by a 10mA beam of 1GeV protons.

Table A.5: Φ for different k_{eff}
in the inner core of the ADS neutronic benchmark reactor
(volume-integrated values per source neutron, V=$1.3548 \cdot 10^6 cm^3$)

^{233}U enrichment (at %)	k_{eff}	$\Phi^{total} = \Phi^{E<20MeV} + \Phi^{E>20MeV}$	$\Phi^{E>20MeV}$	$\Phi^{E>20MeV}/\Phi^{total}$
8.0	.90833610	$2.10886 \cdot 10^3$	$7.64088 \cdot 10^{-2}$	$3.623 \cdot 10^{-5}$
8.2	.92298652	$2.42869 \cdot 10^3$	$7.64139 \cdot 10^{-2}$	$3.146 \cdot 10^{-5}$
8.7216	.96000690	$4.23891 \cdot 10^3$	$7.64380 \cdot 10^{-2}$	$1.803 \cdot 10^{-5}$

Table A.6: $(\Sigma_{fiss}\phi)$ for different k_{eff}
in the inner core of the ADS neutronic benchmark reactor
(volume-integrated values per source neutron)

k_{eff}	$(\Sigma_{fiss}\phi)^{total}$	$(\Sigma_{fiss}\phi)^{E>20MeV}$	$\frac{(\Sigma_{fiss}\phi)^{E>20MeV}}{(\Sigma_{fiss}\phi)^{total}}$
.90833610	2.90163	$4.32453 \cdot 10^{-4}$	$1.490 \cdot 10^{-4}$
.92298652	3.41595	$4.33725 \cdot 10^{-4}$	$1.270 \cdot 10^{-4}$
.96000690	6.30007	$4.37098 \cdot 10^{-4}$	$6.938 \cdot 10^{-5}$

Table A.7.: $(\nu\Sigma_{fiss}\phi)$ for different k_{eff}
in the inner core of the ADS neutronic benchmark reactor
(volume-integrated values per source neutron)

k_{eff}	$(\nu\Sigma^{fiss}\phi)^{total}$	$(\nu\Sigma^{fiss}\phi)^{E>20MeV}$	$\frac{(\nu\Sigma_{fiss}\phi)^{E>20MeV}}{(\nu\Sigma_{fiss}\phi)^{total}}$
.90833610	7.26422	$2.79226 \cdot 10^{-3}$	$3.844 \cdot 10^{-4}$
.92298652	8.55276	$2.79863 \cdot 10^{-3}$	$3.272 \cdot 10^{-4}$
.96000690	$1.57778 \cdot 10^{1}$	$2.81553 \cdot 10^{-3}$	$1.784 \cdot 10^{-4}$

Table A.8: Φ for different k_{eff}
in the outer core of the ADS neutronic benchmark reactor
(volume-integrated values per source neutron, V=$3.5226 \cdot 10^{6} cm^{3}$)

^{233}U enrichment (at %)	k_{eff}	$\Phi^{total} = \Phi^{E<20MeV} + \Phi^{E>20MeV}$	$\Phi^{E>20MeV}$	$\Phi^{E>20MeV}/\Phi^{total}$
8.0	.90833610	$1.95065 \cdot 10^{3}$	$1.46423 \cdot 10^{-3}$	$7.506 \cdot 10^{-7}$
8.2	.92298652	$2.41209 \cdot 10^{3}$	$1.47044 \cdot 10^{-3}$	$6.096 \cdot 10^{-7}$
8.7216	.96000690	$5.14388 \cdot 10^{3}$	$1.50640 \cdot 10^{-3}$	$2.929 \cdot 10^{-7}$

Table A.9: $(\Sigma_{fiss}\phi)$ for different k_{eff}
in the outer core of the ADS neutronic benchmark reactor
(volume-integrated values per source neutron)

k_{eff}	$(\Sigma_{fiss}\phi)^{total}$	$(\Sigma_{fiss}\phi)^{E>20MeV}$	$\frac{(\Sigma_{fiss}\phi)^{E>20MeV}}{(\Sigma_{fiss}\phi)^{total}}$
.90833610	3.16816	$9.76367 \cdot 10^{-6}$	$3.082 \cdot 10^{-6}$
.92298652	3.99642	$9.82752 \cdot 10^{-6}$	$2.459 \cdot 10^{-6}$
.96000690	8.95846	$1.01103 \cdot 10^{-5}$	$1.129 \cdot 10^{-6}$

Table A.10.: $(\nu\Sigma_{fiss}\phi)$ for different k_{eff}
in the outer core of the ADS neutronic benchmark reactor
(volume-integrated values per source neutron)

k_{eff}	$(\nu\Sigma^{fiss}\phi)^{total}$	$(\nu\Sigma^{fiss}\phi)^{E>20MeV}$	$\frac{(\nu\Sigma_{fiss}\phi)^{E>20MeV}}{(\nu\Sigma_{fiss}\phi)^{total}}$
.90833610	7.93075	$6.34130 \cdot 10^{-5}$	$7.996 \cdot 10^{-6}$
.92298652	$1.00058 \cdot 10^{1}$	$6.37453 \cdot 10^{-5}$	$6.371 \cdot 10^{-6}$
.96000690	$2.24390 \cdot 10^{1}$	$6.52262 \cdot 10^{-5}$	$2.907 \cdot 10^{-6}$

Table A.11: Φ for different k_{eff}
in the radial blanket of the ADS neutronic benchmark reactor
(volume-integrated values per source neutron, V=$1.0956 \cdot 10^{6} cm^{3}$)

^{233}U enrichment (at %)	k_{eff}	$\Phi^{total} = \Phi^{E<20MeV} + \Phi^{E>20MeV}$	$\Phi^{E>20MeV}$	$\Phi^{E>20MeV}/\Phi^{total}$
8.0	.90833610	$1.98436 \cdot 10^{2}$	$5.72702 \cdot 10^{-6}$	$2.886 \cdot 10^{-8}$
8.2	.92298652	$2.51580 \cdot 10^{2}$	$5.92079 \cdot 10^{-6}$	$2.353 \cdot 10^{-8}$
8.7216	.96000690	$5.72217 \cdot 10^{2}$	$7.09424 \cdot 10^{-6}$	$1.240 \cdot 10^{-8}$

Table A.12: $(\Sigma_{fiss}\phi)$ for different k_{eff}
in the radial blanket of the ADS neutronic benchmark reactor
(volume-integrated values per source neutron)

k_{eff}	$(\Sigma_{fiss}\phi)^{total}$	$(\Sigma_{fiss}\phi)^{E>20MeV}$	$\frac{(\Sigma_{fiss}\phi)^{E>20MeV}}{(\Sigma_{fiss}\phi)^{total}}$
.90833610	$4.95105 \cdot 10^{-3}$	$3.34094 \cdot 10^{-8}$	$6.748 \cdot 10^{-6}$
.92298652	$6.37031 \cdot 10^{-3}$	$3.43419 \cdot 10^{-8}$	$5.391 \cdot 10^{-6}$
.96000690	$1.50329 \cdot 10^{-2}$	$3.99774 \cdot 10^{-8}$	$2.659 \cdot 10^{-6}$

Table A.13.: $(\nu\Sigma_{fiss}\phi)$ for different k_{eff}
in the radial blanket of the ADS neutronic benchmark reactor
(volume-integrated values per source neutron)

k_{eff}	$(\nu\Sigma^{fiss}\phi)^{total}$	$(\nu\Sigma^{fiss}\phi)^{E>20MeV}$	$\frac{(\nu\Sigma_{fiss}\phi)^{E>20MeV}}{(\nu\Sigma_{fiss}\phi)^{total}}$
.90833610	$1.15537 \cdot 10^{-2}$	$2.21243 \cdot 10^{-7}$	$1.915 \cdot 10^{-5}$
.92298652	$1.48661 \cdot 10^{-2}$	$2.26246 \cdot 10^{-7}$	$1.522 \cdot 10^{-5}$
.96000690	$3.50840 \cdot 10^{-2}$	$2.56399 \cdot 10^{-7}$	$7.308 \cdot 10^{-6}$

Table A.14: Φ for different k_{eff}
in the inner lead region of the ADS neutronic benchmark reactor
(volume-integrated values per source neutron, V=$5.4752 \cdot 10^5 cm^3$)

^{233}U enrichment (at %)	k_{eff}	$\Phi^{total} = \Phi^{E<20MeV} + \Phi^{E>20MeV}$	$\Phi^{E>20MeV}$	$\Phi^{E>20MeV}/\Phi^{total}$
8.0	.90833610	$9.73402 \cdot 10^2$	$9.39528 \cdot 10^{-1}$	$9.652 \cdot 10^{-4}$
8.2	.92298652	$1.06990 \cdot 10^3$	$9.39529 \cdot 10^{-1}$	$8.781 \cdot 10^{-4}$
8.7216	.96000690	$1.61078 \cdot 10^3$	$9.39529 \cdot 10^{-1}$	$5.833 \cdot 10^{-4}$

Table A.15: Φ for different k_{eff}
in the upper and lower lead regions of the ADS neutronic benchmark reactor
(volume-integrated values per source neutron, V=$4.9863 \cdot 10^7 cm^3$)

^{233}U enrichment (at %)	k_{eff}	$\Phi^{total} = \Phi^{E<20MeV} + \Phi^{E>20MeV}$	$\Phi^{E>20MeV}$	$\Phi^{E>20MeV}/\Phi^{total}$
8.0	.90833610	$1.81750 \cdot 10^3$	$3.48196 \cdot 10^{-6}$	$1.916 \cdot 10^{-9}$
8.2	.92298652	$2.19696 \cdot 10^3$	$3.48218 \cdot 10^{-6}$	$1.585 \cdot 10^{-9}$
8.7216	.96000690	$4.41665 \cdot 10^3$	$3.48333 \cdot 10^{-6}$	$7.885 \cdot 10^{-10}$

Table A.16: Φ for different k_{eff}
in the outer lead region of the ADS neutronic benchmark reactor
(volume-integrated values per source neutron, V=$3.9392 \cdot 10^7$)

^{233}U enrichment (at %)	k_{eff}	$\Phi^{total} = \Phi^{E<20MeV} + \Phi^{E>20MeV}$	$\Phi^{E>20MeV}$	$\Phi^{E>20MeV}/\Phi^{total}$
8.0	.90833610	$2.32648 \cdot 10^3$	$2.73756 \cdot 10^{-6}$	$1.177 \cdot 10^{-9}$
8.2	.92298652	$2.91125 \cdot 10^3$	$2.78399 \cdot 10^{-6}$	$9.563 \cdot 10^{-10}$
8.7216	.96000690	$6.41045 \cdot 10^3$	$3.06282 \cdot 10^{-6}$	$4.778 \cdot 10^{-10}$

Table A.17: Φ for different k_{eff}
in the axial reflector of the ADS neutronic benchmark reactor
(volume-integrated values per source neutron, V=$7.1675 \cdot 10^6 cm^3$)

^{233}U enrichment (at %)	k_{eff}	$\Phi^{total} = \Phi^{E<20MeV} + \Phi^{E>20MeV}$	$\Phi^{E>20MeV}$	$\Phi^{E>20MeV}/\Phi^{total}$
8.0	.90833610	$2.17513 \cdot 10^3$	$9.82732 \cdot 10^{-4}$	$4.518 \cdot 10^{-7}$
8.2	.92298652	$2.61146 \cdot 10^3$	$9.83185 \cdot 10^{-4}$	$3.765 \cdot 10^{-7}$
8.7216	.96000690	$5.15198 \cdot 10^3$	$9.85633 \cdot 10^{-4}$	$1.913 \cdot 10^{-7}$

Appendix B

Calculation of the Neutron Source used as Input for TWODANT

For the ADS neutronic benchmark, [3], (Fig. A.1), the neutron source has been provided as an energy dependent source homogeneously distributed within a cylindrical region (r=10cm, h=50cm) in the center of the reactor. In Fig. A.1 this source region is marked as target. The source spectrum was originally given in a 25 energy groups structure up to 19.4MeV and has been used for our benchmark solutions [2].
For further calculations with the S_N code TWODANT [25] especially for tests of group constants up to 50MeV [26] we calculated new neutron source spectra with LAHET/ HTAPE [6]. These calculations have been carried out for a 1GeV proton beam with radius 10cm and with parabolic profile. In accordance with the specification of the IAEA-ADS neutronic benchmark the proton beam enters the subcritical reactor from above along its center axis and hits the lead 25cm above the reactor midplane.
In the LAHET/HTAPE calculations the neutron production spectrum (and the proton production spectrum) was averaged over the zone marked as target in Fig. A.1, namely the cylindrical volume with radius 10cm and height 50cm with its centrum in the reactor center.
Four neutron source spectra have been calculated: two source spectra up to 20MeV, one averaged over the volume marked as target in Fig. A.1 (Table B.1), and the other one averaged over the entire reactor of Fig. A.1 (Table B.2). In Table B.3 the source spectrum up to 50MeV averaged over the 'target' is given; Table B.4 shows the source up to 50MeV averaged over the whole reactor.

Neutron source up to 20MeV

The following Table shows the proton- and neutron-production spectra in the energy range 10^{-5}eV to 20MeV calculated by LAHET/HTAPE. The results are per primary proton. The Monte Carlo calculation has been carried out for 20.000 proton histories, the neutron cutoff energy in LAHET (ELON) was 20MeV.

Table B.1: nucleon production **in the target** of the ADS neutronic benchmark reactor (Fig. A.1) for neutron cutoff energy ELON=20MeV

lahet-calculation of neutron source for ADS neutronic benchmark
1000MeV circular beam (r=10cm) with parabolic proton density
distribution over the radius
the calculation has been carried out for 20.000 proton histories

The mean values of the number of protons (neutrons)
and the statistical errors are given for each
energy interval per primary proton

upper energy [MeV]	proton		neutron	
5.000D-09	0.000D+00	.000	0.000D+00	.000
7.550D-05	0.000D+00	.000	0.000D+00	.000
1.487D-04	0.000D+00	.000	2.500D-05	1.000
3.673D-04	0.000D+00	.000	1.250D-04	.447
9.069D-04	0.000D+00	.000	2.750D-04	.301
1.425D-03	0.000D+00	.000	4.000D-04	.250
2.239D-03	0.000D+00	.000	8.250D-04	.174
3.519D-03	0.000D+00	.000	2.175D-03	.107
5.530D-03	0.000D+00	.000	3.425D-03	.085
9.118D-03	0.000D+00	.000	7.300D-03	.059
1.503D-02	0.000D+00	.000	1.323D-02	.044
2.478D-02	0.000D+00	.000	2.423D-02	.032
4.085D-02	0.000D+00	.000	4.632D-02	.023
6.734D-02	0.000D+00	.000	8.173D-02	.018
1.110D-01	0.000D+00	.000	1.526D-01	.013
1.830D-01	0.000D+00	.000	2.743D-01	.010
3.025D-01	2.500D-05	1.000	4.990D-01	.007
5.000D-01	2.500D-05	1.000	8.849D-01	.006
8.210D-01	0.000D+00	.000	1.472D+00	.005
1.353D+00	2.750D-04	.301	2.325D+00	.004
2.231D+00	1.050D-03	.158	3.152D+00	.004
3.679D+00	8.150D-03	.057	3.478D+00	.004
6.066D+00	1.305D-01	.015	2.987D+00	.004
1.000D+01	6.079D-01	.008	2.022D+00	.005
1.380D+01	3.629D-01	.009	9.015D-01	.006

1.500D+01	9.286D-02	.017	2.112D-01	.011
2.000D+01	3.020D-01	.010	6.330D-01	.007
total	1.506D+00	.006	1.917D+01	.003

Table B.2: **total** nucleon production in the ADS neutronic benchmark reactor (Fig. A.1) for neutron cutoff energy ELON=20MeV

lahet - calculation of neutron source for ADS neutronic benchmark
1000MeV circular beam (r=10cm) with parabolic density
20.000 proton histories

The mean values of the number of protons (neutrons)
and the statistical errors are given for each
energy interval per primary proton

energy [MeV]	proton		neutron	
5.000D-09	0.000D+00	.000	0.000D+00	.000
7.550D-05	0.000D+00	.000	0.000D+00	.000
1.487D-04	0.000D+00	.000	2.500D-05	1.000
3.673D-04	0.000D+00	.000	2.000D-04	.354
9.069D-04	0.000D+00	.000	7.750D-04	.180
1.425D-03	0.000D+00	.000	9.250D-04	.164
2.239D-03	0.000D+00	.000	2.225D-03	.107
3.519D-03	0.000D+00	.000	4.050D-03	.079
5.530D-03	0.000D+00	.000	7.572D-03	.057
9.118D-03	0.000D+00	.000	1.632D-02	.040
1.503D-02	0.000D+00	.000	2.927D-02	.029
2.478D-02	0.000D+00	.000	5.089D-02	.022
4.085D-02	0.000D+00	.000	9.578D-02	.016
6.734D-02	5.000D-05	.707	1.681D-01	.012
1.110D-01	1.500D-04	.408	3.072D-01	.009
1.830D-01	1.000D-04	.500	5.450D-01	.007
3.025D-01	3.250D-04	.277	9.762D-01	.006
5.000D-01	7.500D-04	.183	1.680D+00	.005
8.210D-01	1.150D-03	.147	2.724D+00	.004

1.353D+00	1.600D-03	.127	4.149D+00	.003
2.231D+00	4.425D-03	.076	5.336D+00	.003
3.679D+00	2.875D-02	.031	5.480D+00	.003
6.066D+00	1.668D-01	.014	4.341D+00	.003
1.000D+01	7.148D-01	.007	2.851D+00	.004
1.380D+01	4.687D-01	.008	1.338D+00	.005
1.500D+01	1.270D-01	.014	3.242D-01	.009
2.000D+01	4.338D-01	.008	1.011D+00	.005
total	1.948D+00	.005	3.144D+01	.002

In Fig. B.1 the particle production spectrum in the target of the ADS neutronic benchmark reactor is shown. For comparison the energy distribution of the neutron source given in the specification of the IAEA/ADS neutronic benchmark is given. The maximum for both distributions is between 0.1MeV and 1MeV.

Neutron source up to 50MeV.

The following tables (B.3 and B.4) show the proton- and neutron-production spectra in the energy range up to 50MeV calculated by LAHET/HTAPE with neutron cutoff energy ELON=50MeV. The results are per primary proton. The Monte Carlo calculation has been carried out for 20.000 proton histories.

Table B.3: nucleon production **in the target** of the ADS neutronic benchmark reactor (Fig. A.1) for neutron cutoff energy ELON=50MeV

lahet-calculation of neutron source for ADS neutronic benchmark
1000MeV circular beam (r=10cm) with parabolic proton density
distribution over the radius. (20.000 proton histories)
number of protons (neutrons) for each energy interval per
primary proton (mean values and statistical errors)

energy	proton		neutron	
5.000D-09	0.000D+00	.000	0.000D+00	.000
1.487D-04	0.000D+00	.000	0.000D+00	.000
3.673D-04	0.000D+00	.000	1.000D-04	.500
9.069D-04	0.000D+00	.000	2.250D-04	.333
1.425D-03	0.000D+00	.000	3.500D-04	.267
2.239D-03	0.000D+00	.000	7.750D-04	.180
3.519D-03	0.000D+00	.000	1.825D-03	.117
5.530D-03	0.000D+00	.000	2.450D-03	.101
9.118D-03	0.000D+00	.000	5.625D-03	.066
1.503D-02	0.000D+00	.000	1.053D-02	.049
2.478D-02	0.000D+00	.000	1.848D-02	.037
4.085D-02	0.000D+00	.000	3.507D-02	.027
6.734D-02	0.000D+00	.000	6.336D-02	.020
1.110D-01	0.000D+00	.000	1.183D-01	.015
1.830D-01	0.000D+00	.000	2.181D-01	.011
3.025D-01	2.500D-05	1.000	4.031D-01	.008
5.000D-01	2.500D-05	1.000	7.295D-01	.006
8.210D-01	0.000D+00	.000	1.248D+00	.005
1.353D+00	2.750D-04	.301	2.009D+00	.004
2.231D+00	1.050D-03	.158	2.800D+00	.004
3.679D+00	8.150D-03	.057	3.185D+00	.004
6.066D+00	1.305D-01	.015	2.803D+00	.004
1.000D+01	6.027D-01	.008	1.904D+00	.005
1.380D+01	3.526D-01	.009	8.380D-01	.007
1.500D+01	8.909D-02	.017	1.935D-01	.012
2.000D+01	2.887D-01	.010	5.813D-01	.007
2.300D+01	1.367D-01	.014	2.469D-01	.010
2.710D+01	1.540D-01	.013	2.695D-01	.010
3.680D+01	2.806D-01	.010	4.606D-01	.008
5.000D+01	2.685D-01	.010	4.297D-01	.008
total	2.313D+00	.005	1.858D+01	.003

Table B.4: **total** nucleon production in the ADS neutronic benchmark reactor (Fig. A.1) for neutron cutoff energy ELON=50MeV

lahet - calculation of neutron source for ADS neutronic benchmark
1000MeV circular beam (r=10cm) with parabolic density
distribution over the radius. (20.000 proton histories)
number of protons (neutrons) for each energy interval per
primary proton (mean values and statistical errors)

energy	proton		neutron	
5.000D-09	0.000D+00	.000	0.000D+00	.000
1.487D-04	0.000D+00	.000	0.000D+00	.000
3.673D-04	0.000D+00	.000	1.500D-04	.408
9.069D-04	0.000D+00	.000	4.250D-04	.242
1.425D-03	0.000D+00	.000	5.750D-04	.208
2.239D-03	0.000D+00	.000	1.325D-03	.137
3.519D-03	0.000D+00	.000	2.600D-03	.098
5.530D-03	0.000D+00	.000	4.347D-03	.076
9.118D-03	0.000D+00	.000	1.003D-02	.050
1.503D-02	0.000D+00	.000	1.859D-02	.037
2.478D-02	0.000D+00	.000	3.159D-02	.028
4.085D-02	0.000D+00	.000	5.966D-02	.021
6.734D-02	5.000D-05	.707	1.056D-01	.016
1.110D-01	1.000D-04	.500	1.967D-01	.011
1.830D-01	5.000D-05	.707	3.548D-01	.009
3.025D-01	2.500D-04	.316	6.523D-01	.007
5.000D-01	2.750D-04	.301	1.164D+00	.005
8.210D-01	4.000D-04	.250	1.960D+00	.004
1.353D+00	1.050D-03	.158	3.091D+00	.004
2.231D+00	2.725D-03	.097	4.155D+00	.003
3.679D+00	1.978D-02	.037	4.499D+00	.003
6.066D+00	1.531D-01	.014	3.721D+00	.004
1.000D+01	6.901D-01	.007	2.450D+00	.004
1.380D+01	4.317D-01	.008	1.125D+00	.005
1.500D+01	1.140D-01	.015	2.679D-01	.010
2.000D+01	3.875D-01	.008	8.277D-01	.006
2.300D+01	1.864D-01	.012	3.589D-01	.009
2.710D+01	2.154D-01	.011	3.951D-01	.008
3.680D+01	3.863D-01	.008	6.789D-01	.006
5.000D+01	3.631D-01	.008	6.281D-01	.006
total	2.952D+00	.004	2.676D+01	.002

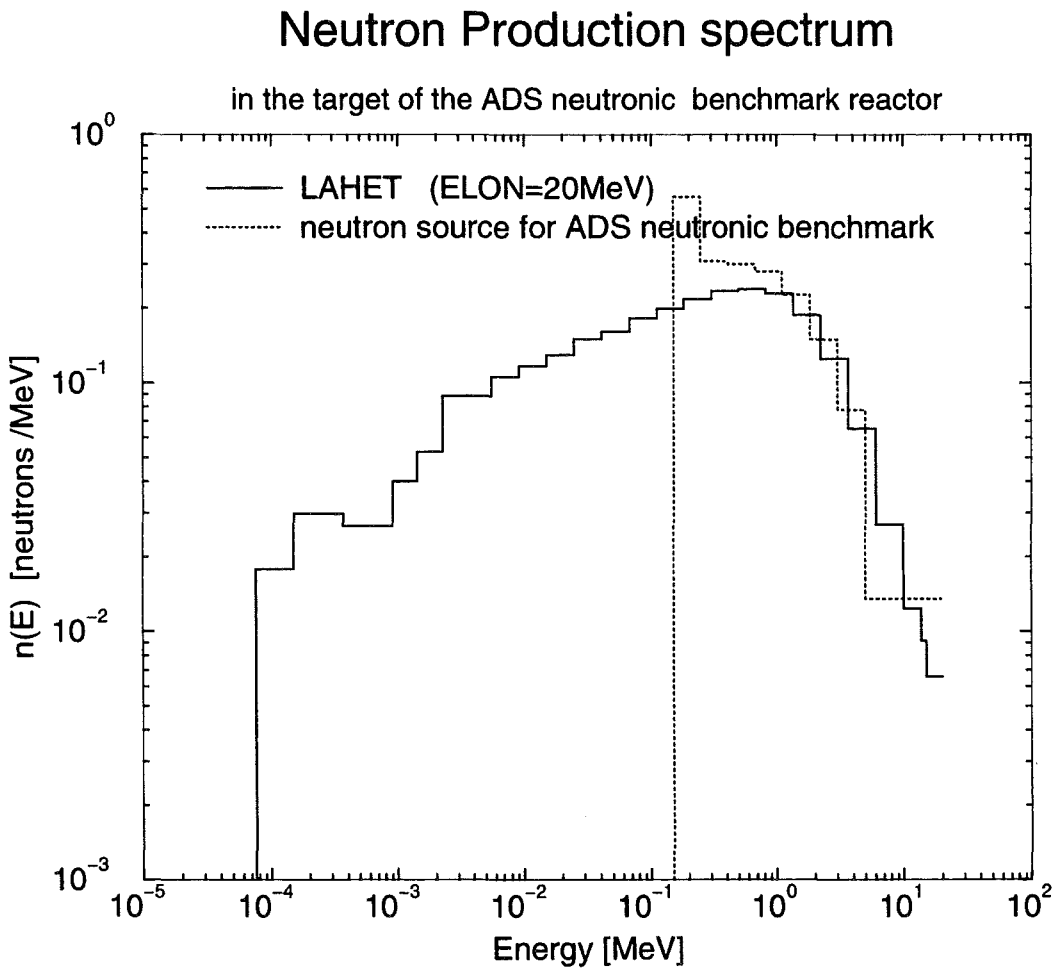

Figure B.1: Neutron production spectrum n(E) in the target of the ADS neutronic benchmark calculated with LAHET. The neutron source given in the benchmark specification is shown for comparison. The spectra are normalized to $\int_{E_{min}}^{E_{max}} n(E)dE = 1$

Appendix C

Input Samples for the LAHET Code System and for MCNPX

Input samples for the LAHET Code System (LCS) are given in [6] and are also distributed together with the LCS code package.
Input samples for MCNPX have been distributed together with the beta-test version on MCNPX (as already mentioned, FZK is beta-tester for MCNPX).
In section C.1 of this chapter we will list the user-defined input files which are needed by the LAHET code system for the calculation of energy deposition and particle production in the different zones of the spallation target shown in Fig. 2.1. In section C.2 we will give the input file for MCNPX for the calculation of the energy deposition in each zone of the target and for the calculation of neutron flux densities

C.1 Input sample for the LAHET Code System

The LAHET Code System needs four input files for the calculation of the energy deposition and of the particle production:

- input file *inh* for LAHET
- input file *int* for HTAPE
- input file *inph* for PHT
- input file *inp* for MCNP

The program TRANSM which prepares the neutron- and γ- source for MCNP needs files that are results provided by LAHET and by PHT but does not need any additional input file.

C.1.1 Example for the input file inh for LAHET

The program LAHET generates two binary files, that are needed in subsequent calculations with HTAPE, PHT, TRANSM and MCNPX

The *neutp* file contains information on the low energy neutrons, that means on the neutrons below the cutoff energy, $E_{cutoff} = 20$MeV in the standard case. (Instead of *cutoff energy*, in MCNPX [18] the expression *'cross-over' energy* is used).
On the history file *histp* detailed information on all particle events is stored.
The structure of both files is given in detail in [6].
In the following input samples for LAHET, HTAPE and PHT a slash (/) means the end of a record. If an input record is terminated by a / before the input list is exhausted, the remaining input items are set equal to their default values.
A comma (,) which is not used as a separator between two numbers means that the default value is used for the corresponding input quantity.
4*, is equivalent to ,,,,. 4*2 is equivalent to 2,2,2,2.

```
lahet - calculation for liquid lead target  (structural material: steel ht9)
600MeV circular proton beam with parabolic proton density profile is
entering from above

100,1000,3,23,4*,1,2*,1/
,-1,1,1/
/
1000./
0,3,3/
82,206,7.45487e-3,22/
82,207,6.83621e-3,22/
82,208,1.62089e-2,22/
0,14,14/
24,52,1.0520e-2,12/
25,55,4.6605e-4,13/
26,54,4.1312e-3,13/
26,56,6.5331e-2,13/
26,57,1.5670e-3,13/
26,58,1.9944e-4,13/
42,98,4.8522e-4,16/
23,51,2.7415e-4,11/
6,12,7.7515e-4,5/
14,28,4.1437e-4,9/
74,182,3.3297e-5,20/
```

```
74,183,1.8104e-5,20/
74,184,3.8994e-5,20/
74,186,3.6209e-5,20/
0,1,1/
2,4,2.6860e-20,1/
    1   3    2.69e-20  -103              8     -9
    2   3    2.69e-20             -203    7     -8
    3   2    8.43e-2   -104        103    8     -9
    4   2    8.43e-2   -202        203    7     -8
    5   1    3.05e-2   -105        104    8     -9
    6   1    3.05e-2   -301        202    6     -8
    7   2    8.43e-2   -302        301    6     -8
    8   2    8.43e-2   -106        105    8     -9
    9   1    3.05e-2   -107        106    8     -9
   10   1    3.05e-2   -107        302    6     -8
   11   2    8.43e-2   -102        101    3     -6
   12   2    8.43e-2   -108        107    2     -9
   13   2    8.43e-2   -205        204    1     -2
   14   1    3.05e-2   -107        102    3     -6
   15   1    3.05e-2   -101               3     -6
   16   1    3.05e-2   -107               2     -3
   17   1    3.05e-2   -204               1     -2
   18   0               108              2     -9
   19   0              -108              9
   20   0                         205          -2

    1   pz     0.0
    2   pz    32.54
    3   pz   141.0
    4   pz   169.71
    5   pz   171.0
    6   pz   181.0
    7   pz   185.0
    8   pz   195.0
    9   pz   215.0
   18   pz   230.0
  101   cz     7.0
```

```
  102  cz     7.9
  103  cz     9.7
  104  cz    10.0
  105  cz    16.8
  106  cz    17.7
  107  cz    31.94
  108  cz    32.54
  201  sz   195.0      9.7
  202  sz   195.0     10.0
  203  sq   0.010628122 0.010628122 0.0103068876 0. 0. 0. -1. 0. 0. 195.
  204  sz   32.54     31.94
  205  sz   32.54     32.54
  301  kz   171.0      0.49
  302  kz   169.71     0.49

in    1 1 1 1 1 1 1 1 1 1 1 1 1 1 1 1 1 1 0 0 0
print

1,-600.,0.0,212.000,7.5,7.5,1.0,0.0,0.0,0.0/
```

The geometry input of LAHET corresponds to the geometry input of MCNP and has to be given twice for a complete LCS calculation. In the MCNP input which will be given in section C.1.1, comment cards are added to the geometry input.

C.1.2 Example for the input file int for HTAPE

HTAPE needs the histp file which optionally is provided by LAHET. The histp-file contains information on all particle types and is used to evaluate quantities like surface current and surface flux for the particles specified on the HTAPE input file int, particle production spectra, track length estimate for neutron flux, energy deposition, information on spallation products, ...

In the following example the HTAPE input is given for the calculation of the energy deposition in the zones of the target given in Fig. 2.1 and for the calculation of the particle production (n, p, π^0, π^+, π^-, deuteron, triton, ^3He and α-particles) in each zone; the total energy production (summed over all zones) and the total particle production are also given in the output of HTAPE.

```
htape - evaluation of energy deposition  600MeV circular proton beam
r=7.5cm parabolic proton density profile   (100000 proton histories)
6,0,0,0,0,20/
1 2 3 4 5 6 7 8 9 10 11 12 13 14 15 16 17 18 19 20 /
htape - evaluation of particle production  600MeV circular proton beam
r=7.5cm parabolic proton density profile   (100000 proton histories)
3,0,0,0,0,20/
1 2 3 4 5 6 7 8 9 10 11 12 13 14 15 16 17 18 19 20 /
```

C.1.3 Example for the input file inph for PHT

The program PHT generates a γ - ray source file (gamtp) which is needed for the calculation of the neutron - γ - source for MCNP.
PHT needs the histp file, provided by LAHET and the input file inph.
Here we give the inph - file which has been used for the LCS calculations discussed in Chapters 2 and 3 of this report.

```
target (r=32.54   h=215cm) with ht9 window
600MeV protons  entrance 212.00 cm in neg.z direction. 100.000 histories
1,4,2000,100,0,0,1.0/
/
```

The TRANSM code uses the neutp - file and the gamtp - file to generate the file rssa, which will be used as neutron - γ - source for MCNP.

C.1.4 Example for the input file inp for MCNP

Within the LAHET Code System, MCNP carries out the Monte Carlo calculations for γ 's and for neutrons below the neutron cutoff energy which is 20MeV in the standard case. Input for MCNP are the file rssa with the neutron - γ - source and the input file inp.
In the following the inp file is given that has been used for the calculation of the energy deposition and the particle production in the zones of the liquid lead target of Fig. 2.1.

Reaction rates for each zone may be specified by tally input. Reaction rates (n,xn), fission and capture for each zone (and total) may also be printed out on the neutron weight balance tables (print table 130) if specified in the print input.

```
lcs/mcnp calculation of the energy deposition and reaction rates
c       for the zones of a liquid lead target. The target is hit from
c       above by a 600MeV circular proton beam with r=7.5cm and with
c       parabolic intensity profile over the radius of the circle.
c
c   internal vacuum in vacuum tube
    1  3   2.69e-20  -103              8    -9
c   internal vacuum in window
    2  3   2.69e-20            -203    7    -8
c   steel vacuumtube
    3  2   8.43e-2   -104       103    8    -9
c   steel window
    4  2   8.43e-2   -202       203    7    -8
c   lead around vacuum tube  10cm<r<16.8cm  195cm<z<215cm
    5  1   3.05e-2   -105       104    8    -9
c   lead between window and funnel 181cm<z<195cm
    6  1   3.05e-2   -301       202    6    -8
c   steel funnel                   181cm<z<195cm
    7  2   8.43e-2   -302       301    6    -8
c   steel flow guide               195cm<z<215cm
    8  2   8.43e-2   -106       105    8    -9
c   lead                  16.8cm<r<17.7cm  195cm<z<215cm
    9  1   3.05e-2   -107       106    8    -9
c   lead outside funnel            181cm<z<195cm
   10  1   3.05e-2   -107       302    6    -8
c   steel (funnel neck)    7cm<r<7.9cm  141cm<z<181cm
   11  2   8.43e-2   -102       101    3    -6
c   steel (target container) 31.94cm<r<32.54cm   32.54cm<z<215cm
   12  2   8.43e-2   -108       107    2    -9
c   steel (target lower head)  0cm<z<32.54cm
```

```
   13  2   8.43e-2   -205       204    1    -2
c   lead outside funnel neck  7.9cm<r<31.94cm    141cm<z<181cm
   14  1   3.05e-2   -107       102    3    -6
c   lead inside funnel neck   r<7cm             141cm<z<181cm
   15  1   3.05e-2   -101              3    -6
c   lead                      r<31.94cm         32.54cm<z<141cm
   16  1   3.05e-2   -107              2    -3
c   lead inside target lower head               0cm<z<32.54cm
   17  1   3.05e-2   -204              1    -2
c   vacuum                    r>32.54cm         32.54cm<z<215cm
   18  0              108              2    -9
c   vacuum                    r<32.54cm         z>215cm
   19  0             -108              9
c   vacuum  outside target lower head  z<32.54cm
   20  0                         205         -2

    1  pz     0.0
    2  pz    32.54
    3  pz   141.0
    4  pz   169.71
    5  pz   171.0
    6  pz   181.0
    7  pz   185.0
    8  pz   195.0
    9  pz   215.0
   18  pz   230.0
  101  cz     7.0
  102  cz     7.9
  103  cz     9.7
  104  cz    10.0
  105  cz    16.8
  106  cz    17.7
  107  cz    31.94
  108  cz    32.54
  201  sz   195.0      9.7
```

```
  202  sz   195.0      10.0
  203  sq   0.010628122 0.010628122 0.0103068876 0. 0. 0. -1. 0. 0. 195.
  204  sz   32.54      31.94
  205  sz   32.54      32.54
  301  kz   171.0       0.49
  302  kz   169.71      0.49

C       all nuclear data taken from endf601
c     liquid lead   particle number densities taken from the ADS neut. bench.
m1     82206.60c     2.44422E-1
       82207.60c     2.24138E-1
       82208.60c     5.31440E-1
c      steel HT9
m2     6000.60c      9.1962E-03
       14000.60c     4.9160E-03
       25055.60c     5.5291E-03
       24052.60c     1.2481E-01
       42000.60c     5.7565E-03
       23000.60c     3.2525E-03
       74182.60c     3.9503E-04
       74183.60c     2.1478E-04
       74184.60c     4.6262E-04
       74186.60c     4.2958E-04
       26054.60c     4.9012E-02
       26056.60c     7.7507E-01
       26057.60c     1.8591E-02
       26058.60c     2.3661E-03
c      he 4 particle number densities mult. by 1.e-15
m3       2004.60c    1.0000
print 40 50 98 110 130 140
imp:n,p      1 1 1 1 1 1 1 1 1 1 1 1 1 1 1 1 0 0 0
ssr
mode   n p
phys:n 20
fc6  energiedeposition [MeV/g] per proton    averaged over zone 1
```

```
f6:n,p  1
fc16  energiedeposition [MeV/g] per proton    averaged over zone 2
f16:n,p 2
fc26  energiedeposition [MeV/g] per proton    averaged over zone 3
f26:n,p 3
fc36  energiedeposition [MeV/g] per proton    averaged over zone 4
f36:n,p 4
fc46  energiedeposition [MeV/g] per proton    averaged over zone 5
f46:n,p 5
fc56  energiedeposition [MeV/g] per proton    averaged over zone 6
f56:n,p 6
fc66  energiedeposition [MeV/g] per proton    averaged over zone 7
f66:n,p 7
fc76  energiedeposition [MeV/g] per proton    averaged over zone 8
f76:n,p 8
fc86  energiedeposition [MeV/g] per proton    averaged over zone 9
f86:n,p 9
fc96  energiedeposition [MeV/g] per proton    averaged over zone 10
f96:n,p 10
fc106  energiedeposition [MeV/g] per proton    averaged over zone 11
f106:n,p 11
fc116  energiedeposition [MeV/g] per proton    averaged over zone 12
f116:n,p 12
fc126  energiedeposition [MeV/g] per proton    averaged over zone 13
f126:n,p 13
fc136  energiedeposition [MeV/g] per proton    averaged over zone 14
f136:n,p 14
fc146  energiedeposition [MeV/g] per proton    averaged over zone 15
f146:n,p 15
fc156  energiedeposition [MeV/g] per proton    averaged over zone 16
f156:n,p 16
fc166  energiedeposition [MeV/g] per proton    averaged over zone 17
f166:n,p 17
fc176  energiedeposition [MeV/g] per proton    averaged over all zones
f176:n,p (1 2 3 4 5 6 7 8 9 10 11 12 13 14 15 16 17)
```

```
fc4    total neutron flux per proton    averaged over zone 4
f4:n     4
fc14   total photonflux per proton    averaged over zone 4
f14:p    4
fc24   absorption rate  per proton    averaged over zone 4
f24:n    4
fm24:n   -1.  1  -2
fc34    n,2n reaction rate  per proton   averaged over zone 4
f34:n    4
fm34:n   -1.  1  16
ctme  300.0
nps 100000
```

C.2 Example for the input file inp for MCNPX

MCNPX is a merge of LAHET, PHT and MCNP
Besides the cross section libraries, MCNPX needs only one input file, called inp.
The physics parameters that are used in LAHET and PHT may be specified in the MCNPX input on four records which are designated lca, lcb, lea and leb. If these cards are not defined in the input the default values of the physics parameters will be used. In the input file given below we have inserted the default values on records lca, lcb, lea and leb.
The following input sample of MCNPX carries out calculations for the target shown in Fig. 2.1. MCNPX calculates the energy deposition for each zone of the target and for the entire target. In addition the neutron flux density spectrum in the target window (zone 4) is evaluated in a 83 energy groups structure from 0eV to 600MeV, 75 energy groups up to 50MeV [26] and 8 energy groups between 50MeV and 600MeV, see also Chapter 3; (note that the group structure differs from that used in Appendix A).
Neutron flux density spectra for all zones (and averaged over the target) are provided in two energy groups: 0eV - 20MeV and 20MeV - 600MeV.
Tally specification +F6 was used in MCNPX for the calculation of the energy deposition according to a recommendation given by H.G. Hughes, LANL, by e-mail of 8 March 1999 as response of a request by C.H.M. Broeders.
The source specification in the MCNPX input is:
sdef sur=19 erg=600. par=9 dir=-1 pos=0. 0. 212.0 rad=d1

si1 7.5

surface 19 (sur=19) is a plane perpendicular to the z-axis, the equation of this plane is $z - 212.0 = 0$.

The corresponding specification of the source in the input of LAHET is:

0,-600.,0.0,212.000,7.5,7.5,1.0,0.0,0.0,0.0/

Input file for MCNPX (inp)

```
mcnpx   calculation for the liquid lead target
c       600MeV protons parallel beam intensity is uniformly distributed
c       over a circle with r=7.5cm
c
    1  3   2.67e-20  -103              8    -9
    2  3   2.67e-20          -203     7    -8
    3  2   8.47e-2   -104      103     8    -9
    4  2   8.47e-2   -202      203     7    -8
    5  1   3.05e-2   -105      104     8    -9
    6  1   3.05e-2   -301      202     6    -8
    7  2   8.47e-2   -302      301     6    -8
    8  2   8.47e-2   -106      105     8    -9
    9  1   3.05e-2   -107      106     8    -9
   10  1   3.05e-2   -107      302     6    -8
   11  2   8.47e-2   -102      101     3    -6
   12  2   8.47e-2   -108      107     2    -9
   13  2   8.47e-2   -205      204     1    -2
   14  1   3.05e-2   -107      102     3    -6
   15  1   3.05e-2   -101              3    -6
   16  1   3.05e-2   -107              2    -3
   17  1   3.05e-2   -204              1    -2
   18  0              108              2    -9
   19  0             -108              9
   20  0                       205          -2

    1  pz     0.0
    2  pz    32.54
    3  pz   141.0
    4  pz   169.71
    5  pz   171.0
    6  pz   181.0
    7  pz   185.0
    8  pz   195.0
```

```
    9  pz   215.0
   18  pz   230.0
   19  pz   212.0
  101  cz     7.0
  102  cz     7.9
  103  cz     9.7
  104  cz    10.0
  105  cz    16.8
  106  cz    17.7
  107  cz    31.94
  108  cz    32.54
  201  sz   195.0      9.7
  202  sz   195.0     10.0
  203  sq   0.010628122 0.010628122 0.0103068876 0. 0. 0. -1. 0. 0. 195.
  204  sz   32.54     31.94
  205  sz   32.54     32.54
  301  kz   171.0      0.49
  302  kz   169.71     0.49

C       all nuclear data taken from endf601
c     liquid lead (particle number density is  3.05e-2 atoms/cm**3
m1    82206.60c    2.44422E-1
      82207.60c    2.24138E-1
      82208.60c    5.31440E-1
c     steel 1.4970 (particle number density is 8.47e-2 atoms/cm**3
m2    24052.60c  1.59951404E-01
      26056.60c  6.72643423E-01
      42000.60c  7.22431252E-03
      28058.60c  1.41655743E-01
      23000.60c  3.26902373E-04
       6000.60c   4.61629359E-03
      14000.60c  8.48860294E-03
      22000.60c  5.09327976E-03
c     he-4 particle number densities multiplied by 1.e-15
c     (2.69e-20)
m3    2004.60c     1.0000
sdef sur=19 erg=600. par=9 dir=-1 pos=0. 0. 212.0 rad=d1
si1 7.5
print 40 50 98 110 130 140
imp:n,p             1 1 1 1 1 1 1 1 1 1 1 1 1 1 1 1 0 0 0
imp:h/,|,z,d,t,s,a  1 1 1 1 1 1 1 1 1 1 1 1 1 1 1 1 0 0 0
mode   h n p / | z d t s a
```

```
phys:n 700. 0.0  20.0
phys:h 700.
fc4 neutron flux spectrum in cell 4 (window)
f4:n     4
C        83 energy groups structure from 0Mev to 600MeV
e4      0.
         0.005E-6 0.010E-6 0.015E-6 0.020E-6 0.025E-6 0.030E-6 0.035E-6
         0.042E-6 0.050E-6 0.058E-6 0.067E-6 0.080E-6 0.100E-6 0.140E-6
         0.180E-6 0.220E-6 0.250E-6 0.280E-6 0.300E-6 0.320E-6 0.350E-6
         0.400E-6 0.500E-6 0.625E-6 0.780E-6 0.850E-6 0.910E-6 0.950E-6
         0.972E-6 0.996E-6 1.020E-6 1.045E-6 1.071E-6 1.097E-6 1.123E-6
         1.150E-6 1.300E-6 1.500E-6 2.100E-6 2.600E-6 3.300E-6 4.000E-6
         9.877E-6 15.968E-6 27.700E-6 48.052E-6 75.5014E-6 148.728E-6
         367.262E-6 906.898E-6 1425.1E-6 2239.45E-6 3519.1E-6 5530.0E-6
         0.009118 0.01503 0.02478 0.04085 0.06734
         0.111 0.183 0.3025 0.500 0.821 1.353 2.231 3.679 6.0655 10.
         13.8 15.0 20.0 27.1 36.8 50.0 60.0 100.0 150.0 200.0 300.0
         400.0 500.0  600.
c        volumen des zylinders:
c        teilchenzahldichte des pb-208: .0305
c        volumen * teilchenzahldichte zur multiplikation der tallies:
c
fc6  energydeposition [MeV/proton] averaged over zone 1
+f6:n,p 1
fc16  energydeposition [MeV/proton] averaged over zone 2
+f16:n,p 2
fc26  energydeposition [MeV/proton] averaged over zone 3
+f26:n,p 3
fc36  energydeposition [MeV/proton] averaged over zone 4
+f36:n,p 4
fc46  energydeposition [MeV/proton] averaged over zone 5
+f46:n,p 5
fc56  energydeposition [MeV/proton] averaged over zone 6
+f56:n,p 6
fc66  energydeposition [MeV/proton] averaged over zone 7
+f66:n,p 7
fc76  energydeposition [MeV/proton] averaged over zone 8
+f76:n,p 8
fc86  energydeposition [MeV/proton] averaged over zone 9
+f86:n,p 9
fc96  energydeposition [MeV/proton] averaged over zone 10
+f96:n,p 10
```

```
fc106  energydeposition [MeV/proton] averaged over zone 11
+f106:n,p 11
fc116  energydeposition [MeV/proton] averaged over zone 12
+f116:n,p 12
fc126  energydeposition [MeV/proton] averaged over zone 13
+f126:n,p 13
fc136  energydeposition [MeV/proton] averaged over zone 14
+f136:n,p 14
fc146  energydeposition [MeV/proton] averaged over zone 15
+f146:n,p 15
fc156  energydeposition [MeV/proton] averaged over zone 16
+f156:n,p 16
fc166  energydeposition [MeV/proton] averaged over zone 17
+f166:n,p 17
fc176  energydeposition [MeV/proton] averaged over all zones
+f176:n,p                                    &
(1 2 3 4 5 6 7 8 9 10 11 12 13 14 15 16 17)
fc204  neutronflux averaged  over zone 1
f204:n    1
e204 0. 20. 600.
fc214  neutronflux averaged  over zone 2
f214:n    2
e214 0. 20. 600.
fc224  neutronflux averaged  over zone 3
f224:n    3
e224 0. 20. 600.
fc234  neutronflux averaged  over zone 4
f234:n    4
e234 0. 20. 600.
fc244  neutronflux averaged  over zone 5
f244:n    5
e244 0. 20. 600.
fc254  neutronflux averaged  over zone 6
f254:n    6
e254 0. 20. 600.
fc264  neutronflux averaged  over zone 7
f264:n    7
e264 0. 20. 600.
fc274  neutronflux averaged  over zone 8
f274:n    8
e274 0. 20. 600.
fc284  neutronflux averaged  over zone 9
```

```
f284:n    9
e284 0. 20. 600.
fc294  neutronflux averaged  over zone 10
f294:n    10
e294 0. 20. 600.
fc304  neutronflux averaged  over zone 11
f304:n    11
e304 0. 20. 600.
fc314  neutronflux averaged  over zone 12
f314:n    12
e314 0. 20. 600.
fc324  neutronflux averaged  over zone 13
f324:n    13
e324 0. 20. 600.
fc334  neutronflux averaged  over zone 14
f334:n    14
e334 0. 20. 600.
fc344  neutronflux averaged  over zone 15
f344:n    15
e344 0. 20. 600.
fc354  neutronflux averaged  over zone 16
f354:n    16
e354 0. 20. 600.
fc364  neutronflux averaged  over zone 17
f364:n    17
e364 0. 20. 600.
fc374  neutronflux averaged  over alle zonen
+f374:n     &
(1 2 3 4 5 6 7 8 9 10 11 12 13 14 15 16 17)
e374 0. 20. 600.
c       ctme  500.0
ctme  15.0
nps 100000
```

Acknowledgement

We would like to thank Dr. E. Kiefhaber for discussions and remarks and W. Götzmann for the preparation of some of the figures.

Bibliography

[1] C. Broeders, I. Broeders,
Calculations of the Energy Deposition in the Target of an ADS
in: Wissenschaftliche Berichte FZKA 6300 (pages 663 - 672)
September 1999

[2] C. Broeders, I. Broeders
Calculations for the IAEA coordinated ADS NEUTRONIC BENCHMARK
in: Wissenschaftliche Berichte FZKA 5963 (pages 464 - 472)
September 1997

[3] I. Slessarev, A. Tschistiakov,
IAEA-ADS BENCHMARK (Stage 1)
RESULTS and ANALYSIS
TCM-Meeting, Madrid, 17-19 September 1997

[4] J.U. Knebel
private communication

[5] X. Cheng, J.U. Knebel, F. Hofmann
Thermohydraulic Design of an ADS with three Spallation Targets
Conference on Accelerator-Driven Systems
Praha, June 7-11, 1999

[6] R.E. Prael and H. Lichtenstein
User Guide to LCS: The LAHET Code System
LA-UR-89-3014 Los Alamos National Laboratory
Revised September 15, 1989
http://www-xdiv.lanl.gov/XCI/PROJECTS/LCS/lahet-doc.html
and

R.E. Prael

Upgrade Package for LCS with LAHET2.7

LA-UR-97-4981

December 1, 1997

[7] R.E. Prael

A Review of Physics Models in the LAHET^{TM} Code

LA-UR-94-1817

and in

Intermediate Energy Nuclear Data: Models and Codes

Proceedings of a Specialists' meeting

Issy-Les-Moulineaux (France)

OECD Documents

30 May-1 June 1994 (pages 159 - 182)

[8] P. Cloth, D. Filges, R.D. Neef, G. Sterzenbach, Ch. Reul, T.W. Armstrong, B.L. Colborn, B. Anders, H. Brückmann

HERMES A Monte Carlo Program System for Beam-Materials Interaction Studies

Jül-2203, May 1988

[9] J.F. Briesmeister, Editor

MCNP-A General Monte Carlo N-Particle Transport Code, Version 4B

LA-12625-M, Version 4B

Issued: March 1997

[10] H.W. Bertini

Intranuclear-Cascade Calculations of the Secondary Nucleon Spectra from Nucleon-Nucleus Interactions in the Energy Range 340 to 2900MeV and Comparisons with Experiment

Phys. Rev. 188, 1711, 1969

[11] R.E. Prael and Michael Bozoian

Adaption of the Multistage Preequilibrium Model for the Monte Carlo Method

LA-UR-88-3238, Los Alamos National Laboratory (September 1988)

http://www-xdiv.lanl.gov/XCI/PEOPLE/rep/index.html

[12] E. Gadioli, P. Hodgson

Pre-equilibrium nuclear reactions

Clarendon Press, Oxford, 1992

[13] F. Atchison

Spallation and Fission in Heavy Metal Nuclei under Medium Energy Proton Bombardment

Proc. of Mtg. on Targets for Neutron Beam Spallation Sources

Jül-Conf-34, January 1980 (pages 17 - 45)

[14] A.V. Ignatyuk, G.N. Smirenkin, and A.S. Tishin

Phenomenological description of the energy dependence of the level density parameter

Sov. J. Nucl. Phys.21(1975) p.255

[15] H. Glasbrenner, K. Stein-Fechner

Chemical composition of HT9 steel

personal communication

[16] G. Musiol, J. Ranft, R. Reif, D. Seeliger

Kern- und Elementarteilchenphysik

Lizenzausgabe der VCH Verlagsgesellschaft, D-6940 Weinheim

VEB Deutscher Verlag der Wissenschaften Berlin 1988

[17] S.J. Lindenbaum

Particle-Interaction Physics at High Energies

CLARENDON PRESS · OXFORD, 1973

[18] Laurie S. Waters, Editor

MCNPX^{TM} User's Manual

Version 2.1.5

TPO-E83-G-UG-X-00001, Revision 0, November 1999

http://mcnpx.lanl.gov

see also

H.G. Hughes, R.E. Prael, R.C. Little

MCNPX - The LAHET/MCNP Code Merger

Los Alamos National Laboratory Report XTM-RN(U)97-012, April 22, 1997,

LA-UR-97-4891

and

H.G. Hughes, K.J. Adams, M.B. Chadwick, J.C. Comly, S.C. Frankle, J.S. Hendricks, R.C. Little, R.E. Prael, L.S. Waters, and P.G. Young, Jr.

Status of the MCNP^{TM} / LCS^{TM} Merger Project

To be published in

Proceedings of the Radiation Protection and Shielding Topical Conference held in Nashville, Tennessee, April 19-23, 1998

http://www-xdiv.lanl.gov/XTM/hughes/

[19] Yu. Korovin, A. Konobeyev, P. Pereslavtsev, V. Sosnin, M. Vecchi, L. Latysheva

Study of Target Window for Accelerator-Driven Sub-critical Reactor

Conference on Accelerator-Driven Systems

Praha, June 7-11, 1999

[20] J.R. Lamarsh

NUCLEAR REACTOR THEORY

1965

ADDISON-WESLEY PUBLISHING COMPANY, INC.

Reading, Massachusetts, U.S.A.

ADDISON-WESLEY (CANADA) LIMITED

[21] R.E. Prael

HTAPE3X for Use with MCNPX

LA-UR-99-1992 Los Alamos National Laboratory (April 1999)

[22] M. Segev, C. Broeders, I. Broeders

Forschungszentrum Karlsruhe Internal Report

Januar 1999

[23] M. Salvatores, G.S. Bauer, G. Heusener

Internal PSI report, 1999

[24] Yu.A. Korovin, A.Yu. Konobeyev, P.E. Pereslavtsev, A.Yu. Stankovsky, C. Broeders, I. Broeders, U. Fischer, U. v. Möllendorff, P. Wilson, D. Woll

Evaluation and Test of Nuclear Data for Investigation of Neutron Transport, Radiation Damage and Processes of Activation and Transmutation in Materials Irradiated by Intermediate and High Energy Particles

G. Reffo, editor

Internat. Conf. on Nuclear Data for Science and Technology, Trieste, May 19-24, 1997. Italian Physical Society, Conference Proceedings, Vol.59, Part I, 1997 (pages 851 - 855)

[25] RSIC COMPUTER CODE COLLECTION, DANTSYS 3.0, One-, Two-, and Three-Dimensional, Multigroup, Discrete Ordinates Transport Code System, contributed by: Los Alamos National Laboratory, Los Alamos, New Mexico (1995)

http://www-xdiv.lanl.gov/XTM/

[26] C. Broeders, I. Broeders,

Generation of a Group Constant Library for Neutron Energy until 50MeV, Tests and Applications

in: Wissenschaftliche Berichte FZKA 6126 (pages 580 - 586)

September 1998